THE IMPACTS OF INFLAMMATION ON ADULT PROSTATE STEM CELLS

by

Paula Cooper

A Dissertation

Submitted to the Faculty of Purdue University

In Partial Fulfillment of the Requirements for the degree of

Doctor of Philosophy

Department of Comparative Pathobiology

West Lafayette, Indiana

August 2020

THE PURDUE UNIVERSITY GRADUATE SCHOOL
STATEMENT OF COMMITTEE APPROVAL

Dr. Timothy L. Ratliff, Chair

Department of Comparative Pathobiology

Dr. Stephen F. Konieczny

Department of Biological Sciences

Dr. Shihuan Kuang

Department of Animal Sciences

Dr. Suresh K. Mittal

Department of Comparative Pathobiology

Approved by:

Dr. Jason R. Cannon

For my husband, Monte, whose excellent taste in music made this work possible

ACKNOWLEDGMENTS

It is true that no great feat is accomplished alone. This work has been supported by a small army of friends, family, and colleagues, without whom it would not have been possible. I am the luckiest person in the world for having them all in my life.

I would like to thank the members of my thesis committee: Dr. Suresh Mittal, Dr. Shihuan Kuang, and Dr. Stephen Konieczny for their guidance, wisdom, and insight. I am especially grateful for Dr. Timothy Ratliff's mentorship. His relentless optimism is contagious, and I am lucky to have the privilege of calling him my PhD advisor.

I would also like to thank the past and current members of the Ratliff lab: Dr. Scott Crist, Dr. Jiang Yang, Dr. Ben Elzey, Dr. Grant Burcham, Dr. Cansu Çimen Bozkus, Dr. Hsing-Hui Wang, Dr. Renee Vickman, Dr. Meaghan Broman, Dr. Gregory Cresswell, Dr. Erin Kischuk, Elia Farah, Sandra Torregrosa-Allen, and Tripti Bera. They have become a second family to me, and the conversations, jokes, and successes we all shared brought such joy to my time at Purdue.

The work described here could not have been completed without Dr. Jill Hutchcroft. I am forever grateful for her endless patience every time my compensations did not work, or I was, "running about 15 minutes late!" Nor would the work be as impactful without Dr. Nadia Atallah Lanman, who was always there to answer any odd question about statistics or bio informatics.

Some of the most important contributions were from people who were farthest away. I want to thank my friends, for their bottomless encouragement and support. Elizabeth Jansen Zissen, Dr. Judy Bordson-Young, Dr. Caitlin Stallings, and Monica Hensley were always there to lend an ear. Thanks to them, this work was a little brighter and more filled with horse gelatin.

Words are not enough to thank my family for their love and support. My mamá, Patricia, always told me that if I didn't want to go to class, I could stay home and clean. Those words drove me through nearly 30 years of school. Despite my dad, Jimmy, insisting that I drop out and become a park ranger, he has been a pillar of support and an example of what it means to be dedicated to your work. His meticulous nature and love of exploration have guided my hands in the lab for the past decade. Carmen, Patty, and Teresa, my sisters, have inspired me through their own hard work and dedication to learning. I look up to all of them.

And last, but most importantly, I would like to thank my husband, Monte Cooper. His brilliance, strength, and optimism make every day a joy. He challenges me to be a better person and inspires me to be a better scientist. I love you, and I am so excited for what is to come.

TABLE OF CONTENTS

LIST OF TABLES 9
LIST OF FIGURES 10
ABSTRACT 12
CHAPTER 1. INTRODUCTION AND LITERATURE REVIEW 13
1.1 The Prostate 13
1.1.1 Basic Biology of the Human and Murine Prostate 13
1.2 The Epithelial Cell Components of the Prostate 15
1.2.1 Luminal Cells 15
1.2.2 Neuroendocrine Cells 15
1.2.3 Basal Cells 16
1.3 The Androgen Receptor 17
1.3.1 Structure and Function of the Androgen Receptor 17
1.3.2 Aberrant Androgen Receptor Signaling 18
1.3.3 Interleukin 1 Alpha and AR signaling 19
1.4 The Major Diseases of the Prostate 19
1.4.1 Prostatitis 20
1.4.2 Benign Prostate Hyperplasia 21
1.4.3 Prostate Cancer 22
1.5 Basic Immunology of the Prostate 23
1.6 Introduction to Research Questions and Methodology 25
1.7 Purpose of Studies 26
CHAPTER 2. INFLAMMATION-INDUCED ANDROGEN RECEPTOR SIGNALING VIA THE INTERLEUKIN 1 ALPHA PATHWAY IN BASAL PROSTATE STEM CELLS 33
2.1 Abstract 33
2.2 Introduction 33
2.3 Methods 34
2.3.1 RNA and Protein Isolation by Trizol Reagent 34
2.3.2 cDNA synthesis 35
2.3.3 Real-Time Quantitative Polymerase Chain Reaction 35

2.3.4 Western blot 35
2.3.5 Histology 36
2.3.6 3D organoids 36
2.3.7 BrdU labeling 37
2.3.8 Mice 37
POET3: 37
2.3.9 Renal grafts 37
2.3.10 Orchiectomy 38
2.3.11 Human prostate samples 38
2.3.12 Murine AR target gene array 39
2.3.13 ATAC sequencing 39
2.3.14 Single Cell RNA Sequencing 40
2.3.15 Human Organoid RNA seq 43
2.3.16 3'RACE 47
2.3.17 pGL3 Luciferase Reporter 47
2.4 Results 47
2.4.1 Androgen Receptor in Prostate Stem Cells 47
2.4.2 Androgen Receptor in 3D Prostate Organoids 49
2.4.3 Interleukin 1 Alpha and Androgen Receptor Signaling 52
2.4.4 In Vivo Analysis of Inflammation-Mediated AR and PSC Proliferation 54
2.4.5 AR in Human Prostate Stem Cells 54
2.5 Discussion 56
2.6 Tables and Figures 60
CHAPTER 3. T CELL REGULATION BY ADULT PROSTATE STEM CELLS 96
3.1 Abstract 96
3.2 Introduction 96
3.3 Methods 98
3.3.1 OT-I Activation for Suppression 98
3.3.2 Cell Sorting 99
3.3.3 Liquid Organoid Culture and Suppression Assay 99
3.3.4 Flow Cytometry 99

3.4 Results 99
3.5 Discussion and future directions 101
3.6 Tables and Figures 103
REFERENCES 107

LIST OF TABLES

Table 2.1. Genes over-expressed in inflamed LSC vs. naïve LSC. 60

Table 2.3. Genes upregulated in inflamed LSC as compared to naïve. 61

Table 2.4. Interleukin 1 alpha and its signaling component genes upregulated in inflamed LSC as compared to naïve. 62

Table 3.1. Differential Expression of Immune Regulatory Genes in Inflamed LSC vs Naïve 103

LIST OF FIGURES

Figure 1.1. The Human Prostate.. 28
Figure 1.2. Cellular Structure of Prostatic Ducts. 29
Figure 1.3. The Murine Prostate. 31
Figure 1.4. Cytokeratin Staining in the Prostate. 32
Figure 2.1. Identification of AR activity in inflamed $Lin^{-}Sca1^{+}CD49f^{+}$ (LSC) population ex vivo. 63
Figure 2.2. Identification and modulation of AR activity in naïve and inflamed organoids. 65
Figure 2.3. Androgen Synthesis in organoid cultures.. 67
Figure 2.4. Abrogation of AR activity via AR antagonists abolishes basal PSC characteristics. 68
Figure 2.5. 3'RACE (Rapid amplification of cDNA ends).. 70
Figure 2.6. Inflammation induces CDK-1 mediated phosphorylation of AR.. 71
Figure 2.7. Quality Control for Single Cell mRNA Sequencing.. 72
Figure 2.8. Heatmap showing results of unsupervised clustering. 74
Figure 2.9. Upstream regulator IFNG and its predicted mechanistic network. 75
Figure 2.10. Differentially expressed genes between naïve and inflamed. 76
Figure 2.11. Canonical Interleukin 1 pathway.. 77
Figure 2.12. PGL3 Luciferase IL-1α Reporter Assay. 78
Figure 2.13. Interleukin 1 Alpha Treatment of Organoid Cultures.. 79
Figure 2.14. Interleukin 1 Receptor Antagonist in 3D Organoids. 80
Figure 2.15. Interleukin 1 Receptor Antagonist Impacts Androgen Receptor Signaling.. 81
Figure 2.16. Genomic Manipulation of AR and IL-1RA. 82
Figure 2.17. ATAC Sequencing.. 83
Figure 2.18. Short-term Inflammation Castration and BrdU incorporation. 84
Figure 2.19. Short-term Inflammation Castration Representative H&E Staining. 85
Figure 2.20. Short-term Inflammation Castration Representative AR Staining. 86
Figure 2.21. Short-term Inflammation Castration Representative p63 Staining.. 87
Figure 2.22. Enzalutamide Treatment of Human Organoids. 88
Figure 2.23. Quality Control for RNA Sequencing of Human Organoids 89

Figure 2.24. Clustering Analysis of Human Organoid RNA Sequencing. 90

Figure 2.25. Heatmap showing the expression data of the 40 most highly expressed genes of comparison and all samples. 91

Figure 2.26. Antigen Presentation Canonical Pathway in Human Organoids. 92

Figure 2.27. Protein Digestion and Absorption (hsa04974) in Human Organoids. 93

Figure 2.28. Heatmap Showing Expression Data for Genes of Interest. 94

Figure 2.29. Production of Inflammable Recombinant Prostate Grafts in Renal Capsule Assay. 95

Figure 3.1. PD-L1 expression in naïve and inflamed LSC 104

Figure 3.2. Suppression Assay With Anti-PD-L1 Neutralizing Antibody Despite the increase in PD-L1 in inflamed LSC 105

Figure 3.3. LSC Suppression Assays. 106

ABSTRACT

Adult prostate stem cells (PSC) are a rare epithelial progenitor population in the prostate. While essential for normal homeostasis, they have also been implicated in hyperplasia and cancer initiation (1-7). While studies have shown that inflammatory growth factors and cytokines can fuel stem cell expansion, the impact of inflammation on PSC is not well understood (1, 8, 9). To study the impact of inflammation on the prostate, the Ratliff laboratory developed the Prostate Ovalbumin Expressing Transgenic 3 (POET3), an inducible mouse model of abacterial T cell mediated prostate inflammation, which functions as a model for human autoimmune prostatitis (10). Previous studies using the POET3 demonstrated that inflammation increased proliferation and differentiation of PSC enrichments (11). Based on these findings, it was speculated that inflammation impacts prostate stem cells to enhance mechanisms of survival, possibly as a means of tissue protection.

Since androgen receptor (AR) signaling is the major driver of cellular differentiation and survival in the prostate, it was further hypothesized that inflammation promotes AR signaling in the PSC. To address this hypothesis, PSC and their resulting organoids from inflamed and non-inflamed (naïve) POET3 mice as well as human patient samples were assessed for AR and its signaling components.

These data were expanded by single cell mRNA sequencing using Fluidigm's C1 platform, which revealed changes in stem cell populations, differential expression of interleukin 1 alpha (IL-1α) and its signaling components, and upregulation of various genes associated with immune regulation. Thus, experiments described herein probed the impacts of inflammation on AR, IL-1α, and T cell regulatory abilities in the PSC.

The results of these studies indicate that indeed, inflammation increases PSC survival. Inhibition of IL-1α via inflammation-mediated up-regulation of IL-1 receptor antagonist (IL-1RA) promotes AR signaling, resulting in proliferation, differentiation, and AR target gene expression which can be modulated by Enzalutamide (a clinical AR inhibitor). Furthermore, PSC from inflamed mice are able to suppress cytotoxic T cell function in *ex vivo* assays. These studies set the foundation for new ways to treat proliferative diseases of the prostate by targeting IL-1α, AR, and immune regulation in the PSC.

CHAPTER 1. INTRODUCTION AND LITERATURE REVIEW

1.1 The Prostate

1.1.1 Basic Biology of the Human and Murine Prostate

The prostate is a walnut-sized secretory gland. The peak of the cone-shaped prostate encircles the penile urethra, and the base extends toward the bladder (12). While the developing human prostate consists of distinct "lobes," the adult prostate is composed of less distinct "zones" described by McNeal et al. in 1981 (13, 14) (Figure 1.1). The majority of the prostate (70%) is comprised of the peripheral zone, which surrounds the wedge-shaped central zone (25%) (12, 13). These two zones contain the major secretory ducts. The third lobe is described as the transition zone, which lacks ducts of its own but is traversed by ducts of the peripheral zone. The anterior prostate is composed of thick fibromuscular stroma (13). These distinct zones function to produce the fluids that nourish and protect the sperm, making the prostate essential for mammalian reproduction (15).

Architecturally, the glandular tissue of the human prostate is composed of acini and ducts that are described as undulating and papillary (with small rounded projections) in appearance (12) (Figure 1.2). It is fairly homogeneous, although the central zone contains more notable papillae. The prostatic acini are lined by tall, cuboidal luminal cells that are the functional cells of the prostate. Interspersed among them are rare neuroendocrine cells. These sit upon a layer of basal cells, which separate the lumen from a prominent fibromuscular stroma (12). These cellular ducts run toward the urethra, and function together to secrete prostatic fluids.

The prostate is prone to diseases including prostatitis, benign prostate hyperplasia (BPH), and prostate cancer (PCa), which impact male fertility and quality of life (15); however, it is impossible to study the development and changes between healthy and diseased tissues in living humans. Therefore, we rely on animal models to provide insight to prostate development and reveal the underlying causes and mechanisms of progression of prostate disease.

The murine prostate, while performing the same function as the human prostate, has several key differences. Similar to the human prostate, murine prostate lobes contain acini lined by epithelial cells composed of cuboidal to columnar luminal cells, interspersed basal cells, and rare neuroendocrine cells surrounded by fibromuscular stroma cells (these cell types are described in

detail below). Generally, the murine prostatic stroma is less prominent than that of the human prostate (16). While the human prostate has no external lobe structures, the mouse prostate has 4 pairs of distinct lobes, which can be easily identified by eye (Figure 1.3). These consist of the anterior lobes, dorsal lobes, lateral lobes, and ventral lobes (17, 18). The characteristics are defined in detail by Oliveria et al. (18). Along with being physically distinct, hematoxylin and eosin (H&E) staining reveals architectural and cellular differences between murine lobes. The anterior lobes consist of large, open acini that are described as "cribriform" or "papillary" in shape and form prominent infoldings. The dorsal lobes are characterized by small acini with sparse infoldings. The lateral lobes possess acini of varying sizes with flat epithelial borders that lack infoldings; and while similar in appearance to the lateral lobes, the ventral lobes lack the eosinophilic luminal secretions present in the other murine lobes (12, 13, 16, 18). The secretions produced by each lobe are also different in composition; however, the end result is similar to that produced by humans in role and makeup (19, 20).

In terms of prostatic morphology and the development and progression of cancer, canine models may be most similar to human (21, 22). However, canine studies are difficult to control and mainly dependent on patient samples (23), while the mouse is easy to manipulate and control in a laboratory setting (16, 24). Thus, while it is difficult to draw direct comparisons between the zones and lobes of murine and human prostate, the mouse remains the most prominent and well-studied model of prostatic development and disease.

Despite the apparent differences between murine and human prostate composition, there are many similarities between the two organs. The human peripheral zone, where the majority of prostate cancer (PCa) occurs, is often compared to the dorsolateral murine prostate in terms of gene expression (13, 25).The human central zone most closely resembles the anterior prostate of the mouse (18), while the transition and anterior zones have no murine equivalent. This is unfortunate since the transition zone is the origin of benign prostate hyperplasia and a subset of PCa with distinct characteristics from those that originate in the peripheral zone (13, 26-29). This lack of essential regions hindered the use of mouse models in studies of prostate disease until recently. With the development of widely applicable genetic modifications and xenograft models, the mouse has provided substantial insight to the areas of prostatitis, benign prostate hyperplasia, and invasive carcinoma (24, 30-32).

1.2 The Epithelial Cell Components of the Prostate

In order to understand the diseases of the prostate described below, an understanding of the cellular components is required. The human and murine prostatic ducts are composed of two major cellular layers: the fibromuscular stroma and the epithelium (Figure 1.3). The stroma is essential for prostate development, fueling proliferation and differentiation with growth factors and paracrine signals, and plays a supportive role in mature prostate function (33, 34). These same factors may contribute to prostatic disease (35); however, the topic of this work is the epithelium, which will be the focus of the discussion below. The epithelium can be divided into functional luminal cells, supportive basal cells, and rare neuroendocrine cells. Each of these cell types plays an essential role in prostate function and contributes to different aspects of prostate disease. The cellular composition is similar between species; therefore, the following section is relevant to both human and murine prostate.

1.2.1 Luminal Cells

The luminal cells are the functional secretory cells of the prostate. They are predominantly columnar in shape and line the prostatic acini described above. They are the functional cells of the prostate and produce three major components of seminal fluid to help buffer and nourish the sperm. These include prostatic acid phosphate (PAcP), beta-microseminoprotein, and, in humans, prostate specific antigen (PSA) (36, 37). Mature luminal cells are recognized by their expression of androgen receptor (AR), Nkx3.1, cytokeratin 8, cytokeratin 18, and kallikreins (38). They are most sensitive to circulating androgens, particularly dihydrotestosterone (DHT) and its less potent precursor testosterone (T). If there is loss of circulating androgens, the luminal cells undergo rapid apoptosis resulting in drastic involution and a reduction in prostate size. Upon reintroduction of androgens, the prostate regenerates and resumes normal function (39, 40). Luminal cells have been implicated in prostate cancer initiation (41, 42); however, their role is debated as they may arise from trans-differentiation and maturation of transformed basal cells described below (5, 43-45).

1.2.2 Neuroendocrine Cells

Neuroendocrine cells compose a small percentage (<1%) of the prostate (46). They are thought to play a role in development, and they produce various growth factors including

transforming growth factor alpha (TGF-α) and vascular endothelial growth factor (VEGF) (47). Coupled with their lack of AR expression and resistance to androgen deprivation therapy, this makes them particularly pernicious in the tumor setting. Because of these features, neuroendocrine cells are studied extensively for their role in treatment resistant prostate cancer (46, 48). In the normal setting, these rare cells exist interspersed among the basal and luminal cells. They are difficult to identify morphologically, but express unique markers chromogranin A (CgA), neuron specific enolase (NSE), and synaptophysin (SYN) at varying intensities (48). Neuroendocrine cells are heterogeneous, and there is great variability in the number and density of these cells from person to person (49, 50), leaving room for speculation about their importance and contribution to normal prostate biology.

1.2.3 Basal Cells

The basal cells of the prostate play a supportive role in prostate function and are the focus of the studies described herein. In the mature prostate, they exist in a dispersed layer between the functional luminal cells and the stroma, and are characterized by their expression of p63, cytokeratin 5, cytokeratin 14, and CD49f (integrin alpha-6) (Figure 1.4). Despite some controversy, basal cells are considered the developmental origin of the prostate epithelium. Fetal urogenital sinus epithelial cells of p63 knockout mice can form prostate grafts that lack basal cells but maintain luminal and neuroendocrine populations (51); however, this does not definitively rule out basal cells as the developmental source of the prostate epithelium, as the inductive stroma used in these experiments can drive bladder and urethral epithelium to generate functional prostate lumens (52). Furthermore, lineage tracing studies indicate that basal, luminal, and rare neuroendocrine cells all originate from $p63^+$ basal cells (53).

A small percentage of basal cells retains these multipotent capabilities in the adult prostate. As early as the 1980s, based on the prostate's ability to regenerate after a period of involution post-castration, a portion of the human prostate epithelium was speculated to possess stem cell functions (54, 55). Over a decade later, stem like cells were found to reside proximal to the urethra (56). These cells were further characterized as basal stem cells, due to their lack of luminal markers and expression of basal cytokeratin 5 and 14 (57, 58). More recent studies also demonstrated high expression of CD49f (integrin alpha-6), CD133, and later by stem cell antigen-1 (sca-1) in the mouse (59, 60). Upon *in vitro* 3D culture, these cells form prostate spheres, also called organoids

or spheroids (61, 62); or they can be implanted with fetal urogenital sinus mesenchyme *in vivo* to regenerate a representative prostate (63, 64). Thus, while still containing substantial transit-amplifying (cells with limited bipotential differentiation capacity) (65), these enrichments are useful for studying the prostate stem cell response to treatment, stimulation, and transformation. They have also been invaluable for investigating prostate development, maintenance, and response to disease.

More recently, rare luminal progenitors have been identified and isolated. This led to the finding that, while basal prostate stem cells can produce daughter cells of all epithelial types, luminal and basal progenitor cells remain fairly lineage restricted during normal homeostasis (41, 62, 66, 67). This has been the topic of debate in the realm of inflammation and tissue destruction, where tissue integrity may be disrupted beyond the capacity of luminal progenitor repair. While the extent of their contribution to luminal regeneration remains unclear, it is apparent that adult basal progenitor cells can trans-differentiate to luminal cells and that inflammation and subsequent loss of luminal cells induces proliferation and trans-differentiation from basal cells (11, 43, 44, 62, 68, 69).

1.3 The Androgen Receptor

1.3.1 Structure and Function of the Androgen Receptor

The androgen receptor (AR) is a zinc finger transcription factor, which mediates the cellular effects of male hormones (androgens). Its gene is located on the X chromosome and spans 2757 nucleotides and 8 exons. The resulting protein is 110 kilodaltons (kDa) and composed of 919 amino acids (AA) (70). It is similar to other steroid hormone receptors. The N-terminal region (AA 1-555) is responsible for transcriptional activity. The DNA binding domain (AA 555-623) contains two zinc-fingers that interact directly with cellular DNA. The hinge region (AA 623-665), connects the C-terminal ligand binding domain (AA 665-919), which is responsible for binding dihydrotestosterone and, to a lesser degree, testosterone (70-73). Nuclear import and export signals are located within the DNA binding and ligand binding regions. These signals are responsible for engaging other proteins that shuttle the AR into or out of the nucleus, depending on the presence of ligand (mainly androgens such as testosterone (T) and dihydrotestosterone (DHT) (74).

The AR is essential for prostate development and function. Under normal conditions, the AR remains in the cytoplasm, bound by heat shock proteins (HSP) that hold it in the proper conformation to accept ligand (75). Once bound to ligand, the AR is imported to the nucleus where it forms a dimer and binds androgen response elements (ARE) of the DNA (74). It then recruits various cofactors and coactivators to initiate transcription of a multitude of targets, including TMPRSS2, NKX3A, and KLK (PSA) genes resulting in the proliferation and maturation of prostate cells (76).

In addition to ligand binding, the AR can be regulated through post-translational modifications (PTM) including phosphorylation, methylation, SUMOylation, acetylation, and ubiquitination (77). AR activation and nuclear translocation can also be induced by inflammatory molecules such as interleukin 6 (78). These noncanonical AR activating mechanisms are associated with aberrant AR signaling and prostate cancer severity (79).

1.3.2 Aberrant Androgen Receptor Signaling

Aberrant AR signaling plays a role in two major diseases of the prostate: benign prostate hyperplasia and prostate cancer (explained in detail below). In fact, AR has been studied in the context of prostate disease since groundbreaking work by Huggins and Hodges in 1941 demonstrated a castration-induced decrease in prostate cancer markers in patients (80). Aberrant AR signaling can occur by numerous mechanisms. At the genomic level, it may undergo amplification leading to over expression of the protein (81), or it may gain activating mutations that promote constitutive signaling or promiscuous ligand binding (82). At the protein level, along with the post-translational modifications described above, it may undergo alternative splicing events during translation. These androgen receptor splice variants (ARSV) often lack the ligand binding domain while retaining functional DNA binding domains and nuclear localization signals. This allows them to function in the absence of androgens and evade clinical inhibitors that target the ligand binding domain (83).

Since prostate cancer is also associated with inflammatory disease of the prostate (8, 9, 27, 84-86), various cytokines have been studied for their impact on AR. To this end, interleukin 6 (IL6) has been found to activate AR and promote transcription of target genes associated with luminal phenotype (78, 87, 88). Other cytokines, such as interleukin 1 (IL-1) have also been studied in this context (89, 90).

1.3.3 Interleukin 1 Alpha and Androgen Receptor Signaling

Cytokines are molecules that broadly function by binding cell membrane receptors and initiating signaling cascades. They can act in an autocrine (same cell), paracrine (nearby cell), or endocrine (distant cell) manner. They play an essential role in immune system function, as they can be produced at the site of infection or injury to recruit the cells necessary to repair damage or eliminate a pathogen (91). Cytokines can be classified into pro-inflammatory and anti-inflammatory categories, with some overlap between the two groups mediated by receptor interactions.

Interleukin cytokines, first identified in leukocytes, are no different. Interleukin 1 alpha (IL-1 α) and beta (IL-1 β) both signal through the same receptor, the interleukin 1 receptor 1 (IL-1R1). This complex recruits the interleukin 1 receptor activating protein IL-1RAcP), which activates Myd88 and phosphorylates IRAK, resulting in activation of nuclear factor κB (NFκB), JNK, and p38 mitogen activated kinase (p38MAPK). The result is a change in expression of hundreds of genes including IL-6, IL-8, MCP-1, COX-2, IκBα, IL-1α, IL-1β, MKP-1 (92).

While IL-1 α and IL-1 β are very similar, they possess several key differences. IL-1 β is produced and secreted by cells under stress as opposed to constitutive expression of IL-1 α, which remains intracellular until released by cell death (93). As the interleukin pathway is highly inflammatory, there are many mechanisms in place to control its signaling. This includes decoy receptor IL1R2, soluble versions of the IL1R1, and the naturally occurring inhibitor, interleukin 1 receptor antagonist (IL-1RA), which has the sole function of blocking IL-1 signaling (92).

The IL1 pathway has been predominantly studied for its role in immune function; however, there is evidence to suggest it could contribute to prostate cancer progression (94). Notably, IL-1 α can enhance AR signaling (89). Conversely, IL-1 α can also induce senescence and decreased AR signaling in basal cells of the prostate (95), indicating a dual role for the signaling pathway in normal and malignant cells.

1.4 The Major Diseases of the Prostate

Benign and malignant prostate diseases have a tremendous impact on male health. Their study spans centuries, with documents from the 1800s speculating their prevalence and causes (96,

97). The three major afflictions include prostatitis, benign prostate hyperplasia, and prostate cancer. Each of these diseases will be discussed in this section.

1.4.1 Prostatitis

Prostatitis encompasses two major types of inflammatory prostate disease, bacterial and abacterial, that may or may not include symptoms of pain and urine retention. A lack of clearly defined criteria led to conflicting information and debate among researchers (98), until a thorough categorization was implemented by the National Institutes of Health (NIH) in 1999 (99). At that point, prostatitis was defined as four categories: category I, acute bacterial prostatitis, category II, chronic bacterial prostatitis, category III, chronic prostatitis/pelvic pain syndrome, and category IV, asymptomatic inflammatory prostatitis (99). Categories III and IV are distinct in their lack of bacterial cause. Despite the category system, the prevalence of each is not entirely clear due to inconsistencies between physician diagnosis and pathology (100, 101); however, the overall impact of prostatitis on men's health is immense. The economic burden of prostatitis alone was estimated to be $84 million in 2000 in the United States, and it is speculated that up to 15% of men will experience symptomatic prostatitis during their lifetimes (102, 103).

The most common form of prostatitis encompasses categories III and IV, chronic abacterial prostatitis. Despite the widespread use of antibiotics to treat symptomatic prostatitis, only 10% of cases are estimated to be bacterial (100). Additionally, in spite of attempts to clarify, these abacterial syndromes remain nebulous in definition and study. In fact, due to the lack of defined symptoms, many men only come to be diagnosed after biopsy for prostate cancer (the third major disease of the prostate, which will be discussed in detail below) (101). There remains some controversy as to the bacterial origin of categories III and IV; however, treatment with antibiotics remains ineffective and sensitive methods of detection, such as polymerase chain reaction (PCR) have failed to detect the presence of pathogenic bacteria (104, 105).

Treatment options for prostatitis are limited. They consist of antibiotics, nonsteroidal anti-inflammatory drugs, and alpha blockers to relieve symptoms (100). These all fail to address chronic abacterial prostatitis, which is poorly understood and thus, difficult to treat.

In addition to its prevalence and impact on male health, chronic prostatitis is associated with more severe pathologies of the prostate. There is an abundance of evidence that chronic prostatitis can contribute to benign hyperplasia and invasive carcinoma, especially in mouse models of

disease (9, 27, 84, 86, 106-108). Indeed, inflammatory cytokines can fuel hyperplastic growth (86, 109-111). Yet, despite the clear correlation between prostatitis and hyperplastic disease, a mechanism by which chronic prostatitis may persist and result in hyper proliferation of prostate cells remains elusive.

1.4.2 Benign Prostate Hyperplasia

The next major disease of the prostate is benign prostate hyperplasia (BPH). BPH may begin as early as age 30, affecting 50% of 60-year-old men, and its incidence continues to increase with age (112, 113). Its source is an enlargement of the transition zone of the prostate, which eventually compresses the urethra (26). Symptoms include frequent need to urinate, urination at night (nocturia), weak or intermittent stream, difficulty starting urination, incomplete voiding, and dribbling with urination. In extreme cases, BPH may even lead to urinary tract infections and renal failure due to retention of urine (114, 115).

Since BPH is a benign disease, therapy is aimed at symptom relief. Treatment of BPH consists of alpha blockers, which relax the smooth muscle cells of the stroma to release the urethral constriction (116), or 5 alpha reductase inhibitors (5ARI), which block conversion of testosterone to the more potent dihydrotestosterone leading to decreased prostate epithelium (117). Unfortunately, pharmaceutical intervention is rarely effective, and patients often require surgical intervention (118, 119). This is partly due to a great deal of heterogeneity in BPH nodules, which may be composed predominantly of epithelium or stroma) and partly due to resistance of epithelial basal cells to androgen deprivation (7, 120).

While the symptoms and histopathology of BPH are well established, the cause of BPH is not clear. There are a few predominant theories that include: 1) an age-related accumulation of dihydrotestosterone as opposed to testosterone, 2) a reactivation of developmental processes, and 3) a shift in the balance of growth factors (121). Reactivation of developmental processes and a plethora of growth factors are associated with inflammation (1, 8, 9). Indeed, the correlation between BPH and prostatitis (inflammation of the prostate, described above) is well established. Up to 80% of BPH patients have concurrent inflammation (84, 122), and the presence of prostatitis contributes to BPH progression (107). Mouse models also point to a relationship between prostatitis and BPH (123); however, there is controversy as to whether one is causal to the other (124-126).

In addition to the uncertainty regarding the role of prostatitis in BPH initiation and progression, immune infiltrating cells are also poorly characterized in BPH patients. Studies by Robert et al. found a high prevalence of macrophages, B cells, and T cells in BPH patient samples (122). More specifically, BPH samples possess prominent chronically activated $CD4^+$ T cell populations, indicating a potential for chronic inflammation (127-129). These authors speculated that chronic inflammation could cause a cycle of tissue destruction and regeneration enriching the environment for growth factors and cytokines that could promote BPH. Further study is required to validate these findings; thus, this is the goal of some of the studies described below, which examine the response of regenerative prostate stem cells to cytotoxic T cell mediated inflammation.

While BPH is characterized by abnormal expansion of epithelial and stromal components of the transition zone of the prostate, it is a benign disease. Cancer of the prostate may begin with preinvasive lesions or intraepithelial neoplasia (PIN); however, as these lesions progress, the tissue architecture becomes disrupted, leading to invasive carcinoma (130). Similar to BPH, there is evidence to suggest that prostatitis contributes to initiation and progression (27).

1.4.3 Prostate Cancer

Prostate cancer is one of the most impactful and prevalent cancers. It is the second leading cause of male cancer deaths worldwide (131). The American Cancer Society Cancer Statistics for 2020 predicts prostate cancer to account for 21% of male cancer diagnoses (not including squamous cell skin cancer) and cause over 33,000 deaths (132). While the five year survival rate for local prostate cancer is >99%, for cases where distant metastases occur, five year survival is closer to 30% (132). With the advent of improved screening by use of the prostate specific antigen (PSA) test in the early 1990's, documented cases surged (133); however, the androgen sensitive and non-essential role of the prostate, which lends itself to surgical removal, allowed for a high survival rate (132). The American Cancer Society recognizes multiple kinds of prostate cancer. The most common is adenocarcinoma, with few cases of small cell carcinoma, transitional cell carcinoma, sarcoma, and neuroendocrine tumors. Mucinous, signet ring cell, ductal, and adenosquamous cancers of the prostate are also possible, but exceedingly rare (134). As localized prostate cancer has a very good outcome and five year survival rate, the following discussion will be focused on metastatic adenocarcinoma, which is the fatal form of prostate cancer.

As the prostate is an androgen-responsive organ, most of modern pharmaceutical intervention for metastatic prostate cancer has focused on control of the androgen receptor (discussed above). The simplest way to target the androgen receptor is to remove circulating androgens through androgen deprivation therapy (ADT) via physical or chemical means (135). Unfortunately, the effects of ADT are temporary and tumor growth resumes in the form of castration resistant prostate cancer (CRPC, also referred to as hormone refractory prostate cancer) within 2-3 years.

The mechanisms by which CRPC may circumvent ADT are many, and most involve reactivation of the androgen receptor (AR) by intratumoral androgen synthesis or other aberrant AR signaling processes described above. Thus, the most recently developed pharmaceutical agents against CRPC target the AR directly (74, 136). Unfortunately, even these leave great room for improvement; direct AR inhibition can only extend life 5 months over placebo (137).

With the advent of cancer immunotherapy, the contribution of immune infiltrates to prostate cancer has drawn massive attention. Indeed, cancer immunotherapy was named breakthrough of the year in 2013 by the journal *Science* (138). The main goal of cancer immunotherapy is to help the patient's own immune system to recognize and eliminate cancer cells to boost efficacy of existing chemotherapy (139). This can be achieved using vaccines against tumor antigens, adoptive transfer of T cells with chimeric antigen receptors (CAR T cells), or checkpoint inhibitors. These major focal areas all aim to take advantage of cytotoxic T cells, which can target and kill other cells (139-141).

To that end, immunotherapy has proven ineffective against prostate cancer (142-145). This is possibly because prostate cancer possesses a "cold" tumor microenvironment. This means that while there may be significant peritumoral inflammation, the tumor mass lacks infiltrating immune cells (144). Thus, the invigorated anticancer T cell response that immunotherapy aims for cannot exert an effect. The treatment options for BPH and CRPC are ineffective It is clear that an increased understanding of prostate disease and its cellular signaling processes, particularly those mediated by inflammation, is necessary in order to improve treatment options and patient outcomes.

1.5 Basic Immunology of the Prostate

To better understand the mechanisms by which chronic prostatitis may contribute to BPH and prostate cancer, an understanding of the normal immune landscape of the prostate is

necessary. The normal human prostate contains low levels of infiltrating myeloid and lymphoid cells (146, 147). More recently, innovative studies by Henry et al. of the Strand laboratory performed unbiased analysis of young patient samples by single cell RNA sequencing, but were unable to obtain sufficient leukocytes (CD45 positive) for analysis (34). While this may have been due to digestion protocols used, the low numbers were not addressed. However, these data are consistent with murine prostates, where studies by Haverkamp et al. found CD45 positive cells in non-inflamed murine prostates to be as low as 0.93% (148).

In addition to being vague in symptoms, studies regarding the immunology of prostatitis are lacking. There is evidence that an autoimmune component is involved; animal models have been utilized to induce sensitization to prostatic proteins leading to prostatitis (149, 150), and human studies indicate a role for both the innate and adaptive immune responses (146). In fact, T cells from prostatitis patients were shown to react to native prostate proteins, including prostate specific antigen (PSA) (151-153). This is indicative of an autoimmune component; however, the extent of their contribution to chronic prostatitis is unclear.

Studies of BPH patient samples are more conclusive. CD45 positive cells may account for up to 45% of prostate cells, based on flow cytometry analysis (90); and studies by Henry et al. indicated that 50% of these were CD11b positive monocytes (of which 36% were also positive for M2 markers typically associated with anti-inflammatory properties), 0.3% were CD4 positive T cells and 3% were CD8 positive (64). Unpublished data from the Ratliff and Hayward laboratories also revealed that the $CD4^+$ and $CD8^+$ T cell populations were enriched for genes associated with exhaustion and anergy that would indicate chronic inflammation and an immune suppressive environment.

Prostate cancer is also thought to possess immune suppressive characteristics. The current paradigm for prostate cancer is that it is characterized by a "cold" microenvironment. While the periphery may contain prominent inflammatory cells, the bulk of the tumor tends to exclude leukocytes (144, 154). This has become an important topic of study due to the advent of cancer immunotherapies. Indeed, even the surrounding lymphocytes were found to have decreased function (154, 155).

All three of these diseases exhibit characteristics of aberrant T cell function, whether autoimmune activation (chronic prostatitis), blockade (prostate cancer), or suppression (BPH), for which the causes are unclear or debated. They illustrate the tug-of-war between an

autoimmune response to endogenous prostate proteins and failing tolerance mechanisms that may contribute to an overly suppressive environment conducive to tumor formation. By studying the response of the epithelial stem cells to the infiltrating cytotoxic T cells, we may begin to identify targets to improve patient outcomes and non-surgical options for disease treatments.

1.6 Introduction to Research Questions and Methodology

The discovery that adult prostate stem cells (PSC) could be enriched by fluorescence activated cell sorting (FACS) as lineage$^-$ (CD45$^-$/CD31$^-$) sca-1$^+$ CD49f$^+$ (LSC) ushered in a new era for studying the normal and pathological development of the prostate (62, 64, 66). Their ability to recapitulate the source prostate made them invaluable for assessment of the overall impacts and contribution of inflammation on BPH and PCa. After the Ratliff laboratory characterized inflammation associated with epithelial and stromal hyperplasia in the Prostate Ovalbumin Expressing Transgenic 3 POET3 mouse, the next logical step was to assess the overall changes to their PSC. Thus, studies were initiated by the Ratliff lab to define PSC expansion in response to abacterial autoimmune inflammation. To this end, Wang et al. found that PSC from inflamed mice were not only more proliferative, but they skewed more toward a transit amplifying (CK5$^+$/CK8$^+$) phenotype and their resulting organoids were larger and more differentiated (11). Since these are features of AR signaling, it was hypothesized that inflammation increased AR signaling in the PSC to promote proliferation and differentiation.

Initial experiments in inflamed prostate tissues revealed increased AR protein in freshly isolated LSC and cultured 3D organoids and a surprising dependence on AR for organoid formation. This observation was contrary to previous studies in non-inflamed prostate LSC that showed only degraded AR, suggesting that the PSC were AR-independent (61). Thus arose the questions of 1) whether that increase in AR was the cause of proliferation and differentiation in the inflamed PSC, 2) by what mechanism inflammation increased AR, and 3) how inflammation-mediated PSC proliferation and differentiation would impact human prostate disease. By continuing to utilize FACS, flow cytometry, 3D organoid culture, and other basic molecular biology techniques as well as more specialized methods such as RNA (ribonucleic acid) sequencing, orchiectomy and renal graft implantation, these questions were explored.

At the initiation of these studies, prostate basal cells were assumed to function independently of AR signaling due to their AR low-to-negative state and survival during

castration-mediated involution of the prostate. Thus, the results of experiments to inhibit AR signaling by enzalutamide, which indicated an essential role for AR by severely impacting organoid formation, were surprising. Unfortunately, this also impacted the ability to measure the impact of reduced AR signaling. These findings were later corroborated by Xie, et al. in 2017 (156).

Multiple avenues for inflammation-mediated increases in AR signaling were also pursued to various levels of success. With the advent of single cell mRNA sequencing, the authors saw the opportunity not only to identify broader inflammation-mediated changes to PSC biology, but also to identify the true stem cells from the mixed population of LSC (discussed in chapter 4). Once a putative mediator of AR signaling (the IL-1 α pathway) was identified, experiments to manipulate this effect using transgenic mice, chemical inhibitors, and neutralizing antibodies in 3D organoid cultures were initiated.

A major benefit of single cell RNA sequencing is that it is not restricted by the lens of the researcher's questions. Due to the unlimited nature of the assay, it was revealed that multiple genes associated with immune regulation were modulated in the LSC by inflammation. To this end, suppression assays and other tests of activation were adapted to examine the impact of LSC on T cell function.

1.7 Purpose of Studies

The overall purpose of these studies is to define the mechanism(s) by which inflammation modulates AR and contributes to prostate stem cell survival. Through understanding these mechanism(s), the foundation will be set for improving prognosis and treatment options for men with prostate disease. While this end result will require decades of continued investigation, by gaining insight to the alterations that inflammation induces in adult prostate stem cells, we hope to identify key changes that can be targeted in the clinic. These targetable areas include an inflammation-mediated increase in AR signaling as well as immune regulatory capabilities that may contribute to persistent inflammation and epithelial hyperplasia.

While much is known about AR signaling in prostate cancer and luminal cells, there is very little information on its signaling and role in normal basal stem cell biology. It was only recently that they were found to be dependent on AR for proliferation and differentiation (156). Since basal cells are enriched in BPH and a potential source of prostate cancer, understanding their complex

signaling processes, especially AR signaling, remains essential for improvement of treatment options (7, 41).

Because of their roles in BPH and prostate cancer, the discovery of a novel immune-regulatory component to basal stem cell biology provides an exciting new avenue for the development of treatment options. The studies described herein set the foundation for recognition and further analysis of these cells as key players in shaping the immune landscape of the prostate.

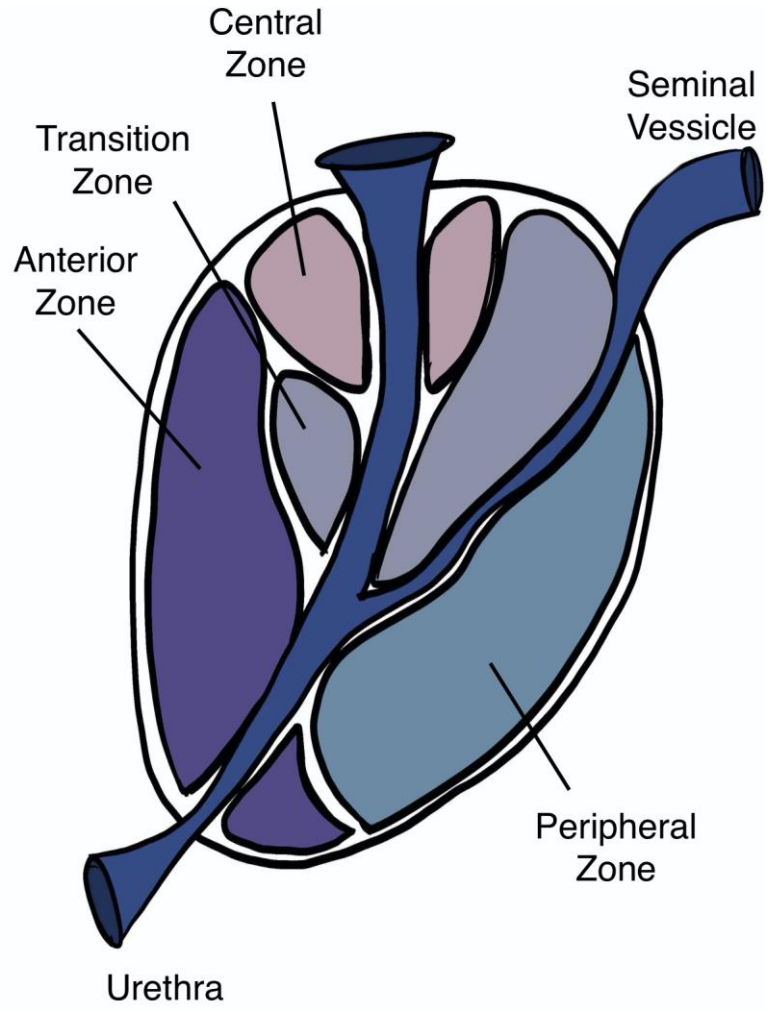

Figure 1.1. The Human Prostate. The human prostate, consisting of the central zone, transition zone, peripheral zone, and anterior zone. It is located at the base of the bladder and surrounds the urethra. Adapted from Toivanen, R. and Shen M. M. (157).

Figure 1.2. Cellular Structure of Prostatic Ducts. The human and murine prostate is composed of acini and ducts. These are lined by epithelial cells. Functional, secretory luminal cells are surrounded by interspersed basal cells and rare neuroendocrine cells. A small percentage of basal cells maintain stem like abilities and can produce basal, luminal, and neuroendocrine cells, through an intermediate transit amplifying cell. The epithelium is supported by a fibromuscular stromal cell layer that consists predominantly of smooth muscle and fibroblast cells.

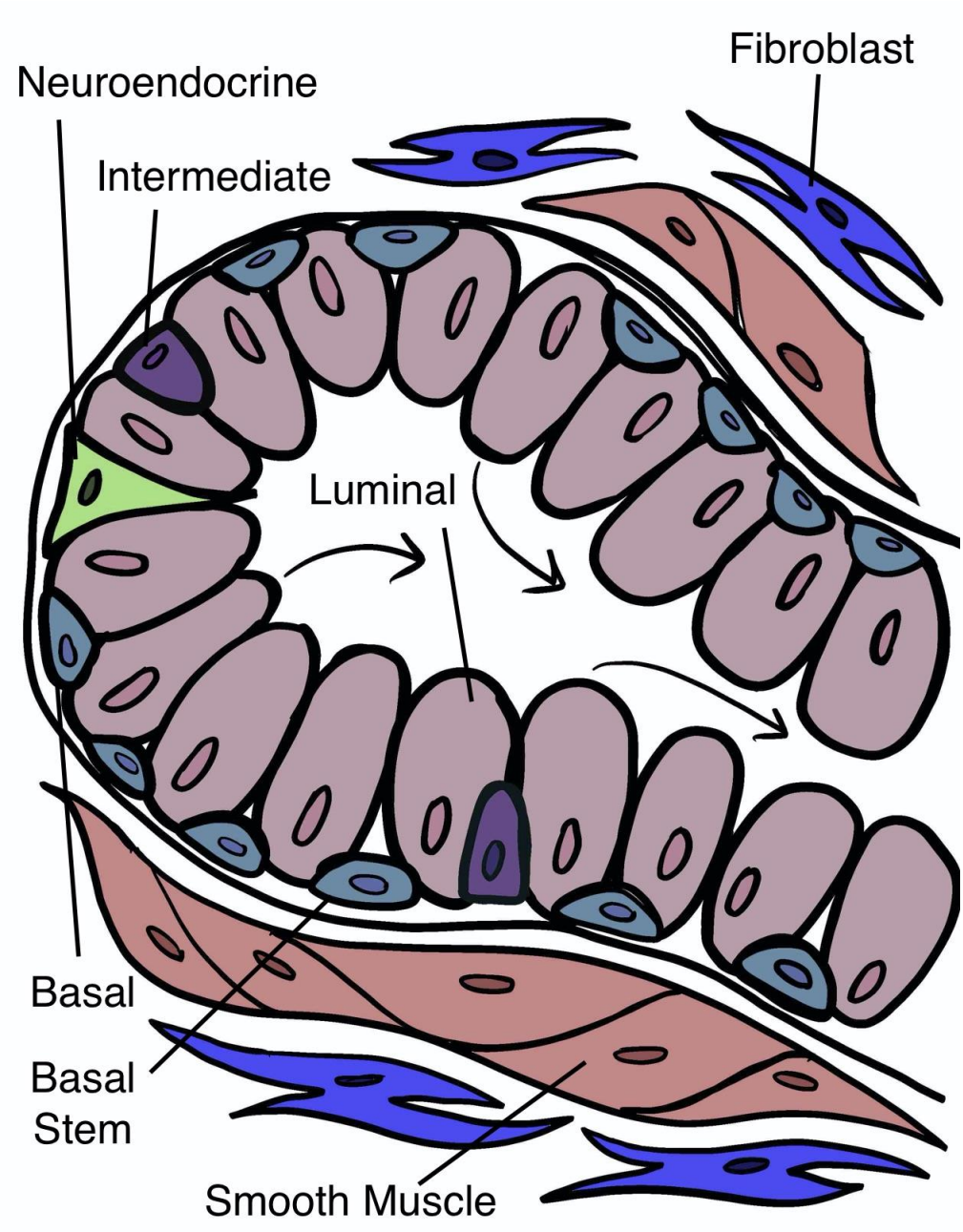
Fibroblast
Neuroendocrine
Intermediate
Luminal
Basal
Basal
Stem
Smooth Muscle

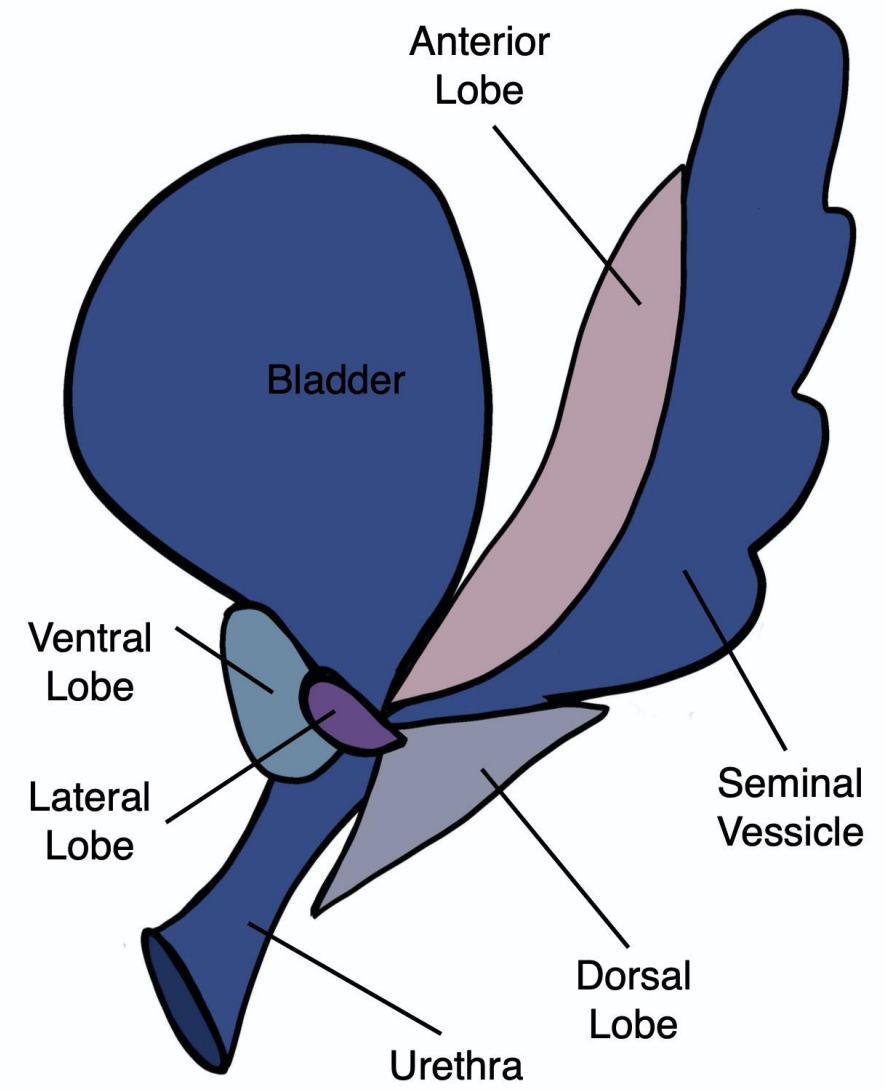

Figure 1.3. The Murine Prostate. The murine prostate, consisting of 4 pairs of distinct lobes. These surround the urethra, at the base of the bladder and extend toward the seminal vesicles. Adapted from Toivanen, R. and Shen M. M. (157).

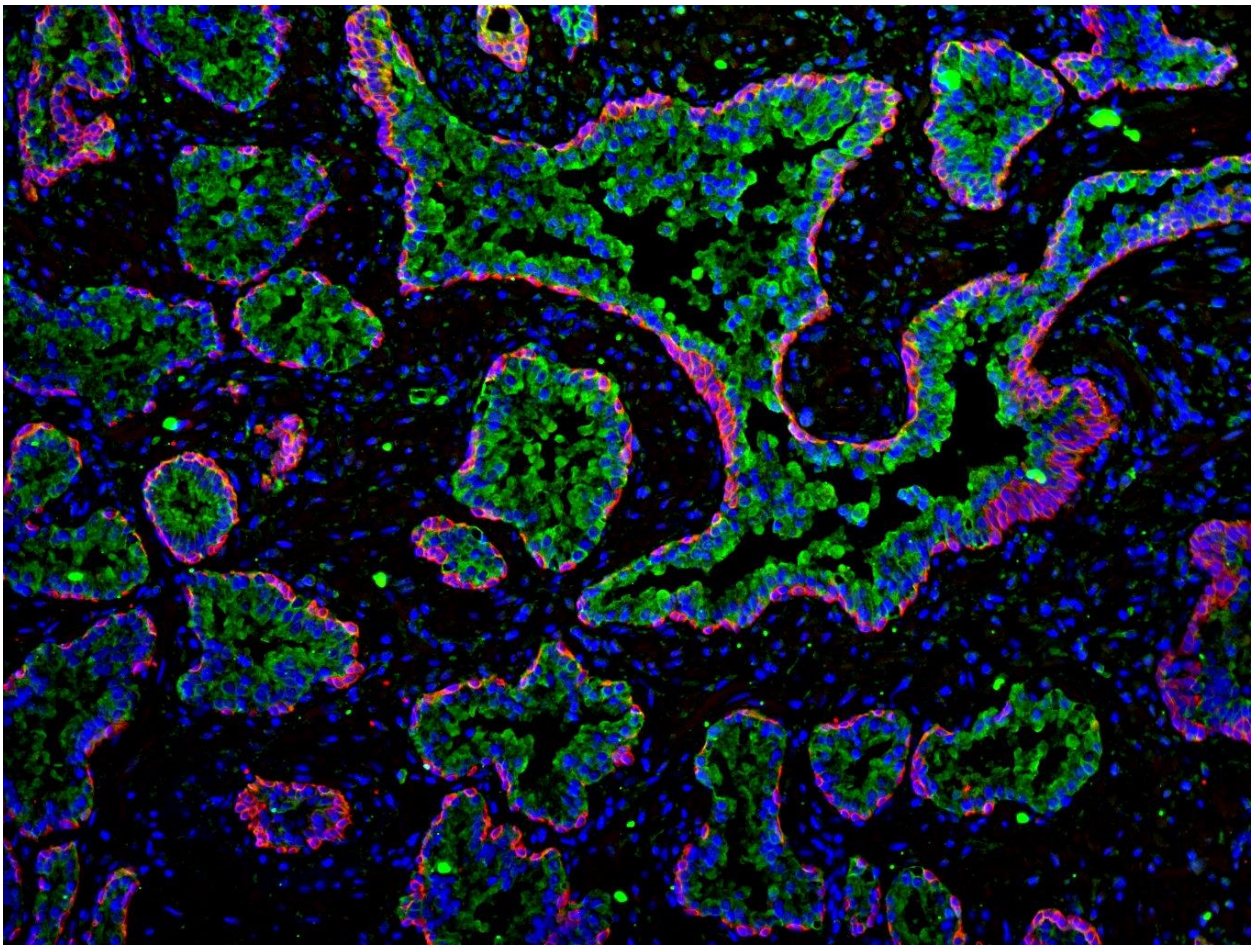

Figure 1.4. Cytokeratin Staining in the Prostate. A representative immunofluorescent image of a human prostate. Luminal cells are positive for cytokeratin 8 (green), while basal cells are positive for cytokeratin 5 (red). Intermediate cells are positive for both cytokeratin 5 and 8 (yellow).

CHAPTER 2. INFLAMMATION-INDUCED ANDROGEN RECEPTOR SIGNALING VIA THE INTERLEUKIN 1 ALPHA PATHWAY IN BASAL PROSTATE STEM CELLS

2.1 Abstract

Adult prostate stem cells (PSC) are a rare epithelial progenitor population in the prostate. PSC are rare and often difficult to isolate; thus, they tend to be overlooked during bulk analysis of tissues. Despite their lack of abundance, these cells possess tremendous proliferative capacity and have been implicated in benign and malignant hyperplasia (5, 7, 41, 158, 159). While it is recognized that stem cells can respond to tissue damage and inflammatory cytokines, the impact of inflammation on PSC is not well understood (1, 8, 9). Previous studies using the Prostate Ovalbumin Expressing Transgenic 3 (POET3) demonstrated that inflammation increased proliferation and differentiation of PSC (11). Since androgen receptor (AR) signaling is the major driver of differentiation in the prostate, it was hypothesized that inflammation affects AR signaling in the basal PSC. To address this, PSC enrichments were isolated from inflamed and naïve (not inflamed) POET3 mice and assessed by molecular, *in vitro*, and *in vivo* methods to demonstrate 1) an essential role for AR in both murine and human PSC, 2) inflammation-induced AR and its target genes in these cells, 3) persistence of inflammation-induced changes to PSC through androgen deprivation, and 4) that increased AR signaling is mediated by inhibition of interleukin-1 alpha (IL-1α) by interleukin-1 receptor antagonist.

These findings have implications for the development and persistence of treatment-resistant prostate hyperplasia. They set the foundation for further study and potential targeting of PSC pathways in the clinic.

2.2 Introduction

Adult stem cells are implicated in many hyperplastic diseases and often respond to inflammation in a proliferative manner (5, 6). While prostate stem cells (PSC) have also been implicated in prostate disease, their response to inflammation is poorly understood (5, 158, 159). Studies from the Ratliff lab previously demonstrated that the Prostate Ovalbumin Expressing Transgenic 3 (POET3) mouse model of autoimmune prostate inflammation develops epithelial and

stromal hyperplasia closely modeling autoimmune prostatitis, and PSC from inflamed POET3 produce larger, more differentiated organoids in 3D androgen-free culture (11). These data, along with the finding that basal cell enrichment occurs in human benign prostate hyperplasia (BPH) (7), led to the hypothesis that PSC may contribute to BPH and other inflammation-induced androgen-independent conditions of the prostate.

The androgen receptor (AR) plays a critical role in normal prostate biology; however, AR is also prone to aberrant signaling, which has been studied extensively due to its role in hormone refractory prostate cancer where AR can be activated promiscuously by other ligands or may form constitutively active splice variants that lack the ligand binding domain entirely (160-164). It may also be activated by phosphorylation by kinases such as CDK1 and p38 MAPK (79, 161) or by upstream signaling from inflammatory cytokines including interleukin 1 and 6 (35, 89, 165). Basal prostate stem cells are generally considered AR negative or low, due to their very low expression levels that often go undetected (62). Despite the apparent lack of AR in basal PSC, studies by Xie et al. showed that these cells require AR for proliferation and differentiation *in vivo* (156). These data, coupled with Wang et al.'s findings that PSC from inflamed mice produce more differentiated organoids in androgen-free conditions (11), indicate a potential role for increased AR signaling in the PSC's response to inflammatory conditions.

The studies described herein assess the impact on and persistence of inflammation-induced increased AR signaling in the PSC, concluding with an investigation into interleukin 1α signaling as a mediator of the effects.

2.3 Methods

2.3.1 RNA and Protein Isolation by Trizol Reagent

Tissue samples and cells were lysed using Trizol (Thermo Fisher Scientific) reagent according to manufacturer protocol. Briefly, samples were suspended 1:10 in Trizol reagent and homogenized by passage through 22G needle. BCP (1-bromo-2 chloropropane) was added to separate RNA from the organic phase containing DNA and protein. RNA was precipitated by addition of glycogen and isopropanol (IPA), then washed with 75% ethanol (EtOH) and re-suspended in RNAse free water before measure by NanoDrop (ThermoFisher). RNA was then processed for cDNA synthesis, described below. The remaining organic phase was further

fractioned by addition of 100% EtOH, and protein precipitated by addition of IPA. Protein pellet was washed in 3M guanidine hydrochloride (GuHCL) in 95% EtOH before final cleanup in 100% EtOH. Resulting pellet was resuspended in 1% sodium dodecyl sulfate (SDS), measured by NanoDrop, and stabilized with protease inhibitor cocktail.

2.3.2 cDNA synthesis

Fifty –100 ng of RNA was added to 250μM dNTPs (Amresco), 0.5 μM random hexamers (Promega), 0.5 μM oligo(dT) 15 primers (Promega), 1 μl of RNase inhibitor (NEB), and 200 units of M-MuLV reverse transcriptase were combined in 10X reaction buffer (NEB) for a 20 μl reaction. The reaction occurred at 25°C for 5 minutes, 42°C for 30 minutes, 85°C for 5 minutes, and 4°C hold using a Bioer GenePro thermalcycler. The resulting cDNA was diluted in 80 or180 μl Buffer EB (Qiagen).

2.3.3 Real-Time Quantitative Polymerase Chain Reaction

Analysis of relative gene expression was performed using real-time quantitative polymerase chain reaction (RT-qPCR). cDNA was added to a 20 μl reaction of PerfeCTa FastMix II (Quanta Biosciences) and 6-FAM/ZEN/IBFQ labeled qPCR probes (Integrated DNA Technologies). These were used in combination with VIC labeled probes for the internal housekeeping gene, 18s (Thermo Fisher Scientific). Relative gene expression was calculated using the formula 2-[Ct(gene)-Ct(18s)] where Ct refers to the threshold cycle number given by the Roche Lightcycler 96 instrument.

2.3.4 Western blot

Protein samples isolated from Trizol reagent (described above) were heated to boiling for 5 minutes with added Dithiothreitol (DTT) and 6X SDS sample loading buffer. Samples were loaded into hand-cast or Novex SDS PAGE 4-12% gradient gels in 1X MOPS SDS running buffer. Electrophoresis was run at continuous voltage for 1 hour or until appropriate resolution was obtained. Protein was transferred on ice in 1X Tris-Glycine 20% methanol (MeOH) transfer buffer to Millipore Immobilon PVDF-FL 0.22 μm pore membrane for 1-3 hours depending on the size of protein. The membrane was blocked for 1-4 hours in 50% Odyssey blocking buffer (LiCOR) in

1X PBS before probing with one or more primary antibodies listed below. Secondary antibody staining was performed according to manufacturer protocol using 680LT or 800CW before imaging and quantification on LiCOR Odyssey imaging system. Where applicable, protein pixel intensity was normalized to beta actin loading control.

2.3.5 Histology

Sample embedding, slide preparation, and staining were performed by Victor Bernal-Crespo at the Purdue University Histology Research Laboratory, a core facility of the NIH-funded Indiana Clinical and Translational Science Institute.

2.3.6 3D organoids

Methods were adapted from Lukacs et al (66) and described in detail in the common methods section. Briefly, after cell isolation and counting, lineage negative (CD45/CD31), stem cell antigen 1 positive, CD49f positive (LSC) was resuspended in 1 part prostate epithelial growth medium (PrEGM, Lonza) to 2 parts Matrigel or growth factor reduced Matrigel (Corning). The mixture was deposited in a ring around the edge of a refrigerated 12-well plate and allowed to solidify for 15 minutes at 37ºC before addition of pre warmed PrEGM with or without treatments to the well. Growth medium was changed every 2-3 days before counting and harvesting on day 7, 8, or 10. The following treatments were used with vehicle controls:

Enzalutamide (Selleckchem S1250)
Dihydrotestosterone (DHT)
R1881 (Sigma Aldrich R0908)
Abiraterone (Selleckchem S1123)
IL1RA, murine recombinant (Sigma SRP6006)
IL1RA, human recombinant (Sigma Aldrich SRP3084)
IL1α, murine recombinant (Sigma Aldrich I5396)
IL1α, human recombinant (Sigma Aldrich I2778)
IL-1α neutralizing antibody (abcam ab7632)
EPI-001 (Selleckchem S7955)
Dinaciclib (Selleckchem S2768)
SB203580 (Selleckchem S1076)

2.3.7 BrdU labeling

Thermo Fisher Scientific BrdU labeling kit (8812-6600-42) was used. Mice were injected intraperitoneally 24 hours before harvest. Permeabilization, DNAse, and antibody labeling steps were performed per manufacturer protocol.

2.3.8 Mice

Due to the exclusively male nature of the prostate, male mice aged 8-12 weeks were utilized for all studies. Mice were maintained in breeding colonies managed by Purdue University under 12-hour light/dark cycles with food and water provided ad libitum. All procedures were performed in accordance to protocols approved by Purdue University Animal Care and Use Committee (PACUC). Mice were euthanized prior to harvest by CO_2 asphyxiation using Euthanex regulators approved and maintained by PACUC, followed by secondary cervical dislocation.

POET3:

The Prostate Ovalbumin Expressing Transgenic 3 is an inducible mouse model of abacterial T cell induced inflammation developed by the Ratliff lab. These mice produce probasin-driven ovalbumin, which is restricted to prostate tissues. Upon introduction of OTI cells (described below), they develop T cell-mediated prostatitis that results in epithelial and stromal hyperplasia, functioning as a model for human category III/IV prostatitis (10, 166). Mice were maintained in homozygous colonies. At age 8-12 weeks, inflammation was induced by adoptive transfer of pre-activated OT-I cells via retroorbital injection. Inflammation was allowed to develop for 6 days before euthanasia and prostate harvest. For inflammation/castration studies, mice were inflamed by adoptive transfer two days before surgical orchiectomy. Mice were euthanized and prostates harvested on day 7.

2.3.9 Renal grafts

Rat urogenital sinus mesenchyme cells were a generousgift from Dr. Simon Hayward's lab. Murine urogenital sinus mesenchyme cells were isolated as described by Lukacs et al. (66). These were combined with an equal number of LSC from POET3 mice and/or human PSC in pellet made of type I collagen (rat tail).

Mice were anesthetized using Isoflurane gas and sedation ensured by toe pinch. After shaving and thorough cleaning of the surgical area, a small incision was made below the ribs. The kidney was pushed out through the opening and, using a microdissection scope, the renal capsule was gently lifted using forceps. A small opening was formed using a blunted glass Pasteur pipette for insertion of grafts. After assurance that grafts were well placed with minimal bleeding, the kidney was reinserted. Incisions were sutured before clipping shut the skin with surgical staples. Flunixin and Bupivacaine were administered as analgesics. Mice were monitored until fully alert, and then checked daily to ensure full recovery. Grafts were allowed to grow for 6-8 weeks before induction of inflammation or harvest.

2.3.10 Orchiectomy

Mice were anesthetized using Isoflurane gas and sedation ensured by toe pinch. After thorough cleaning of the surgical area, a small incision was made at the base of the scrotum. Another, smaller incision was made in the inner membrane surrounding the testicle, which is pushed out by gentle pressure on the abdomen. Once extracted, the connective tissue and blood vessels were cauterized with heated forceps before cutting. This was repeated for the second testicle. The incisions were sutured shut. Flunixin and Bupivacaine were administered as analgesics. Mice were monitored until fully alert, and then checked daily to ensure full recovery.

2.3.11 Human prostate samples

Human specimens were obtained from Indiana University Tissue Procurement Core and Indiana University Methodist Hospital. PSC isolation methods were adapted from Strand et al. (64). Briefly, tissue was minced to a paste like consistency before overnight digestion in 25U type II collagenase (Gibco 17101-015) and 0.2 mg/mL Dispase (Gibco 17105-041) in complete RPMI on a shaker at 37ºC and 200 RPM. The next morning, samples were centrifuged to remove digestion medium and further digested in pre warmed TrypLE express (Gibco 12605-010). After neutralization with RPMI, samples were passed through 18G and 22G syringes before filtration through 70 μm nylon cell filters. After Ammonium-Chloride-Potassium (ACK) lysis to remove red blood cells, samples were stained using:

Zombie UV fixable viability dye (Biolegend 423108)
FITC- CD45 (Clone H130, Biolegend 304006)
APC- CD26 (Clone BA5b, Biolegend 302710)
PE- EpCAM (Clone 9C4, Biolegend 324260)
BV421- CD49f (Clone eBioGoH3, Biolegend 313624)

Once stained, fluorescence activated cell sorting was performed by Purdue Flow Cytometry and Cell Sorting Core.

2.3.12 Murine AR target gene array

Global AR target gene array analysis was done by Qiagen RT2 ProfilerTM PCR Array-mouse AR signaling targets (#PAMM-142ZF) and Qiagen online data analyzer (https://www.qiagen.com/us/products/genes%20and%20pathways/data-analysis-center-overview-page/?UID=1746638c-e792-4988-9bfc-e4ef8f6887a7). Differentially expressed genes in both naïve and inflamed groups (threshold cycle <35) were further subjected to statistical analysis, where the significance was determined by α=0.05.

2.3.13 ATAC sequencing

Methods were adapted from Buenrostro et al. (167). Briefly, nuclei were prepared by cell lysis using ice cold lysis buffer (10 mM Tris-Cl, pH 7.4, 10 mM NaCl, 3 mM MgCl2 and 0.1% IGEPAL CA-630) before immediate transposition of DNA in 25 µl 2x TD buffer, 2.5 µl Transposase (Illumina) and 22.5 µl of nuclease free water for 30 minutes at 37ºC. Samples were then purified using Mini Elute Kit (Qiagen). PCR amplification and library prep was performed using 10 µl transposed DNA, 9.7 µl nuclease free H2O, 0.3 µl 100x SYBR Green I** (Invitrogen S-7563), 25 µL NEBNext High-Fidelity 2x PCR Master Mix (New England Labs M0541), and 2.5 µl each of individual 25µM dual unique Nextera PCR primers in a 50 µl reaction. Bioer GenePro thermalcycler was used for all PCR steps. First amplification was:

(1) 72℃, 5 min
(2) 98℃, 30 sec
(3) 98℃, 10 sec
(4) 63℃, 30 sec
(5) 72℃, 1 min
(6) Repeat steps 3-5, 4x
(7) Hold at 4℃

Once the initial amplification was complete, a side reaction was performed to identify the optimal number of cycles to reduce GQ and size bias as follows:

5 µl of the initial 5 cycle PCR amplified DNA was added to 4.44 µl nuclease free H2O, 0.06 µl 100x SYBR Green I, 5 µl NEBNext High-Fidelity 2x PCR Master Mix, and 0.25 µl each of the same individual 25µM dual unique Nextera PCR primers as before, with RT-qPCR as follows:

(1) 98℃, 30 sec
(2) 98℃, 10 sec
(3) 63℃, 30 sec
(4) 72℃, 1 min
(5) Repeat steps 2-4, 19x
(6) Hold at 4℃

Once the RT-qPCR was complete, linear Rn vs cycle number was plotted using Roche Lightcycler 96 instrument and software, with threshold set at 5000 RF. The cycle number that corresponded to ¼ of the maximum fluorescence intensity was determined and used for amplification of the remaining sample (45 µl) as follows:

Completed amplification
(1) 98℃, 30 sec
(2) 98℃, 10 sec
(3) 63℃, 30 sec
(4) 72℃, 1 min
(5) Repeat steps 2-4, for a number of times determined by the side reaction
(6) Hold at 4℃
Purify
Quality control and sequencing (150 million reads) were performed by Purdue Genomics Core Facility. Analysis was performed by Bingyu Yan in Dr. Majid Kazemian's laboratory at Purdue University.

2.3.14 Single Cell RNA Sequencing

Freshly isolated LSC were collected by Purdue Cell Cytometry Facility. After re-sorting for maximum viability, they were loaded to a Fluidigm C1 96 well chip with SMARTer chemistry (Clontech, Mountain View, CA) to generate cDNA from captured single cells. Wells were checked for doublets and viability before lysis and cDNA synthesis were completed by the C1. cDNA concentration was checked by Qubit fluorimetric quantitation. The Purdue Genomics Facility checked quality using an Agilent Bioanalyzer with the High Sensitivity DNA Chip before library

preparation using a Nextera kit (Illumina, San Diego, CA). Single-end 1x50 bp reads were sequenced using the HiSeq2500 on rapid run mode.

Files were downloaded and stored in the Purdue University Data Depot. Reads were quality trimmed and adapter sequences were removed using Trimmomatic v. 0.32 (168). Trimmomatic removed adapter sequences and trimmed short Illumina reads based on quality. Adapters were from the SMARTer kit (Clontech, Mountain View, CA) as well as the Nextera kit (Illumina, San Diego, CA). FastQC v. 0.11.2 (169) was run in order to observe data quality both before and after quality trimming/adapter removal. FastX-Toolkit v. 0.0.13.2 (170) quality trimmer was used to further trim reads based on quality score, and FASTX-Toolkit quality chart was used to make read per-base quality plots. The minimum quality score for trimming reads was 30, based on FastX trimscore, and reads shorter than 30 bases were discarded. Maximum length was set to 151 bases. All plots were checked to ensure the reads that would be used in the remainder of the analysis were of high quality and that there were no obvious problems.

Before any statistical analysis could be performed, reads resulting from sequencing were aligned to a reference in order to quantify relative amounts of genes/transcripts. Tophat2 was used to align reads to the reference genome (171, 172). Tophat2 was run with defaults except that the number of mismatches allowed was 1. The htseq-count script in HTSeq v.0.6.1 was run to count the number of reads mapping to each gene (173). HTSeq used Biopython v.2.7.3 in the analysis. HTSeq was run using the Ensembl GTF file with rRNA genes removed on "intersection-nonempty" mode. The HTSeq feature was set to "exon" to specify which feature from the GTF file was to be used. The HTSeq attribute parameter was set to "gene_id", which specified that the Ensembl gene IDs were to be used as row names in the count files. The Purdue Bioinformatics Core's RNA-Seq pipeline was used in trimming reads, running fastQC, running Tophat, and running HTSeq. Once the pipeline was completely done running, all error and output files were checked to ensure that everything ran as expected. The Samtools flagstat command was run to generate read alignment statistics for each BAM file resulting from the alignment of reads to the reference genome (174).

A popular method for performing differential expression analyses on bulk RNA-seq data is edgeR (175), which uses TMM (Trimmed Mean of M-values) normalization (176) to scale counts into pseudocounts, on which the hypothesis tests are performed. TMM normalization allows for scaling factors to be calculated from the raw data and used in the ensuing statistical

analysis, thus normalizing for differences in library size and also RNA composition. A trimmed mean is the average after removing the upper and lower x% of the data. The pseudocounts were used to represent the counts that would have been observed assuming the fitted model, if sequencing depths for each library had been equal. The edgeR package also used generalized linear models to account for multifactor experimental designs (177). In edgeR, a matrix of raw counts was the input. Then normalization factors were computed and entered into the statistical model. In the current analysis, gene-specific correction factors were entered into the functions as offsets to allow each gene to have a different dispersion.

Before hypothesis test were carried out, when fitting the negative binomial model, edgeR estimated the biological coefficient of variation (BCV), which is the coefficient of variation with which the unknown true abundance of the gene varies between replicated RNA samples. In RNA-seq experiments, the total coefficient of variation is composed of both a technical coefficient of variation and the biological coefficient of variation. The BCV is likely to be the dominant source of uncertainty for high count genes and represents the coefficient of variation that would remain if infinite sequencing depth were possible for biological replicates.

Under the negative binomial model, the reads are distributed as:

$$Y_{gi} \sim NB(M_i p_{gj}, \varphi_g)$$

Where Y_{gijk} is the read count for gene g, from sample i, M_i is the total number of reads for sample i, p_{gis} the proportion of reads mapping to gene g in group j to which sample i belongs, and φ_g is the gene-specific dispersion. The Benjamini-Hochberg false discovery rate correction was used to correct p-values for multiple testing.

Genewise dispersion estimates were used in the analysis, which allowed each gene to have a different dispersion parameter, providing greater flexibility and power in the model. A false discovery rate (FDR) of 5% was used as a cutoff for differential expression and a fold-change cutoff of 2 was employed to ensure that results were biologically replicated and meaningful.

Differentially expressed genes (DEG) identified using edgeR (or genes exhibiting large fold-changes if no differentially expressed genes were identified) were uploaded, along with associated false discovery rate, and log fold-changes, into Ingenuity IPA software and a network analysis was performed (IPA, QIAGEN Redwood City, www.qiagen.com/ingenuity). An upstream regulator analysis, mechanistic networks analysis, causal network analysis, and downstream effects analysis were performed using IPA. Top overrepresented canonical pathways

were also identified within IPA. Default settings were used, and results were filtered based on p-value (results were deemed significant if the p-value<0.01). The upstream regulator analysis identified potential upstream regulators connected to the DEG either directly or indirectly. The mechanistic networks analysis buildt networks based on the putative upstream regulators by connecting regulators likely to be involved in the same signaling pathways or involved in the same processes. The causal effects analysis connects upstream regulators to the DEG both directly and indirectly by adding intermediate regulators which may be involved in the networks. Finally, the downstream effects analysis identifies biological functions and diseases downstream of the DEG and, where possible, predicts whether these functions are likely to be up-regulated or down-regulated as the result of cell type or treatment (178).

2.3.15 Human Organoid RNA seq

Libraries were prepared by the Ratliff Lab. 2x100 bp reads were sequenced using the NovaSeq 6000 in the Purdue Genomics Facility.

Data were processed in a similar manner to those from the Fluidigm C1 (described above), with the exception of a FastX trimscore of 30 (the minimum quality score for trimming reads was 30) and a trim length of 50 (reads shorter than 50 bases were discarded).

Before any statistical analysis can be performed, reads resulting from sequencing must be aligned to a reference in order to quantify relative amounts of genes/transcripts. STAR v2.5.4b (179) was used to align reads to the GRCh38.p12 Ensembl human genome. STAR was run with defaults except that the number of mismatches allowed was 1 and due to the strand-specificity of the library, the library-type was set to “fr-firststrand”.

The htseq-count script in HTSeq v0.7.0 (173) was run to count the number of reads mapping to each gene. HTSeq used Biopython v2.7.3 in the analysis. HTSeq was run on “intersection-nonempty” mode rather than “union” mode. While union mode is the default, it throws away all reads mapping to overlapping genes, even when there is evidence that suggests that the read originated from one gene over another. The HTSeq feature was set to “exon” to specify which feature from the GTF file was to be used. The HTSeq attribute parameter was set to “gene_id”, to indicate that the Ensembl gene IDs were to be used as row names in the count files. The --stranded=reverse option was set for the differential expression analysis. The Purdue Bioinformatics Core’s RNA-Seq pipeline was used in trimming reads, running fastQC, running

STAR, and running HTSeq. Once the pipeline completed, all error and output files were checked to ensure that everything ran as expected.

The Bioconductor package DESeq2 v1.28.0 (180) was used for differential expression analysis. DESeq2 incorporates estimates of dispersion and logarithmic fold changes in negative binomial generalized linear models to test for differential expression of genes. DESeq2 takes raw count data as input, in the form of a matrix with count integers. Columns are samples (libraries) and rows are gene names. These counts are then normalized and corrected to account for library size (differences in sequencing depth).

The differential expression analysis in DESeq2 uses a generalized linear model:

$$K_{ij} \sim \mathrm{NB}(\mu_{ij}, \alpha_i)$$

$$\mu_{ij} = s_j q_{ij}$$

$$\log_2(q_{ij}) = x_j . \beta_i$$

where K_{ij} is the counts for gene i in sample j and the counts are modeled using a negative binomial distribution with fitted mean μ_{ij} and the dispersion parameter α_i, which is specific to every gene. Dispersions are estimated using the expected mean values from the maximum likelihood estimate of $\log_2$ fold changes. The fitted mean is the product of a size factor s_j and the parameter q_{ij}, which is proportional to the expected true concentration of sequence fragments for sample j. For each column of the model matrix X, the β_i coefficients give the $\log_2$ fold changes for gene i. The steps in the DESeq2 differential expression analysis first normalize the data based on the estimated size factors and the estimated dispersions, and finally to fit a negative binomial generalized linear model and to calculate Wald statistics were used to calculate p-values. The Benjamini-Hochberg false discovery rate correction was used to correct p-values for multiple testing.

Generally, many genes in RNA-seq data will have very low counts. These low counts tend to be highly variable, are less robust, and tend to have little or no chance of showing significant differential expression due to their high dispersion. Additionally, these genes lower the ability to detect differentially expressed genes (DEG) by decreasing the power. Thus, generally in RNA-seq projects, filtering of lowly expressed genes is performed in order to increase the power and thus reduces the severity of the multiple testing adjustment made. Initially, rows with only zero counts were filtered to decrease the memory size of the DESeq data object, thus increasing the speed of DESeq2 functions. Later, independent filtering was performed by using the mean of the normalized counts as a filter statistic. A threshold was found which optimized the adjusted p-values

lower than a significance level α. Using the mean of normalized counts is independent in that it does not use any of the variables specified in the design formula. Genes with low normalized counts were filtered out, thus the majority of the low adjusted p-values were kept.

A diagnostic called Cook's distance was used to test for outliers. Cook's distance is a measure of how much a single sample is influencing the fitted coefficients for a gene - the larger the value of Cook's distance, the more likely it is that a count is an outlier. Potential outlier counts were flagged based on comparison with the other biological replicates. If a count was flagged, the p-value and adjusted p-value in the results table were set to "NA". The Cook's distance cutoff used was the 99% quantile of the $F(p,m\text{-}p)$ distribution, with p being the number of parameters including the intercept and m being the number of samples.

For differential expression analysis raw counts and discrete distributions were used; however, for unsupervised data exploration it was useful to work with transformed versions of the data. The regularized logarithm, or rlog, was used in the current data analysis. This incorporated a prior on the sample differences. The rlog function transforms the original count data to the $\log_2$ scale by fitting a model with a term for each sample and a prior distribution on the coefficients which is estimated from the data. The resulting data is of the form:

$$\log_2(q_{ij}) = \beta_{i0} + \beta_{ij}$$

where q_{ij} is a parameter proportional to the expected true concentration of sequence fragments for gene i and sample j, β_{i0} is an intercept (this term does not undergo shrinkage), and β_{ij} is the sample specific effect which is shrunk toward zero based on the dispersion-mean trend over the data. A prior on the sample specific effect terms is added. This regularized log transformation is preferable to other scaling transformations such as the variance stabilizing transformation if the size factors vary widely.

Another popular method for performing differential expression analyses on RNA-seq data is edgeR v3.18.1 (175), which is highly similar to DESeq2 but uses TMM normalization (176) to scale counts into pseudocounts, on which the hypothesis tests are performed. TMM normalization (Trimmed Mean of M-values) allows for scaling factors to be calculated from the raw data and used in the ensuing statistical analysis, thus normalizing for differences in library size and also RNA composition. A trimmed mean is the average after removing the upper and lower x% of the data. The pseudocounts are used to represent the counts that would have been observed assuming the fitted model, if sequencing depths for each library had been equal. The edgeR package also

uses generalized linear models to account for multifactor experimental designs (177). In edgeR, like in DESeq2, a matrix of raw counts is the input. Then, normalization factors were computed and entered into the statistical model. In the current analysis, gene-specific correction factors were entered into the functions as offsets to allow each gene to have a different dispersion.

Before hypothesis test were carried out, edgeR estimated the biological coefficient of variation (BCV), which is the coefficient of variation with which the unknown true abundance of the gene varied between replicated RNA samples. In RNA-seq experiments, the total coefficient of variation is composed of both a technical coefficient of variation and the biological coefficient of variation. The BCV is likely to be the dominant source of uncertainty for high count genes and represents the coefficient of variation that would remain if infinite sequencing depth were possible for biological replicates.

Under the negative binomial model, the reads are distributed as

$$Y_{gi} \sim NB(M_i p_{gj}, \varphi_g)$$

Where Y_{gijk} is the read count for gene g, from sample i, M_i is the total number of reads for sample i, p_{gis} the proportion of reads mapping to gene g in group j to which sample i belongs, and φ_g is the gene-specific dispersion. As in DESeq2, the Benjamini-Hochberg false discovery rate correction is used to correct p-values for multiple testing.

As the DESeq2 analysis, low count genes were removed from the edgeR analysis. Genes were kept in the analysis provided that they were present at a minimum of 0.06 count per million (CPM), which in this dataset corresponds to approximately 6 counts in the smallest sample (MD_37). Genewise dispersion estimates were used in the analysis, which allowed each gene to have a different dispersion parameter, allowing for greater power and flexibility in the model. A false discovery rate (FDR) of 1% was used as a cutoff for differential expression.

DAVID v6.8 (the Database for Annotation, Visualization, and Integrated Discovery) and GAGE v2.26.3 (Generally Applicable Gene-set Enrichment) were used in the annotation of genes and in performing the GO (gene ontology) enrichment analyses. The analyses were performed for differentially expressed genes found using DESeq2. Default settings were used, and results were filtered based on p-value (results were deemed significant if the p-value<0.01).

2.3.16 3'RACE

After harvest of Enza and DMSO-treated murine organoids, First Choice RLM RACE (rapid amplification of cDNA ends) kit was used (Thermo Fisher AM1700M) to select for and amplify full length mRNA. Wide-Sequencing was performed by Purdue Genomics Core Facility, followed by assessment by Drs. Yunlong Liu and Jun Wan.

2.3.17 pGL3 Luciferase Reporter

pGL3-IL-1α Luciferase reporter plasmid (Promega) was a generous gift from Dr. Eugenie S. Kleinerman, M.D. from the University of Texas M. D. Anderson Cancer Center. The reporter construct consists of the IL-1α promoter region fused to the gene for luciferase (181). Cells were transfected with the plasmid using FuGENE HD Transfection reagent (Promega).

2.4 Results

2.4.1 Androgen Receptor in Prostate Stem Cells

Adult prostate stem cells are rare epithelial progenitor cells, predominantly of basal cell lineage. While luminal progenitor cells play an essential role in tissue homeostasis, basal stem cells are recognized to be the developmental source of all epithelial prostate cells (41, 182, 183). These cells are involved in tissue homeostasis and regeneration during disease, but also play a role in abnormal hyperplasia (7, 120). They can be isolated in an enriched population by fluorescence activated cell sorting (FACS) as lineage negative ($CD45^-/CD31^-$), stem cell antigen 1^+ ($Sca\text{-}1^+$), $CD49f^+$ (LSC). Previous studies by Wang et al. revealed freshly isolated LSC to be more proliferative by bromodeoxyuridine (5-bromo-2'-deoxyuridine; BrdU) incorporation and differentiated by cytokeratin 5 and 8 staining (11). Since these are features of androgen receptor (AR) activity, we began to assess expression of *Ar* and its signaling components. The androgen receptor is the major driver of differentiation and proliferation of prostate epithelial cells (72, 184). The zinc finger transcription factor functions predominantly through ligand binding (to testosterone (T) and its more potent ligand, dihydrotestosterone (DHT)). Once bound, it forms a dimer and is transported to the nucleus where it relies on cofactors to mediate the effects of male hormone (71).

To assess AR for gene expression and protein production, several techniques were used. While quantitative reverse transcription polymerase chain reaction (RT-qPCR) showed variability of *Ar* gene expression, flow cytometry and western blot consistently showed high levels of full-length AR protein in the inflamed LSC (Figure 2.1A-C). This indicated that, rather than increased gene expression, the AR protein was being affected by inflammation. The LSC had traditionally been considered AR negative due to lack of detectable expression and their resistance to androgen deprivation (62). More recently, they were found to depend on AR for proliferation and differentiation to luminal lineage (156); however, modulation of AR had not been studied in the context of basal cell response to inflammation. Thus, we continued experiments to test the effects of increased AR in the LSC.

Typically, basal cells are positive for cytokeratin 5 (krt5), while luminal cells are positive for cytokeratin 8 (krt8). Transit-amplifying cells, or those that are intermediates between basal and luminal are positive for both krt5 and 8. Studies by Wang et al. demonstrated that while LSC from naïve mice were predominantly krt5 positive, LSC from inflamed mice were positive for both krt 5 and 8 indicating a transition to luminal cells (11). To investigate the extent of differentiation to from basal to luminal, we tested AR target genes associated with luminal cells by RT-qPCR. We found increased expression of direct AR target gene, *Tmprss2*, while other typical luminal genes such as *Nkx3.1* and *Pbsn* were not upregulated by inflammation (Figure 2.1D). The unexpected lack of luminal gene upregulation supported a partial differentiation or a novel role for AR signaling in basal cell regulation. To paint a more complete picture of the changes in gene expression, an AR target gene array (Qiagen) was run to compare cDNA from naïve and inflamed LSC. Multiple direct AR target genes, signaling components, and cofactors were upregulated by inflammation (Table 3.1, Figure 2.1E). Together, these data indicated that there may be an incomplete differentiation to luminal lineage. Studies by Kwon et al. demonstrated that *E. coli*-mediated inflammation of the prostate induced basal to luminal trans-differentiation that contributed to prostatic carcinoma (43). The incomplete transition from basal to luminal cells identified here requires further study but may contribute to certain features of prostate cancer (PCa), including androgen independence and resistance to androgen deprivation therapy.

These *ex-vivo* experiments confirmed that inflammation impacts AR and its signaling pathway in the LSC. This novel finding provides insight to the means by which inflammation can lead to hyperplasia and prostate disease through partial luminal differentiation and increased

proliferation. Benign prostate hyperplasia (BPH) is characterized by an enrichment of basal cells and is often resistant to androgen deprivation therapy and other treatments that manipulate the AR (7, 120). Thus, we continued studying the AR pathway in the context of 3D organoids which could be more easily manipulated to recapitulate treatment conditions.

2.4.2 Androgen Receptor in 3D Prostate Organoids

In order to be relevant to the clinical features of prostate disease, the increase in AR and resulting proliferation would need to persist once the initial inflammatory conditions had resolved. To test the persistence of inflammation-mediated AR signaling, 3D organoid cultures were used. After 7 days in androgen-free conditions, in an environment free of inflammatory cytokines, we were able to detect nuclear localization of AR in organoids from inflamed POET3 by immunofluorescence (Figure 2.2A-B). Western blot confirmed the presence of full-length AR (Figure 2.2C). Since the AR must translocate to the nucleus to act as a transcription factor and is quickly degraded when not in use, these data suggested that AR was indeed functional (70, 72).

Next, to identify some of the target genes modulated by persistent AR function, the Qiagen AR target gene array described above was used. This array revealed upregulation of various target genes and co-factors, including *Tmprss2*, *Slc26a2*, and *Steap4*, although with less consistency than the LSC (Table 2.2, Figure 2.2D). This was likely due to the androgen free organoid conditions which contrasted with the development of the assay (using LnCAP, a prostate cancer cell line treated with synthetic AR ligand R1881). In accordance, treating organoid cultures with dihydrotestosterone (DHT), the naturally occurring steroid hormone ligand for the androgen receptor, did not further increase expression of AR target genes (Figure 2.2E).

To further validate this finding, organoids were treated with clinical inhibitors for Cytochrome P450 17A1 (CYP17A1) and 5-alpha reductases (5ARI), Abiratirone (Abi) and Dutasteride (Duta), respectively. These reduced organoid numbers; however, adding DHT or R1881 to culture medium did not rescue organoid formation (Figure 2.3 A-B). Abi may also inhibit glucocorticoid and other steroid synthesis pathways (185), and Duta may interact directly with the AR (186, 187). Furthermore, there was no detection of androgens in the medium or cell homogenates. Although the possibility of intracellular DHT synthesis was not ruled out, the reduction in organoid numbers was attributed to off-target effects rather than hormone synthesis.

These data are consistent with the previous experiments showing no change in AR target gene expression upon addition of DHT to culture conditions.

Together, these data indicated that the AR was acting without ligand. Ligand-free AR signaling is generally associated with prostate disease and has been studied extensively with regards to prostate cancer (PCa) (164). When treated by androgen deprivation therapy, PCa becomes enriched for cells that can proliferate and survive in androgen-free conditions. In addition to intracellular androgen synthesis, they often contain amplification of the AR at the genomic locus, mutations to the AR that make it promiscuous to other ligands, or other changes that allow AR signaling in the absence of circulating androgens (81, 135, 161).

AR inhibitors, such as Enzalutamide (Enz) are used in the clinic to block AR signaling; thus, we used Enz to block AR function in 3D organoid cultures. Treatment with Enz reduced organoid size, numbers, and altered morphology in inflamed organoids (Figure 2.4A-D). The resulting organoids more closely resembled naïve, indicating that the effect was AR-mediated. Notably, Enz caused a significant decrease in proliferation (organoid size), LSC from inflamed POET3 still formed significantly more organoids than their naïve counterparts. These secondary findings are most relevant to castration resistant prostate cancer (CRPC), which initially responds to androgen deprivation therapy, but rebounds and metastasizes (136). Treatment of CRPC patients with Enzalutamide results in 3-5 months of prolonged life over placebo, indicating that androgen-independent cellular proliferation persists despite AR inhibition. Continued studies of the inflammation-mediated resistance to Enz may reveal mechanisms by which prostate cancer cells may achieve this deadly state.

These findings suggested that AR target gene expression was not due to androgen, but ligand-free AR signaling. This could be mediated by various factors including splice variants, phosphorylation, or promiscuous ligand binding, which have been studied extensively in prostate cancer and BPH (74, 76, 135, 160, 188). To investigate the source of ligand-independent and noncanonical AR signaling, studies were initiated to test for production of AR splice variants (ARSV). ARSV often lack the C-terminal ligand binding domain yet retain the nuclear localization signal and DNA binding domains. Competitive AR inhibitors, such as Enzalutamide, bind the C-terminal ligand-binding domain to prevent dimerization and nuclear localization. Since ARSV lack this portion, they are able to avoid inhibition and maintain persistent signaling without circulating androgens. ARSV have been extensively studied in human prostate cancer; however, murine

studies are few and rely on genomic alterations rather than alternative mRNA splicing events (162). Thus, reagents are not readily available for mouse studies that are relevant to human disease.

Despite these drawbacks, we began our investigation by performing 3'RACE (rapid amplification of cDNA ends) for AR in naïve and inflamed POET3 organoids. This technique allows for non-specific amplification of cDNA, which allows for detection of sequences that are unknown. This did reveal potential alternative splice locations that could produce a truncated AR lacking the C-terminal ligand binding domain (Figure 2.5); however, further evaluation of these variants and development of reagents to address protein expression were beyond the scope of these studies. Experiments were continued in human organoids described below.

Aberrant AR signaling can also occur when the AR undergoes post-translational phosphorylation (79, 161). Single Cell RNA-seq described below revealed significant up-regulation of kinases involved in post-translational modification of AR, *Mapk14* (p38MAPK) and *Cdk1*. RT-qPCR confirmed significant up-regulation of *Cdk1* and an upward trend in *Mapk1* in freshly isolated LSC (Figure 2.6A-B). Treatment with p38MAPK inhibitor, SB203580, showed no impact on AR by western blot; however, CDK1 inhibitor, Dinaciclib, did reduce full length protein (Figure 2.6C-D). Attempts were made to progress this finding, including immunoprecipitation of AR and proteomics assay to detect phosphorylation; but due to low cell yield and lack of reagents appropriate for murine studies, these were inconclusive.

These studies, along with those by previous students in the lab, all helped to rule out various mechanisms by which inflammation could promote AR signaling; however, definitive results were necessary to draw any meaningful conclusions. To gain a broader perspective, single cell RNA sequencing (scRNA-seq) was performed on Fluidigm's C1 platform. Cells were processed for sequencing by Purdue Genomics Core Facility, as described in the methods section. Quality control indicated high quality sequence data (Figure 2.7A-B). Unsupervised clustering, which allowed for segregation of cells based on gene expression alone, also indicated that the sequencing data were accurate. The cells clustered well based on inflammation status, with naïve segregated from inflamed (Figure 2.7C).

In addition to changes in AR signaling, an assessment of the true stem cells of the mixed LSC population was of interest. In addition to the two major clusters (naïve and inflamed), further analysis (based on gene expression without user input) revealed 5 cell sub clusters: 1) inflamed major, 2) naïve major, 3) inflamed minor 1, 4) inflamed minor 2, and 5) naïve minor 1 (Figure

2.8). While a thorough assessment of the minor populations is in progress, it is reasonable to assume one of these sub populations may contain true stem cells.

Since the source of the changes to AR signaling was yet to be determined, a pathway analysis was performed to identify the major upstream regulator for the changes in gene expression. This analysis used the differentially expressed genes between naïve and inflamed LSC in the single cell RNA sequencing described above to assess potential factors that could drive the changes in expression. This analysis identified interferon gamma (Ifnɣ) as a major upstream regulator (Figure 2.9), which was reasonable, since Ifnɣ is produced in large quantities by the cytotoxic T cells that are present in POET3 inflammation (148, 166). Notably, the IL1 pathway was identified as a major node in this signaling process; however, further analysis is necessary to evaluate the source and role of Ifnɣ in PSC.

To identify major changes in the LSC induced by inflammation, differential gene expression analysis was performed between naïve and inflamed LSC (Figure 2.10). This revealed upregulation of *Il1a* (Interleukin-1α (IL-1α)) and its signaling components, *Il1r1* (Interleukin-1 receptor 1) and naturally occurring inhibitor *Il1rn* (Interleukin-1 receptor antagonist) (Figure 2.11, Table 2.3). While the literature is suggestive that IL-1α can increase AR signaling in prostate cancer and luminal cells, studies of PSC indicate that they do not produce IL1α in detectable quantities and high dose treatment in culture actually decreases AR (95). Whether the PSC regulated AR via IL1α activation of IL1R1 or inhibition by IL-1RN remained unclear; thus, our attention turned to this signaling process.

2.4.3 Interleukin 1 Alpha and Androgen Receptor Signaling

Initially, it was hypothesized that AR signaling promoted IL-1α. Studies were performed using prostate cancer cell line LnCaP and Myc-CaP transfected with PGL3-Luciferase IL-1α reporter. This construct contains the IL-1α promoter region fused to the gene for luciferase. Thus, if transcription of the IL-1α gene were to occur, there would also be production of luciferase (181). These were grown in complete and serum free medium treated with the AR inhibitor, Enzalutamide (Enz). There was no effect of androgen deprivation or AR inhibition on luciferase measures (Figure 2.12). Thus, we continued studies to determine whether IL-1α mediated AR signaling.

To test whether the interleukin 1 pathway contributed to increased AR signaling in inflamed PSC, 3D organoid cultures were used. Initially, the hypothesis was that IL-1α would

promote organoid formation and AR signaling, and inhibition of this pathway would revert the effect; however, the opposite was the case. Treatment with IL-1α decreased organoid numbers significantly (Figure 2.13), while IL-1RA caused an increase in organoid numbers and size (Figure 2.14A-B). Western blot confirmed IL-1RA protein in untreated cells (LSC and organoids) from naïve and inflamed mice (Figure 2.14C), while an assessment of downstream phosphorylated IRAK was inconclusive (Figure 2.14D).

AR signaling was also affected by supplementation with IL-1RA. Immunofluorescence revealed increased AR protein in IL-1RA treated organoids and those treated with IL-1α neutralizing antibody (Figure 2.15A). It also produced an upward trend in AR gene expression and significant upregulation of AR target gene *Steap4* (Figure 2.15B-C).

To validate the hypothesis that IL-1RA treatment was acting through the AR pathway, lentiviral Cre recombinase was used to manipulate these factors at the genomic level. LSC were isolated from *il-1rn* floxed mice (a generous gift from Dr. Cem Gabay from University of Geneva), which possess lox P sites that flank the *il-1rn* gene. Introduction of Cre recombinase results in genomic loss of *il-1rn*. Indeed, when transduced with lentiviral Cre-GFP, there was loss of organoid formation and an upward trend in numbers when treated with IL-1RA (Figure 2.16A). AR floxed mice, which contain lox P sites that flank the N-terminal domain. When Cre recombinase is introduced into these cells, it results in a non-functional AR product. Consistent with previous studies, loss of AR reduced organoid numbers significantly, and addition of IL-1RA was unable to rescue organoid formation (Figure 2.16B). Additionally, the lentivirus inserts a GFP reporter, which would result in GFP-positive transduced cells. Treatment with IL-1RA did not produce a significantly greater number of GFP positive organoids, indicating that the effect was mediated by AR (Figure 2.16C).

Organoid culture experiments described above indicated that changes to AR signaling were persistent in nature. Thus, it was hypothesized that epigenetic changes could be occurring via chromatin remodeling. To address this, a collaborative investigation with students in Dr. Majid Kazemian's lab to assess differences in open regions of the genomic chromatin using an assay for transposase-accessible chromatin using sequencing (ATAC-seq) was begun. This assay uses a transposase reaction to cut and tag DNA fragments, sparing the regions wrapped around chromatin (167). This assay revealed greater open regions of the chromatin at the Il1rn gene of inflamed LSC. Figure 2.17 shows representative quality control of the transposase reaction with notable peaks at

DNA fragment sites and notable peaks (open regions of DNA) at the il1rn gene (Figure 2.17). These open regions of chromatin allow for transcription factor access to the DNA, indicating that the gene may be active. The open regions surrounding the *Il1rn* gene in inflamed LSC confirmed that epigenetic changes were occurring to these regions.

Studies to expand these findings are underway, but thus far it is clear that inhibition of IL-1α contributes to the increased AR signaling seen in inflamed LSC and their resulting organoids. By manipulation of this pathway, it may be possible to ameliorate the symptoms of basal cell hyperplasia in BPH.

2.4.4 In Vivo Analysis of Inflammation-Mediated AR and PSC Proliferation

While 3D organoid cultures are an excellent model of prostate development and disease, it is important to validate the *in vitro* findings *in vivo*, where confounding factors such as neighboring cells and an intact immune system may impact results. Thus *in vivo* inflamed castrate experiments were performed on POET3 mice. Circulating DHT is depleted rapidly after orchiectomy, and upon loss of circulating androgens, prostatic luminal cells undergo apoptosis, leading to an influx of immune cells resulting in inflammation (80). To achieve castrate conditions without induction of castration-induced inflammation, mice were inflamed on day 0, castrated on day 2, and prostates harvested on day 7. BrdU was injected IP 24 hours before harvest. Flow cytometry analysis revealed LSC from inflamed castrate mice to be significantly more proliferative than naïve castrate (Figure 2.18).

Histological evaluation (Figures 2.19-2.21) of castrate inflamed prostates revealed maintenance of epithelial tissue, as well as both nuclear and cytoplasmic AR as compared to naïve castrate. Inflamed castrate also contained a greater presence of p63 positive basal cells, consistent with the hypothesis that they contribute to prostatic disease induced by inflammation. These data confirmed that inflammation induces AR and proliferation in the basal cells that persist despite androgen deprivation.

2.4.5 AR in Human Prostate Stem Cells

In an attempt to validate these findings in human PSC, stem cell enrichments were obtained and cultured as described above. Unfortunately, human samples were obtained from patients with

symptomatic BPH, which contained a tremendous range of inflammation and lacked control (non-inflamed) for comparison. Thus, we were unable to determine whether inflammation of the human prostate impacts AR signaling in PSC in a manner similar to POET3.

Many cancers are able to hijack stem cell mechanisms to resist treatment and proliferate unchecked (110, 158). Since prostate cancer is initially sensitive to androgen deprivation and AR inhibition therapy, but rebounds in a fatal resistant form, we speculate that PSC would provide insight to the mechanisms by which this occurs. We began studying the impact of androgen deprivation on the PSC through organoid cultures and evaluated their response to AR inhibition by enzalutamide. To test their dependence on AR signaling, 3D organoid cultures were treated with Enz. Consistent with the murine findings, Enz treatment significantly reduced organoid numbers (Figure 2.22).

Hormone refractory and treatment resistant prostate cancer may bypass the need for DHT and evade inhibition by Enz. To identify broader changes to gene expression and potential mechanisms by which human organoids may still form upon Enz treatment, RNA sequencing was performed comparing DMSO (vehicle) to Enz treated organoids from four different patients. Assessment by Dr. Nadia Atallah Lanman at Purdue Bioinformatics Core indicated excellent quality and good library size (Figure 2.23A-C). Samples clustered nicely into distinct groups for treated and untreated (Figure 2.24A-C).

Resulting gene expression analysis revealed an assortment of highly expressed genes (Figure 2.25), as well as enrichment for the antigen presentation pathway (Figure 2.26) and protein digestion and absorption (Figure 2.27). A directed analysis did reveal high expression of IL1RN, but no differential expression of cytokines or AR (Figure 2.28). These results provided insight to the changes PSC may undergo to resist AR blockade, and with further study may yield targets for improving patient outcomes.

This still left the question of whether inflammation impacted human PSC in a manner similar to the POET3. To explore human PSC in the context of abacterial inflammation, methods were created for inducible inflammation of recombinant grafts. These were composed of rat urogenital sinus mesenchyme, LSC from POET3, and PSC from human samples in a collagen pellet. Grafts were implanted under the renal capsules of NRG mice to develop for 12 weeks before induction of inflammation by adoptive transfer of pre-activated OT-I cells. While an imperfect means of studying inflammation in the human prostate, this novel technique would provide

valuable insight to the human PSC response to local inflammation. Indeed, the grafts did prove inflammable; however, no human cells were detected by nucleolar staining (Figure 2.28).

2.5 Discussion

Previous studies using POET3 mice demonstrated a striking increase in prostate stem cell (PSC) proliferation and differentiation caused by autoimmune inflammation of the prostate. Since proliferation and differentiation are features of androgen receptor (AR) signaling in prostate cells, it was hypothesized that inflammation was impacting AR signaling resulting in these changes. The finding that indeed, AR and its target genes were impacted in a non-luminal manner were intriguing and had implications in the realm of stem cell differentiation and function during prostate disease. When experiments were initiated, it was believed that PSC were AR negative or non-responsive due to their low AR expression and their persistence during physical or chemical castration (61). Thus, early experiments using chemical inhibition of AR by Enzalutamide were striking in their revelation that AR was necessary for naïve PSC proliferation.

While Xie et al. since performed a more thorough *in vivo* analysis demonstrating a requirement for AR in normal PSC function (156), subsequent studies described here demonstrated that inflammation increased AR and AR signaling in this cell population. This raised the question of whether this was impacting basal to luminal trans-differentiation, which has been associated with loss of luminal cells and initiation of prostate cancer (43, 68). Concordant with previous data from our lab demonstrating higher proliferative capacity and increased CK8 expression in inflamed LSC (11), the increase in AR signaling supported the hypothesis that inflammation promotes basal PSC commitment to differentiation toward luminal lineage. This transition is further supported by high expression of some canonically luminal genes (*Tmprss2*), but not others (*Nkx3.1*, *Pbsn*).

Furthermore, while studies by Horton et al. demonstrated that loss of luminal cells promotes PSC proliferation and differentiation to luminal lineage (68); how this related to inflammation and T cell-mediated cell loss had not been investigated. Trans-differentiation of basal to luminal cells was examined by Kwon et al., in a model of bacterial prostate inflammation (43). In this setting, bacterial inflammation promoted differentiation from basal to luminal cells and accelerated tumor formation in a transgenic mouse model of prostate cancer. They did not, however, identify a mechanism by which this would occur. The studies described here point to an autocrine IL-1RA

function in the PSC response to inflammation that drives AR signaling and promotes trans-differentiation to a luminal-like phenotype.

While there are various mechanisms by which inflammation may increase AR (70, 72, 78, 87, 90), many were ruled out by experiments performed by previous students in the Ratliff lab. Due to the overwhelming focus on luminal cells in the literature, it was reasonable to assume that basal cells, especially rare basal stem cells, may rely on atypical mechanisms of AR regulation. To this end, single cell RNA sequencing revealed upregulation of various interleukin 1 signaling components. Studies by Zhang et al. had examined IL-1α in the context of E. coli-mediated inflammation of the prostate. In their studies, loss of AR in the luminal cells led to decreased integrity of the prostate and promoted inflammation and AR-independent proliferation. This effect was abrogated by ablation of macrophages, indicating that the impact on luminal cells relied on an external source of signaling (90). The studies described here provided a novel examination of autocrine epithelial production and response to IL-1α by over production of IL-1RA in the basal stem cells. In contrast to the luminal data, these experiments revealed a striking IL-1RA-mediated up-regulation of AR in the PSC, which contributed to proliferation and differentiation. The IL-1α pathway is tightly regulated and influenced by many inhibitory and stimulatory molecules (92, 189). The many epithelial and immune cells present in the inflammatory environment of the prostate are conducive to intricate and multifaceted signaling processes, which will be the topic of continued study via lineage tracing and genomic recombination in the POET3 mouse.

The persistent AR signaling revealed in androgen-free 3D organoid cultures of inflamed bPSC reveal striking long-term changes induced by inflammation. Considering the high correlation between inflammation and BPH (1, 113) and the hyperproliferative nature of bPSC from inflamed prostates (11), our findings that inflammation-driven IL1RA induced persistent changes to AR signaling to promote proliferation in the bPSC begin to form a molecular bridge between inflammation and hyperplastic disease. Aberrant AR signaling has recently been identified in BPH specimens, which often become resistant to treatments targeting the AR axis (160). BPH also often contains an enrichment for basal cells (7). Thus, the persistence of AR and its target genes in inflamed LSC point to a possible cell of origin for this resistance.

Another important question that was revealed by these studies was the means by which inflammation impacted PSC in the long term. To this end, epigenetic changes were a likely candidate. The ATAC sequencing experiments described above revealed notable changes in open

regions of DNA at the location of the *Il1rn* gene. Thus, the possibility remains that AR or other factors may be inducing remodeling of chromatin. These and other questions regarding the mechanisms of long-term changes to differential gene expression and PSC function will be the topic of further collaborative study between the Ratliff, Jerde, and Kazemian labs.

While *in vitro* experiments revealed persistent AR signaling and proliferation by isolated PSC in androgen-free conditions, it remained necessary to demonstrate consistency in the complex multicellular environment of the prostate. *In vivo* inflammation-castration experiments revealed similar findings with regards to basal cell enrichment and maintenance of AR protein. These data are particularly relevant to benign prostate hyperplasia, where basal cell enrichment may confer resistance to non-surgical treatments (7, 120). Experiments are currently underway to assess the LSC and other cellular populations from inflamed castrate mice for IL-1α and its signaling components (IL-1RA, IL-1R1, IL-1R2). Additionally, it will be important to validate the findings in human PSC.

The organoid culture system provided an invaluable resource for studying the effects of pharmaceutical agents on PSC biology. Since cancers may hijack developmental pathways utilized by stem cells (5, 159, 190), the results of these studies are applicable to various areas of cancer research. RNA sequencing of comparing Enz treated and untreated human organoid cultures revealed an enrichment for changes in gene expression associated with the antigen presentation and protein digestion pathways. Protein digestion remains unexplored in the PSC; however, the antigen presentation pathway may be relevant for improving immunotherapy for prostate cancer (discussed in the next chapter). Studies by Olson et al. demonstrated that T-cell immunotherapies for prostate cancer are impacted by AR during androgen deprivation (191). The inflammation-induced changes to AR identified by the studies described here may prove relevant to evasion of immune therapy by advanced prostate cancer. With further study, these aspects may lead to new targets for improved patient outcomes.

To summarize, the data presented herein begin to identify a multitude of mechanisms by which inflammation drives PSC to maintain AR signaling and proliferate in the absence of circulating androgens; however, future studies will be required to demonstrate a definitive role for inflammation in human hyperproliferative disease. The data demonstrating an increase in AR and its target genes in bPSC from inflamed prostates provide evidence that chronic abacterial

inflammation contributes to persistent AR-mediated proliferation of prostate tissues by induction of IL-1RA.

2.6 Tables and Figures

Table 2.1. **Genes over-expressed in inflamed LSC vs. naïve LSC.**

Gene Symbol	Fold Regulation	p-value	RefSeq
Abhd2	6.8369	0.00086	NM_018811
Acsl3	5.8835	0.000531	NM_001033606
Adamts1	7.0128	0.000843	NM_009621
Aldh1a3*	13.4233	0.000939	NM_053080
Ell2	3.2944	0.000446	NM_138953
Endod1	2.7638	0.044739	NM_028013
Fkbp5	2.8089	0.035092	NM_010220
Lrrfip2	6.9967	0.000012	NM_027742
Mme	5.9932	0.004442	NM_008604
Map7d1	2.7959	0.044072	NM_144941
Pak1ip1	2.2553	0.000012	NM_026550
Pmepa1*	9.6242	0.004442	NM_022995
Rel	3.9086	0.044072	NM_009044
Sgk1	4.5736	0.000357	NM_011361
Slc45a3	2.8024	0.009049	NM_145977
Snai2	2.0658	0.001819	NM_011415
Stk39	2.0753	0.008354	NM_016866
Tiparp	2.2658	0.038166	NM_178892
Tmprss2*	8.7746	0.000045	NM_015775
Tpd52	2.3674	0.000125	NM_009412
Tsc22d1	2.6208	0.006968	NM_009366
Vapa	3.1895	0.002297	NM_013933
Zbtb16	2.8879	0.002752	NM_001033324

Top three up-regulated genes

Table 2.2. **Genes upregulated in inflamed LSC as compared to naïve.**

Gene Symbol	Fold Regulation	p-value	RefSeq
Ar	3.8444	0.002925	NM_013476
Cited2	2.1377	0.031692	NM_010828
Igfbp5*	9.9365	0.007704	NM_010518
Jun	2.3995	0.014287	NM_010591
Lama1	2.2544	0.034606	NM_008480
Slc26a2*	5.8675	0.016003	NM_010513
Sord	2.4051	0.006992	NM_019928
Steap4*	5.2394	0.00112	NM_013584
Zfp189	2.6197	0.018571	NM_145547

Top 3 differentially upregulated genes.

Table 2.3. **Interleukin 1 alpha and its signaling component genes upregulated in inflamed LSC as compared to naïve.**

Gene	adj_p_value	log2_fc
Il1rn	6.10E-22	10.954
Il1a	7.02E-22	11.106
Il1r1	3.00E-3	4.9969

Fluidigm single cell mRNA sequencing revealed up regulation of interleukin 1 alpha (IL1a), its receptor Il1r1, and the naturally occurring inhibitor Il1rn in inflamed LSC.

Figure 2.1. Identification of AR activity in inflamed Lin$^-$Sca1$^+$CD49f$^+$ (LSC) population ex vivo. (A) Representative FACS analysis of intracellular stained AR in naïve and inflamed POET3 prostates (histogram), in the LSC population. **(B)** Bar graph percentages of AR$^+$ cells within naïve and inflamed LSC populations (Mann-Whitney test, n=10 in naïve and n=5 in inflamed; data value= means ± s.e.). **(C)** Western blot of full-length AR in naïve and inflamed LSC. **(D)** qRT-PCR analysis of conventional AR target genes, Tmprss2, Nkx3.1, and Pbsn, in LSC and its counterpart luminal population (n=3 individual mice, data value= means ± s.e.). **(E)** A heatmap of murine AR regulated gene analysis. (n=3 individual mice, Student's t-test, significance was determined by α=0.05).

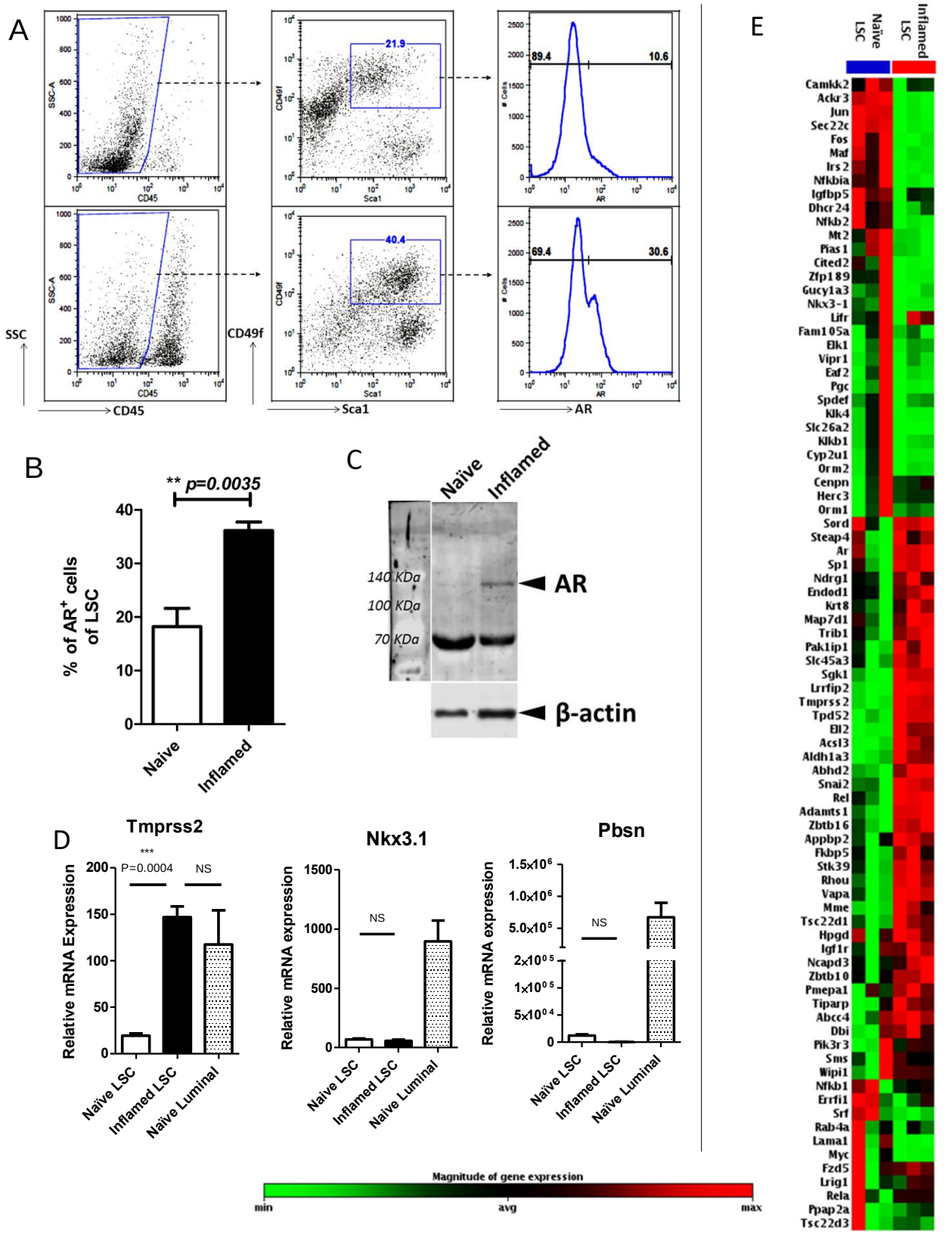
A
SSC
CD45
CD49f
Sca1
AR
21.9
89.4
10.6
40.4
69.4
30.6
B
** p=0.0035
% of AR+ cells of LSC
Naive
Inflamed
C
Naïve
Inflamed
140 KDa
100 KDa
70 KDa
AR
β-actin
D
Tmprss2
***
P=0.0004
NS
Relative mRNA Expression
Naïve LSC
Inflamed LSC
Naïve Luminal
Nkx3.1
Relative mRNA expression
Pbsn
E
Naïve LSC
Inflamed LSC
Camkk2
Ackr3
Jun
Sec22c
Fos
Maf
Irs2
Nfkbia
Igfbp5
Dhcr24
Nfkb2
Mt2
Pias1
Cited2
Zfp189
Gucy1a3
Nkx3-1
Lifr
Fam105a
Elk1
Vipr1
Eaf2
Pgc
Spdef
Klk4
Slc26a2
Klkb1
Cyp2u1
Orm2
Cenpn
Herc3
Orm1
Sord
Steap4
Ar
Sp1
Ndrg1
Endod1
Krt8
Map7d1
Trib1
Pak1ip1
Slc45a3
Sgk1
Lrrfip2
Tmprss2
Tpd52
Ell2
Acsl3
Aldh1a3
Abhd2
Snai2
Rel
Adamts1
Zbtb16
Appbp2
Fkbp5
Stk39
Rhou
Vapa
Mme
Tsc22d1
Hpgd
Igf1r
Ncapd3
Zbtb10
Pmepa1
Tiparp
Abcc4
Dbi
Pik3r3
Sms
Wipi1
Nfkb1
Errfi1
Srf
Rab4a
Lama1
Myc
Fzd5
Lrig1
Rela
Ppap2a
Tsc22d3
Magnitude of gene expression
min
avg
max

Figure 2.2. Identification and modulation of AR activity in naïve and inflamed organoids. (A) Immunofluorescence staining of AR in organoids derived from naïve and inflamed LSC. Representative nuclear localized AR (green, indicated by white arrows) was shown in the inflamed setting (Scale bar: 100μm). **(B)** A bar graph showing the distribution of AR in organoid cells. Significantly higher incidence of nuclear AR vs cytoplasmic AR was observed in inflamed organoids, and nuclear localized AR was higher in inflamed organoids compared to naïve organoids. (Mann Whitney test, n=13-17, collected from 3 independent experiments; data value= means ± s.e.) **(C)** Western blot analysis showing full-length AR in inflamed organoids in the absence of 1nM synthetic AR ligand, R1881. **(D)** A heatmap of global murine AR regulated gene expression (n=3 individual mice, Student's t-test, significance was determined by α=0.05). **(E)** qRT-PCR analysis showing that the top three up-regulated genes in inflamed organoids, *Steap4*, *Slc26a2*, and *Igfbp5*, can be down-regulated by introducing 10μM AR inhibitor, Enzalutamide (n=3 individual mice, data value= means ± s.e.). **(F)** qRT-PCR analysis showing that *Igfbp5* is DHT responsive whereas *Steap4* and *Slc26a2* are not (n=2-4 individual mice, data value= means ± s.e.).

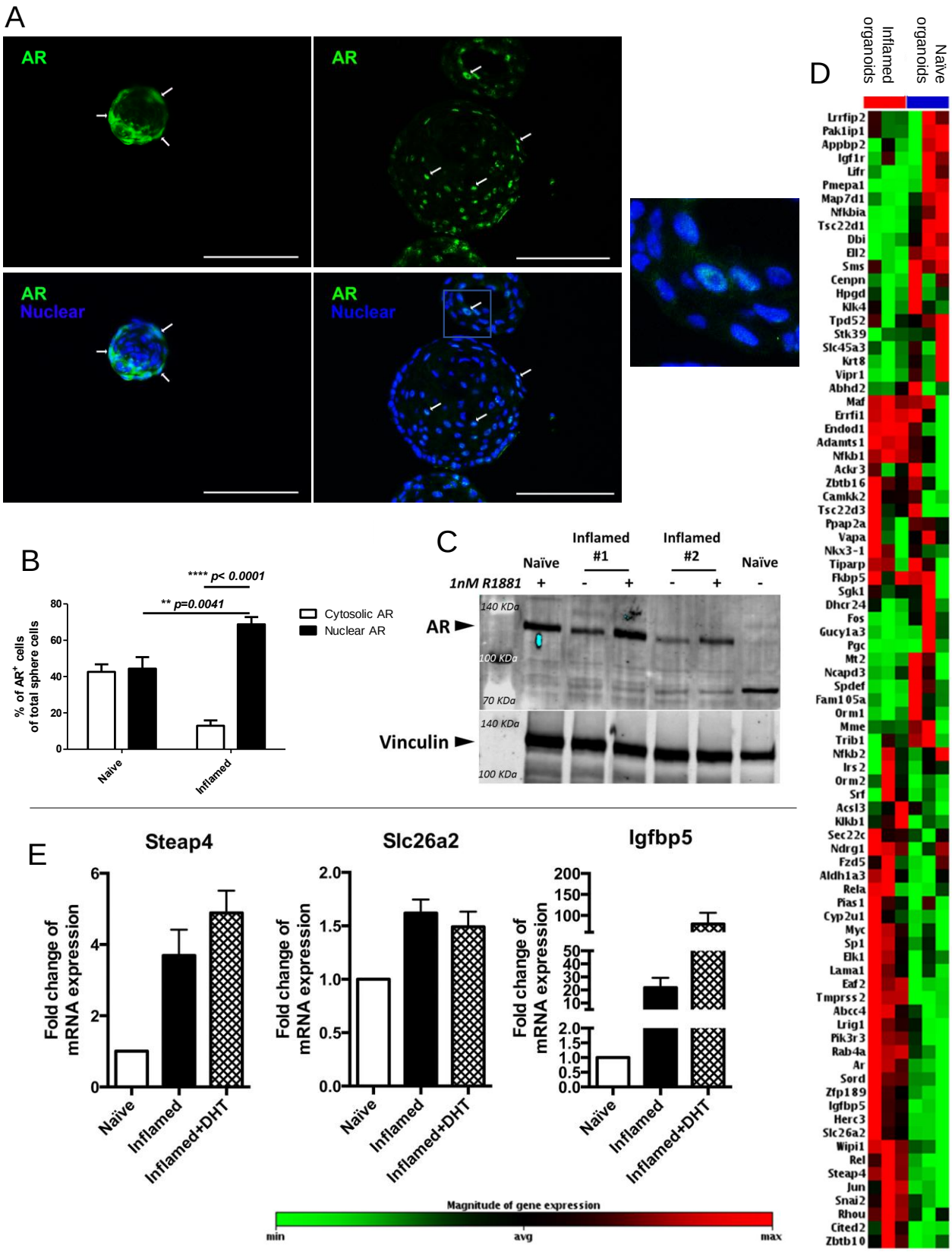
A
AR
AR
AR
Nuclear
AR
Nuclear
B
**** p< 0.0001
** p=0.0041
% of AR+ cells of total sphere cells
Cytosolic AR
Nuclear AR
Naïve
Inflamed
C
Naïve
Inflamed #1
Inflamed #2
Naïve
1nM R1881 + - + - + -
AR
140 KDa
100 KDa
70 KDa
Vinculin
140 KDa
100 KDa
D
Inflamed organoids
Naïve organoids
Lrrfip2
Pak1ip1
Appbp2
Igf1r
Lifr
Pmepa1
Map7d1
Nfkbia
Tsc22d1
Dbi
Ell2
Sms
Cenpn
Hpgd
Klk4
Tpd52
Stk39
Slc45a3
Krt8
Vipr1
Abhd2
Maf
Errfi1
Endod1
Adamts1
Nfkb1
Ackr3
Zbtb16
Camkk2
Tsc22d3
Ppap2a
Vapa
Nkx3-1
Tiparp
Fkbp5
Sgk1
Dhcr24
Fos
Gucy1a3
Pgc
Mt2
Ncapd3
Spdef
Fam105a
Orm1
Mme
Trib1
Nfkb2
Irs2
Orm2
Srf
Acsl3
Klkb1
Sec22c
Ndrg1
Fzd5
Aldh1a3
Rela
Pias1
Cyp2u1
Myc
Sp1
Elk1
Lama1
Eaf2
Tmprss2
Abcc4
Lrig1
Pik3r3
Rab4a
Ar
Sord
Zfp189
Igfbp5
Herc3
Slc26a2
Wipi1
Rel
Steap4
Jun
Snai2
Rhou
Cited2
Zbtb10
E
Steap4
Slc26a2
Igfbp5
Fold change of mRNA expression
Naïve
Inflamed
Inflamed+DHT
Magnitude of gene expression
min
avg
max

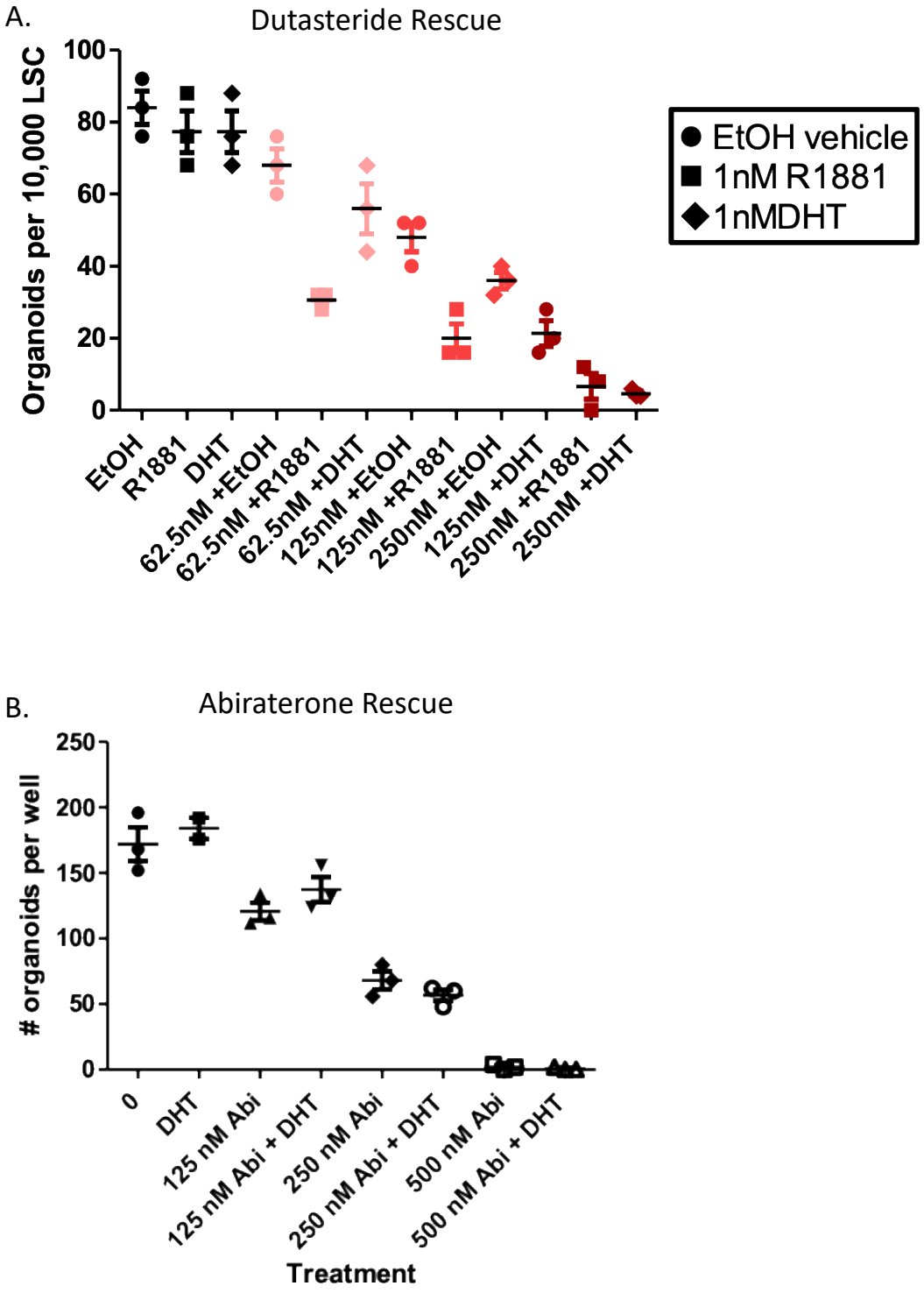

Figure 2.3. Androgen Synthesis in organoid cultures. Treatment of naïve organoids with androgen synthesis inhibitors dutasteride (5 alpha reductase inhibitor) or abiraterone (Cyp17a1 inhibitor) blocks organoid formation, which is not rescued by addition of DHT or R1881.

Figure 2.4. Abrogation of AR activity via AR antagonists abolishes basal PSC characteristics. (A) Representative H&E stained images show a morphological difference between vehicle and Enz treated organoids, where Enz treated more closely resemble naive (Scale bar: 100µm). (B) The number of organoids formed in vehicle and 10µM Enzalutamide in both naïve and inflamed settings. (5 separate experiments in naïve group and 9 separate experiments in inflamed group, each experiment was presented in duplicates; Student's t-test was performed within groups) (C) Inflamed organoids treated with enzalutamide produce more solid organoids and fewer tubule-like. (D) Inflamed organoids are significantly larger than naïve, while Enz treated inflamed are similar in size. (Unpaired T test) (E) CK5 (green) and CK8 (red) staining show lack of organization in Enz treated organoids compared to control (Scale bar: 25µm). (F) qRT-PCR showing that the top three up-regulated genes in inflamed organoids, *Steap4*, *Slc26a2*, and *Igfbp5*, can be down-regulated by introducing 10µM AR inhibitor, Enzalutamide (n=3 individual mice, data value= means ± s.e.).

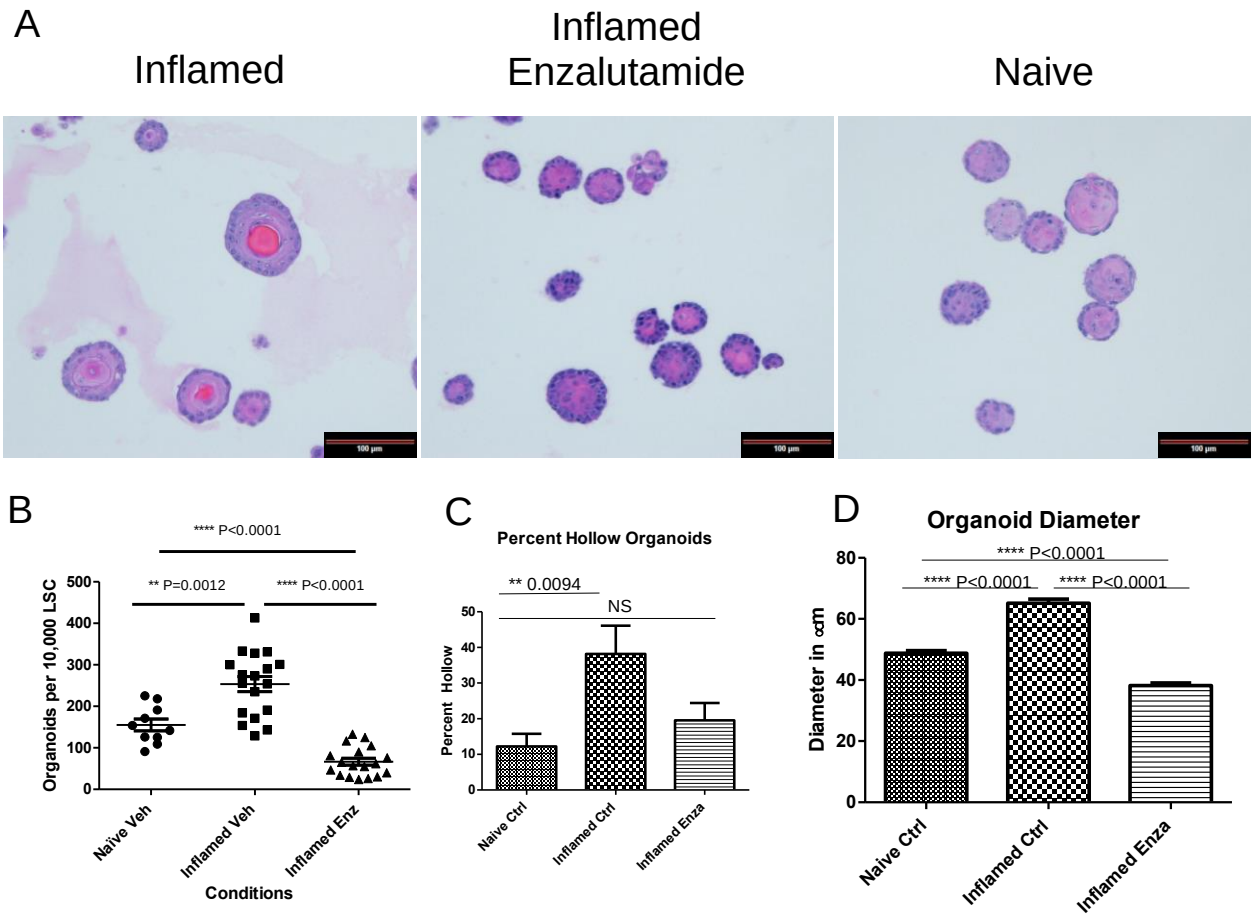
A
Inflamed
Inflamed Enzalutamide
Naive
B
**** P<0.0001
** P=0.0012
**** P<0.0001
Organoids per 10,000 LSC
Naïve Veh
Inflamed Veh
Inflamed Enz
Conditions
C
Percent Hollow Organoids
** 0.0094
NS
Percent Hollow
Naive Ctrl
Inflamed Ctrl
Inflamed Enza
D
Organoid Diameter
**** P<0.0001
**** P<0.0001
**** P<0.0001
Diameter in ∝m
Naive Ctrl
Inflamed Ctrl
Inflamed Enza
E
Inflamed Vehicle
Inflamed Enza
Naïve Vehicle
CK5
CK8
Nuclear
F
AR
Steap4
Slc26a2
Fkbp5
*P=0.0394
Relative mRNA expression
Naïve
Inflamed
Inflamed Enz

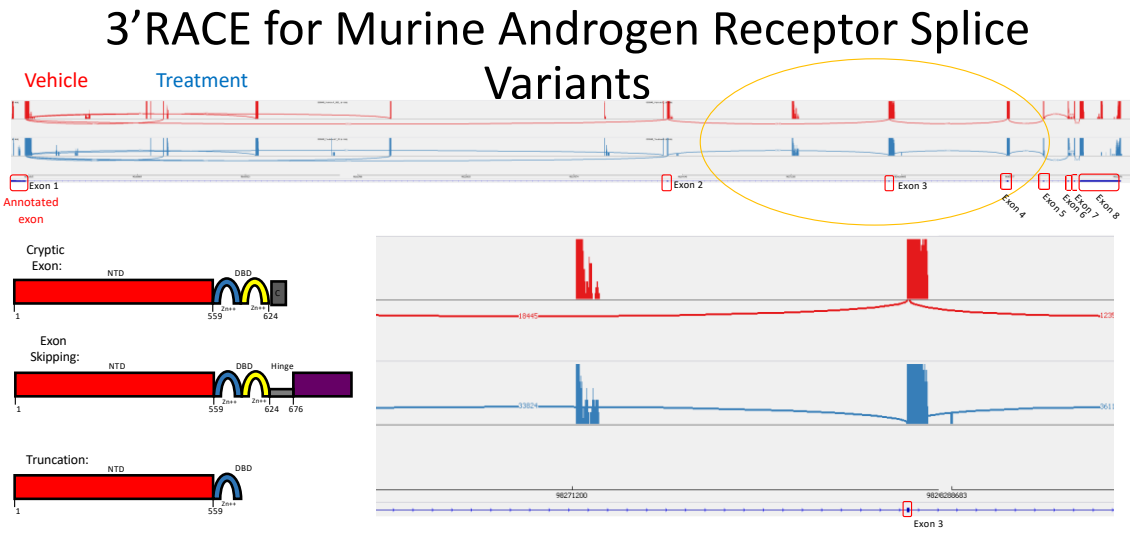

Figure 2.5. 3’RACE (Rapid amplification of cDNA ends). Diagram depicts enrichments for potentially truncated transcriopts that would lack the c-terminal ligand binding domain.

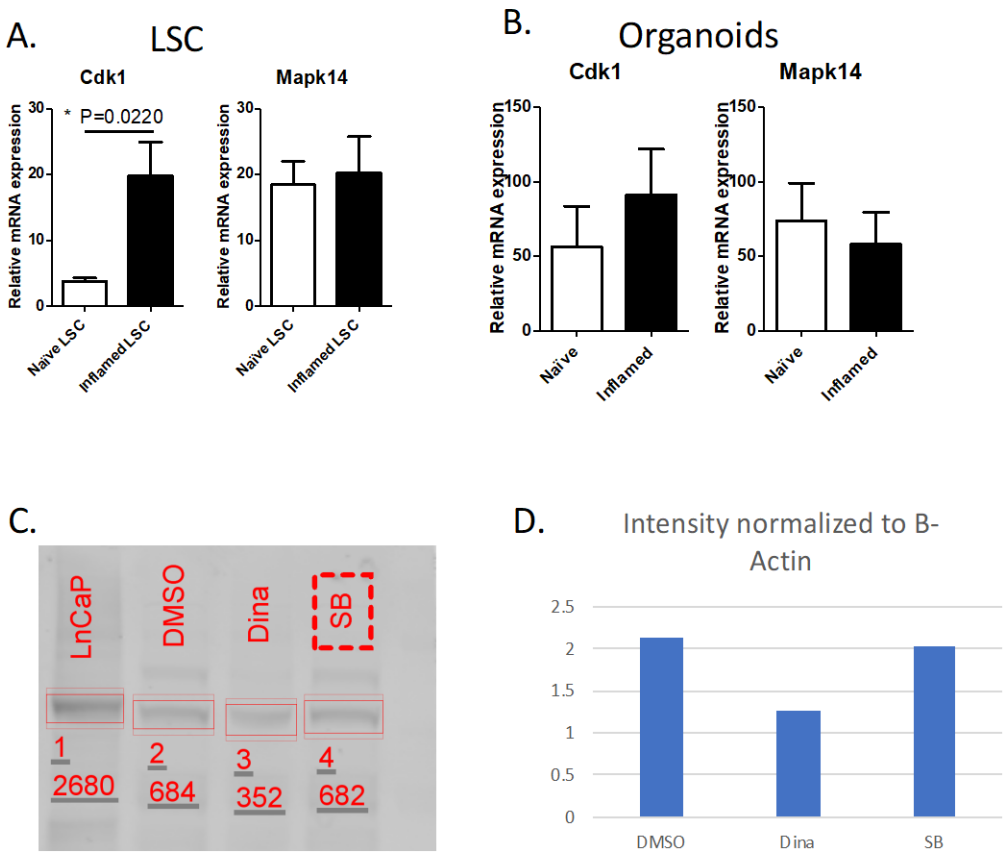

Figure 2.6. Inflammation induces CDK-1 mediated phosphorylation of AR. (A) rt-qPCR showing a significant increase in Cdk1 and no change in Mapk14 in murine LSC. **(B)** rt-qPCR showed no change in Cdk1 or Mapk14 in organoids derived from naïve or inflamed mice. **(C)** Western blot for Androgen Receptor shows no impact of p38MAPK inhibitor, SB203580, while CDK1 inhibitor, Dinaciclib, did reduce full length protein in inflamed organoids. **(D)** bar graph showing quantification of AR protein normalized to B-Actin.

Figure 2.7. Quality Control for Single Cell mRNA Sequencing. **(A)** Per base sequence quality for Inflamed A3 trimmed right reads. The y-axis shows quality scores and the x-axis shows the position in the read. The red line is the median and the blue line is the mean. The yellow box represents the inter-quartile (25%-75%) range, and the upper and lower whiskers represent the 10% and 90% points. The dip in sequence quality at the end of the read is normal and is nearly always observed in Illumina sequencing data. Due in part to trimming, all positions in the reads have high quality. This graph is typical for what was observed across all read files. **(B)** Per sequence quality score for Inflamed A3 trimmed right reads. This plot shows allows identification of samples in which a subset of sequences in the FASTQ file have universally low-quality scores. The Y axis shows the number of sequences and the x axis shows the mean quality score. This plot shows that the reads post-trimming have very high quality. This plot looks similar to all the other per sequence quality score plots seen across the trimmed FASTQ files. **(C)** MDS plot with libraries colored based on inflammation status. Inflamed cells are colored in blue and naïve cells are colored in red. The samples are clustering quite well based on inflammation status.

A.

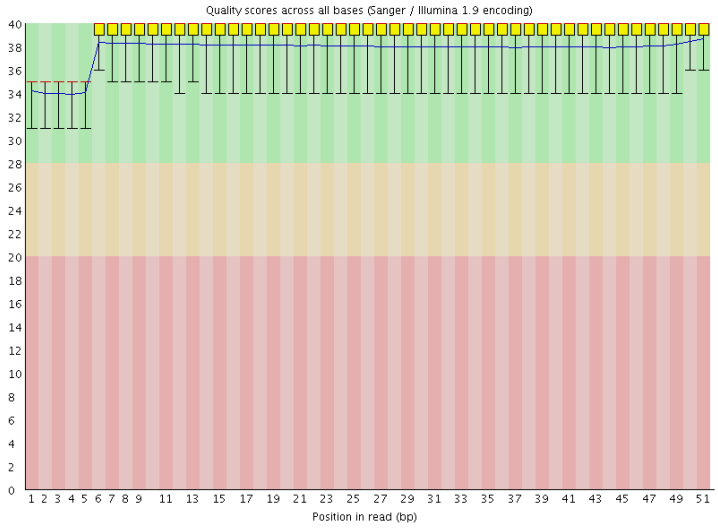
Quality scores across all bases (Sanger / Illumina 1.9 encoding)
Position in read (bp)

B.

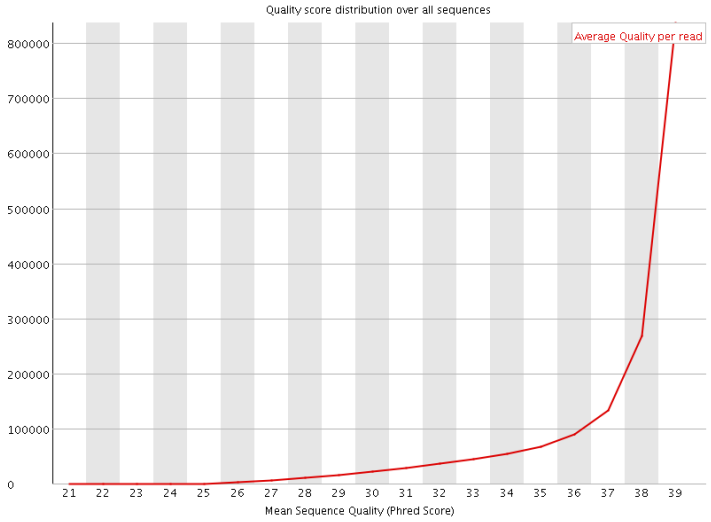
Quality score distribution over all sequences
Average Quality per read
Mean Sequence Quality (Phred Score)

C.

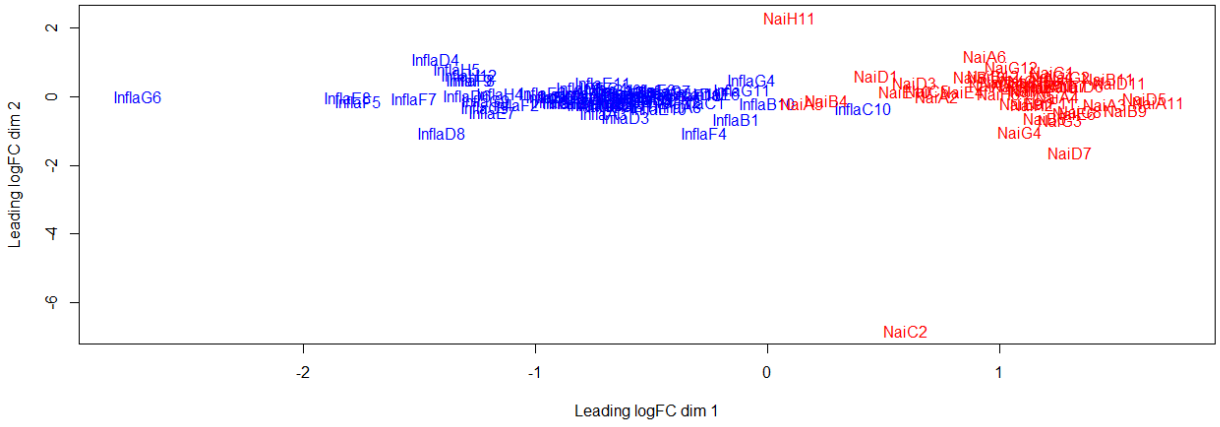
Leading logFC dim 2
Leading logFC dim 1
NaiH11
InflaD4
InflaG6
InflaF5
InflaF7
InflaD8
InflaG4
InflaB1
InflaF4
InflaC10
NaiA6
NaiD1
NaiG4
NaiD7
NaiC2

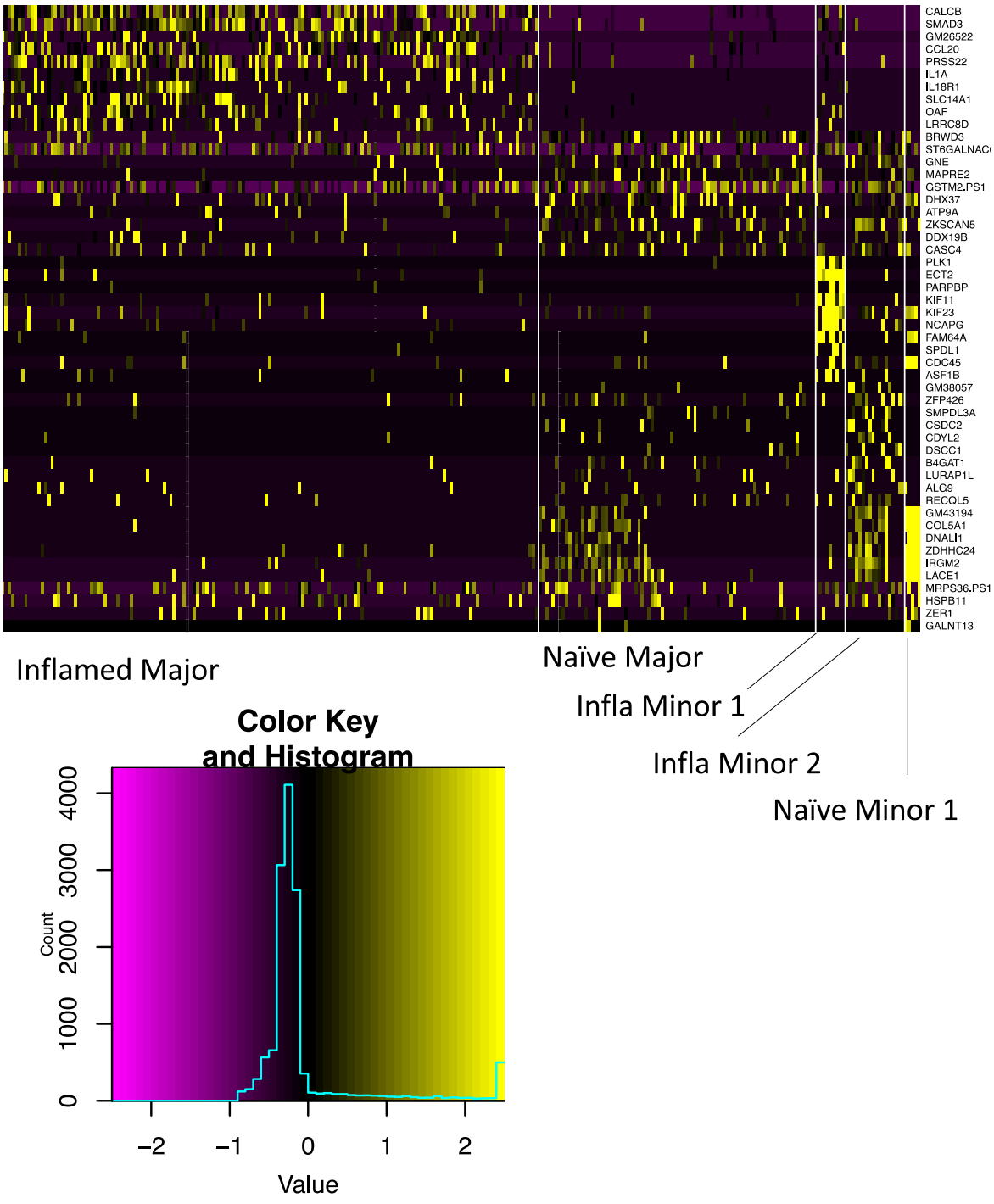

Figure 2.8. Heatmap showing results of unsupervised clustering. Cells were categorized into 4 groups: Inflamed Major, Naïve Major, Inflamed Minor 1, Inflamed Minor 2, and Naïve Minor 3. Vertical columns represent individual cells, while horizontal axis represents top clustering genes. Yellow indicates highest fold change gene expression, while violet indicates lowest. Thanks to Purdue Genomics Core and Bioinformatics Core (Dr. NadiaAtallah Lanman and Emery Goossens)

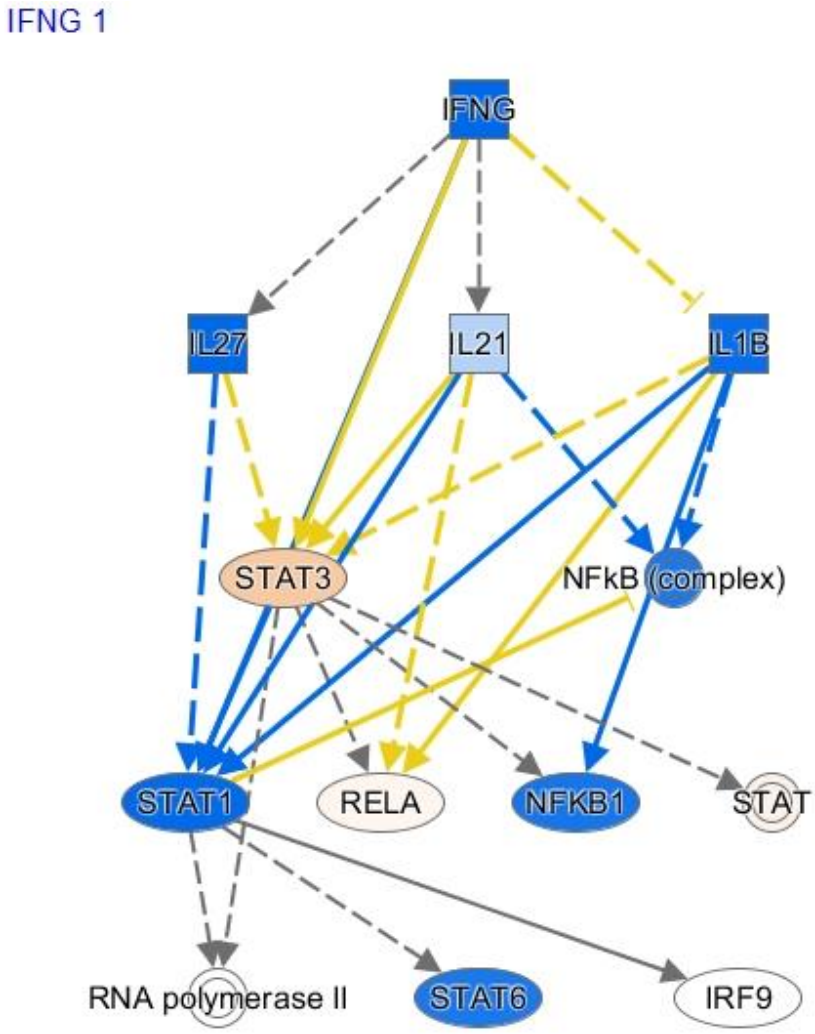

Figure 2.9. Upstream regulator IFNG and its predicted mechanistic network. The list of differentially expressed genes, along with p-values were used as input for the analysis. IFNG is one of the top predicted upstream regulators in the BSC naïve versus inflamed comparison, connecting directly to 45 target molecules in the differentially expressed genes. The list of differentially expressed genes, along with log fold-change and false discovery rates were used as input for the analysis. Nodes shown in orange are also predicted to be upstream activators and those that are predicted to be inhibitors are shown in blue. Orange edges show activating relationships and blue show inhibiting relationships. Black edges do not have an effect predicted and yellow edges show literature findings which are inconsistent with the state of the downstream molecule. This mechanistic network determines which network edges between pre-determined upstream regulators are likely relevant for the causal mechanism behind the dataset. The mechanistic network algorithm is run upon the regulators from the upstream regulator analysis results. Solid edges show direct interactions and dashed lines show indirect interactions between molecules.

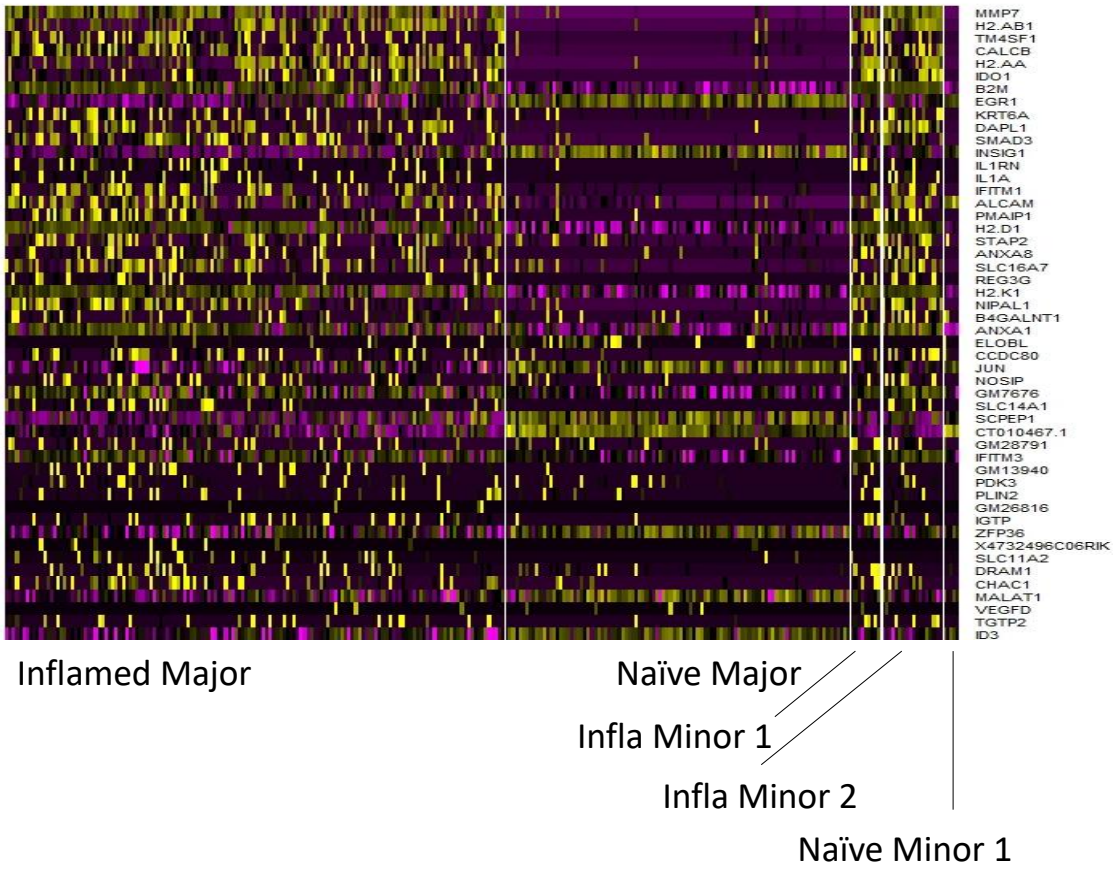

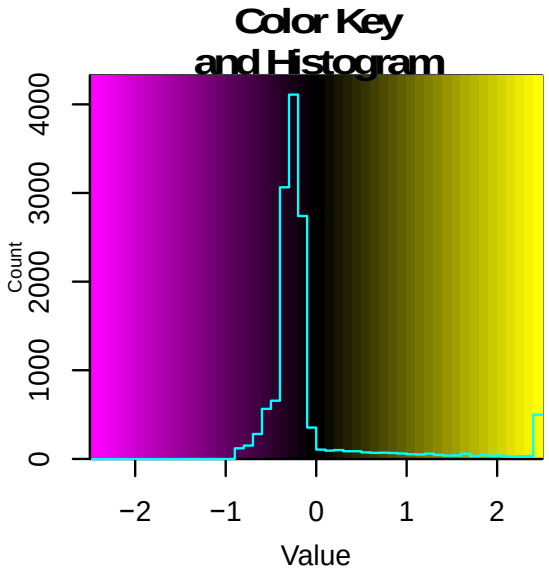

Figure 2.10. Differentially expressed genes between naïve and inflamed. Yellow indicates highest expression while violet is lowest. Vertical columns represent individual cells, while horizontal axis represents top clustering genes. Yellow indicates highest fold change gene expression, while violet indicates lowest. Thanks to Purdue Genomics Core and Bioinformatics Core (Dr. Nadia Atallah Lanman and Emery Goossens)

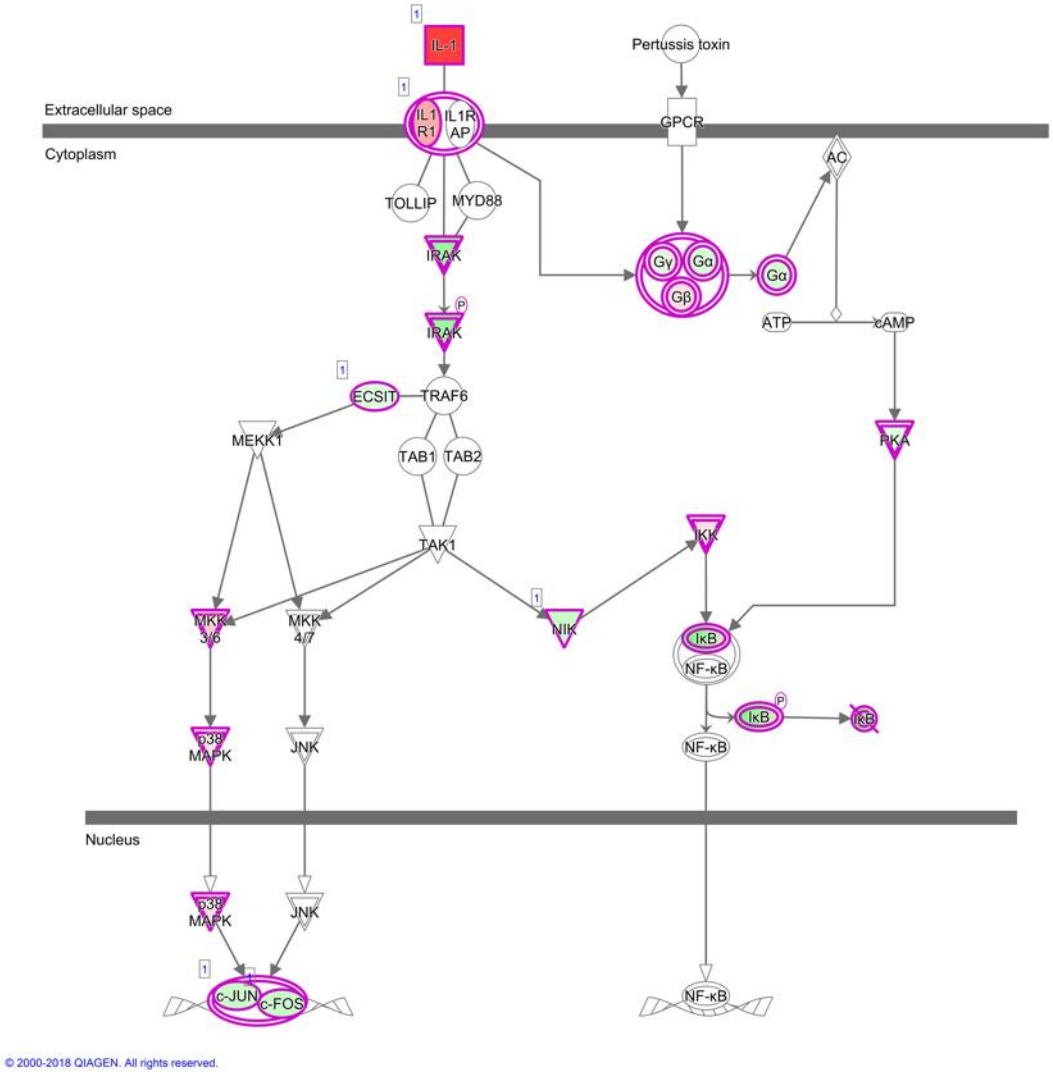

Figure 2.11. Canonical Interleukin 1 pathway. The diagram shows the interleukin 1 pathway, one of the overrepresented pathways found in the naïve versus inflamed LSC comparison by IPA. Genes in the pathway which are present in the differentially expressed gene list are shown outlined in pink. Upregulated molecules are colored in red and downregulated molecules in green. The intensity of the color indicates the degree of down or upregulation. The expression value used in coloring the molecules was the log p-value. Thanks to Dr. Nadia Atallah Lanman.

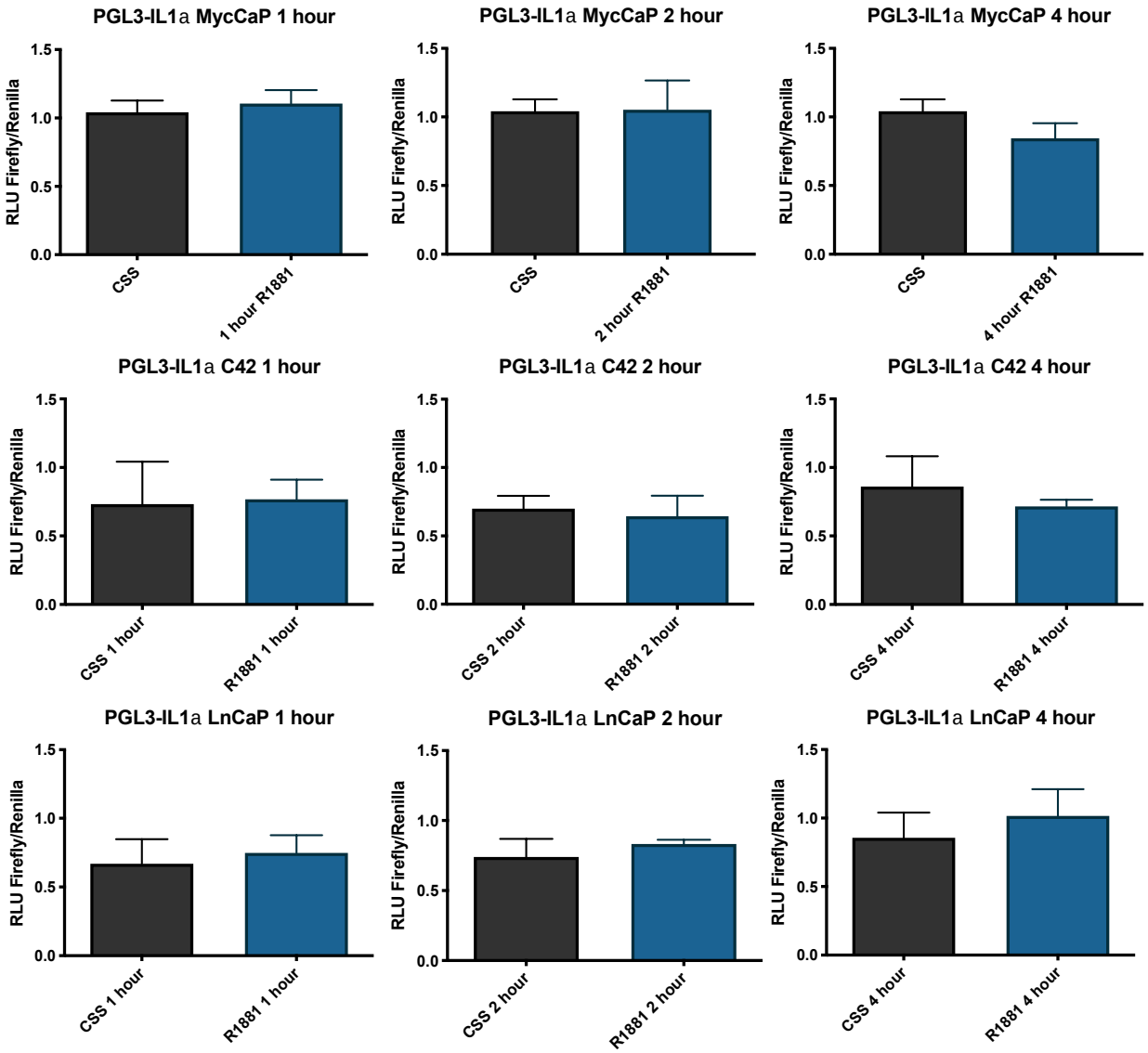

Figure 2.12. PGL3 Luciferase IL-1α Reporter Assay. Murine prostate cancer cell line, Myc-CaP, as well as human lines LnCAP and C42 were transfected with PGL-3 luciferase IL-1α reporter. These were then incubated in RPMI 1640 with charcoal stripped serum and supplemented with R1881 for 1, 2, and 4 hours before lysis and assessment of luciferase activity by fluorometric assay. There was no change in luciferase activity in any cell line at any timepoint.

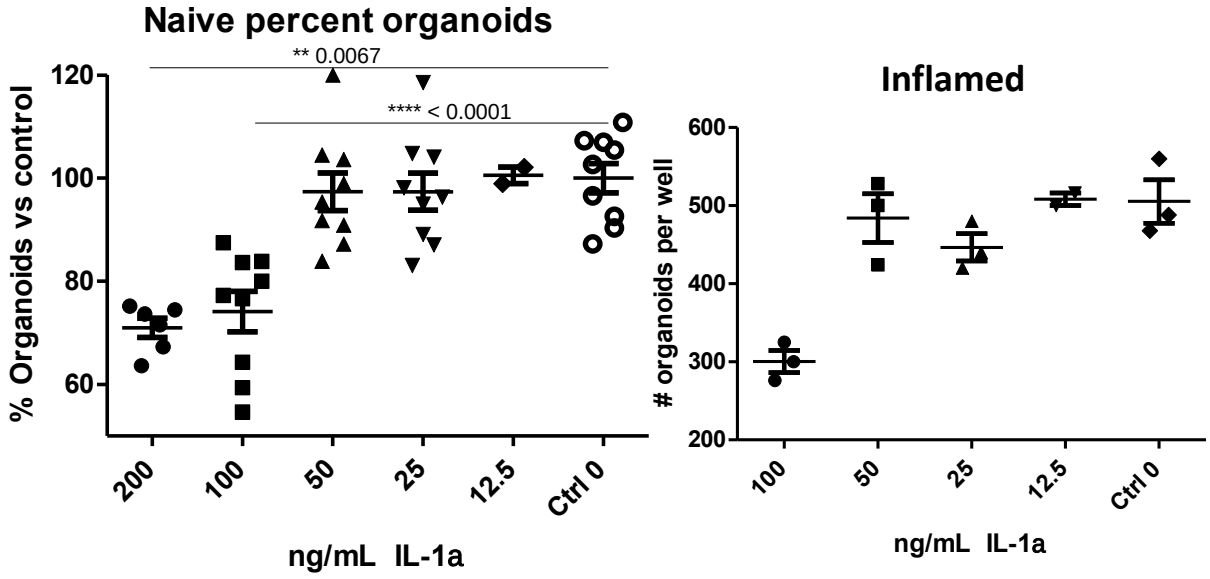

Figure 2.13. Interleukin 1 Alpha Treatment of Organoid Cultures. 3D organoid cultures of naïve and inflamed LSC were treated with various concentrations of synthetic interleukin 1 alpha. Contrary to the hypothesis, treatment decreased organoid numbers.

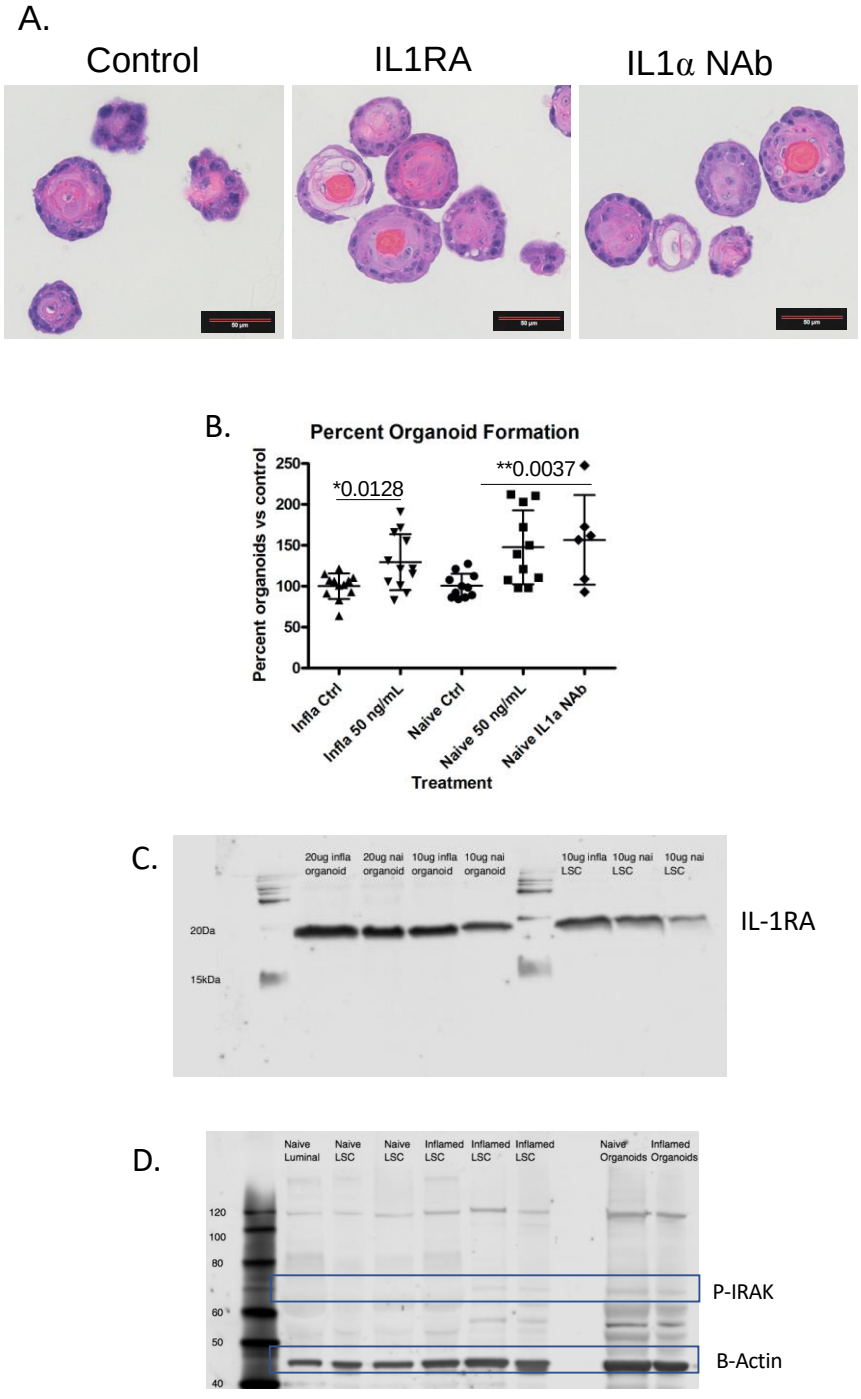

Figure 2.14. Interleukin 1 Receptor Antagonist in 3D Organoids. 3D organoid cultures were treated with 50ng/ml of IL-1RA or a 1:100 dilution of IL-1α neutralizing antibody. **(A)** Representative H&E images demonstrate an increase in stratification and size of treated organoids. **(B)** Treatment also induced a significant increase in organoid numbers. **(C)** Western blot for IL-1RA showed expression in naïve and inflamed LSC and organoids. **(D)** Western blot to assess downstream phosphorylation of IRAK protein proved inconclusive.

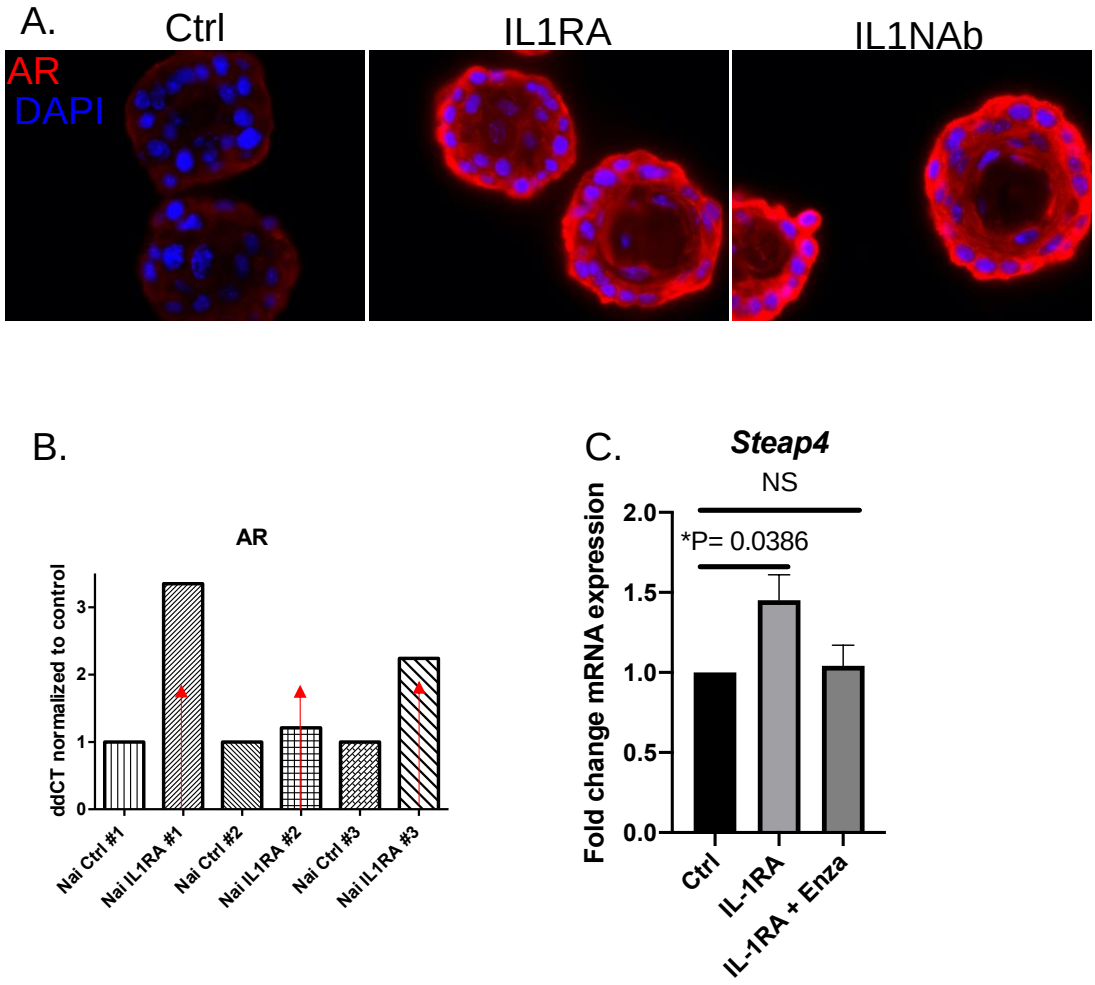

Figure 2.15. Interleukin 1 Receptor Antagonist Impacts Androgen Receptor Signaling. (A) Representative immunofluorescence images show increased AR in naïve organoids treated with 50ng/ml IL-1RA and an IL-1α neutralizing antibody. **(B)** rt-qPCR for Ar showed an upward trend in gene expression in treated organoids and **(C)** significant modulation of AR target gene, *Steap4*, which returned to baseline upon inhibition of AR by Enzalutamide.

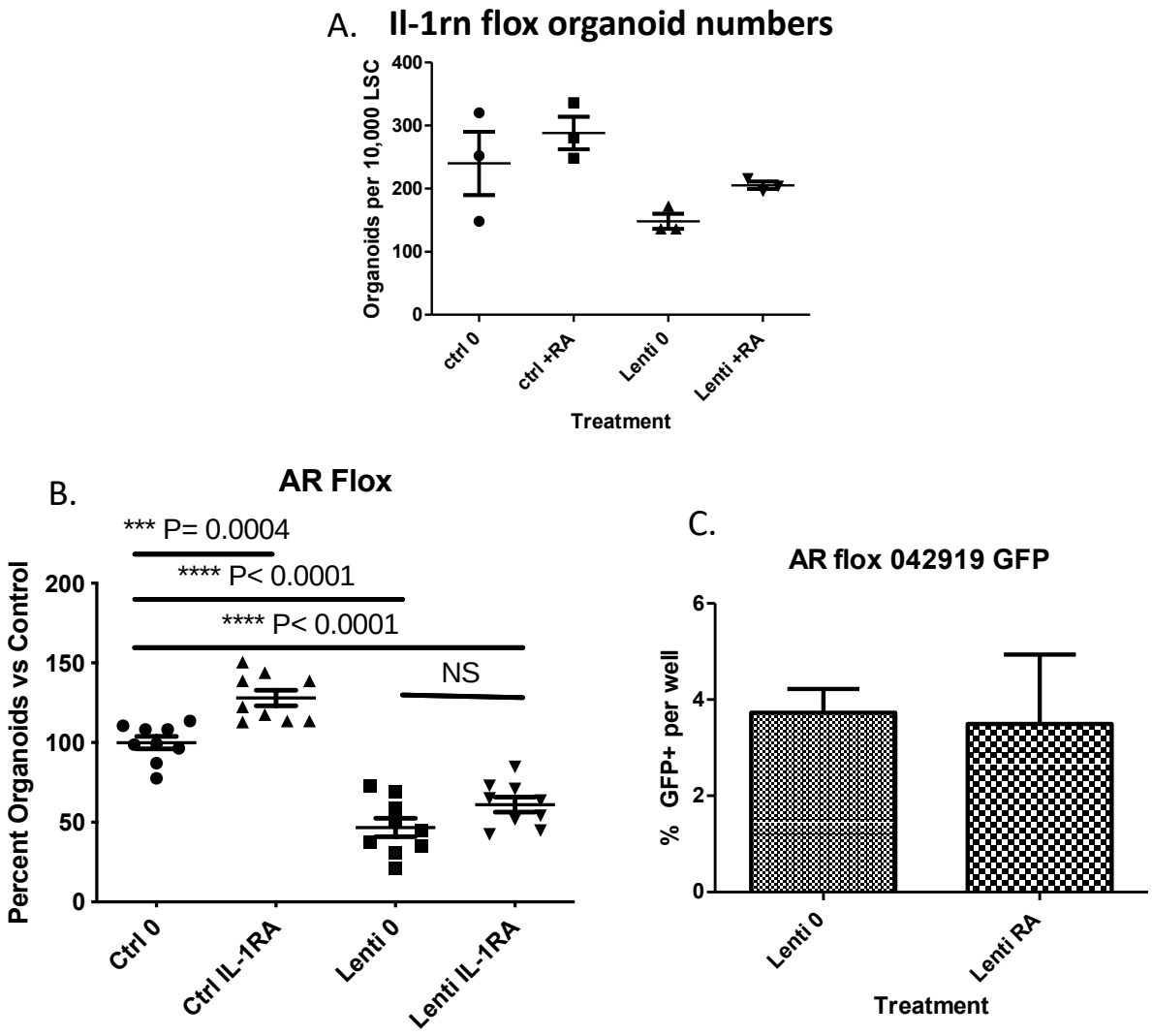

Figure 2.16. Genomic Manipulation of AR and IL-1RA. (**A)** LSC from *Il-1rn* floxed mice were transduced with lentiviral Cre-GFP, resulting in loss of organoid formation. An upward trend in numbers was noted upon treatment with IL-1RA. **(B)** LSC from *Ar* floxed mice were treated in the same manner, with similar results. **(C)** However, there was no rescue of GFP positive organoid formation by addition of IL1-RA to the culture conditions.

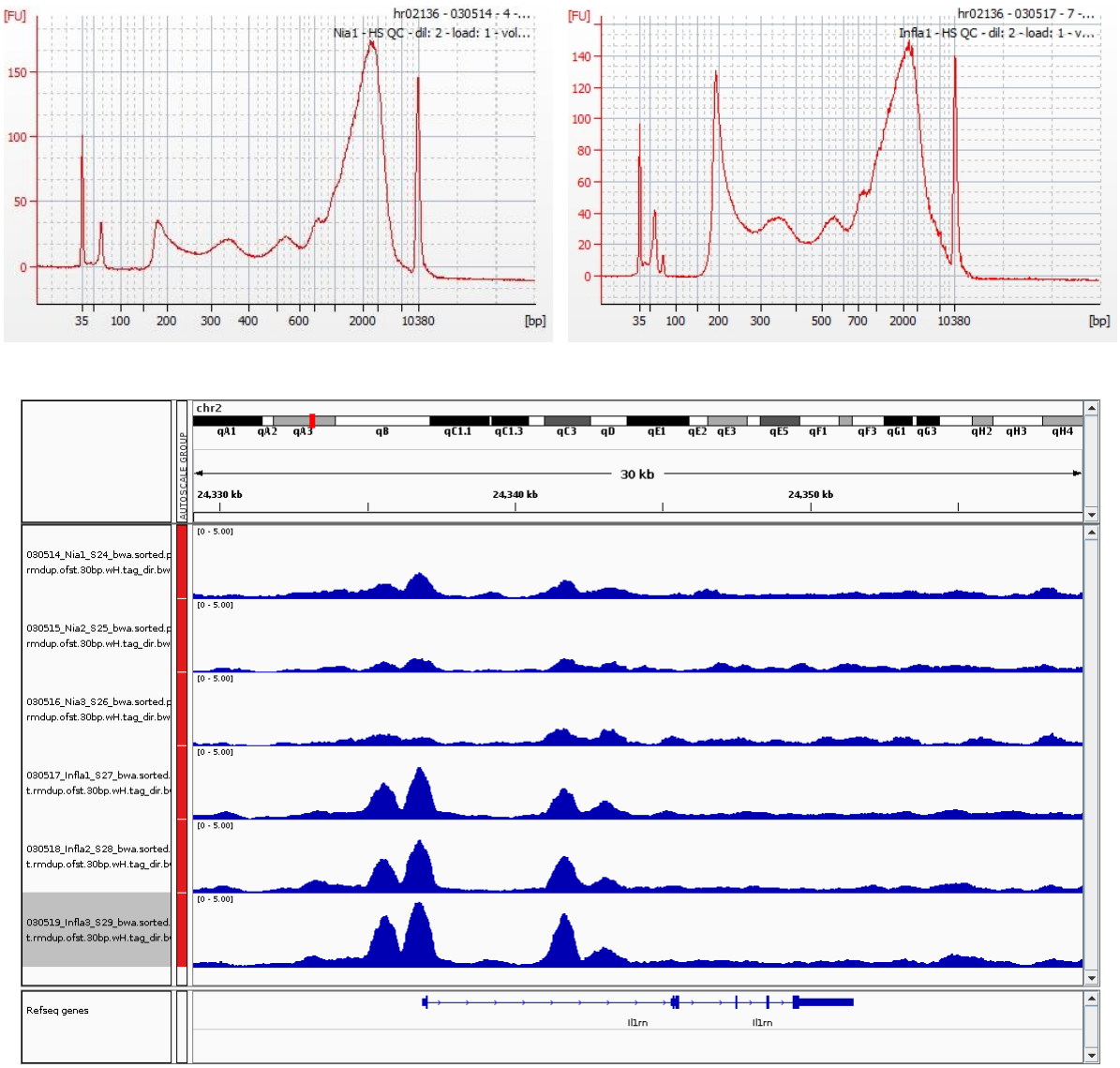

Figure 2.17. ATAC Sequencing. Representative quality control plots showing notable peaks where the DNA was transposed around chromatin regions. The plot below portrays enrichment for open regions in the DNA of inflamed LSC at *il1rn*.

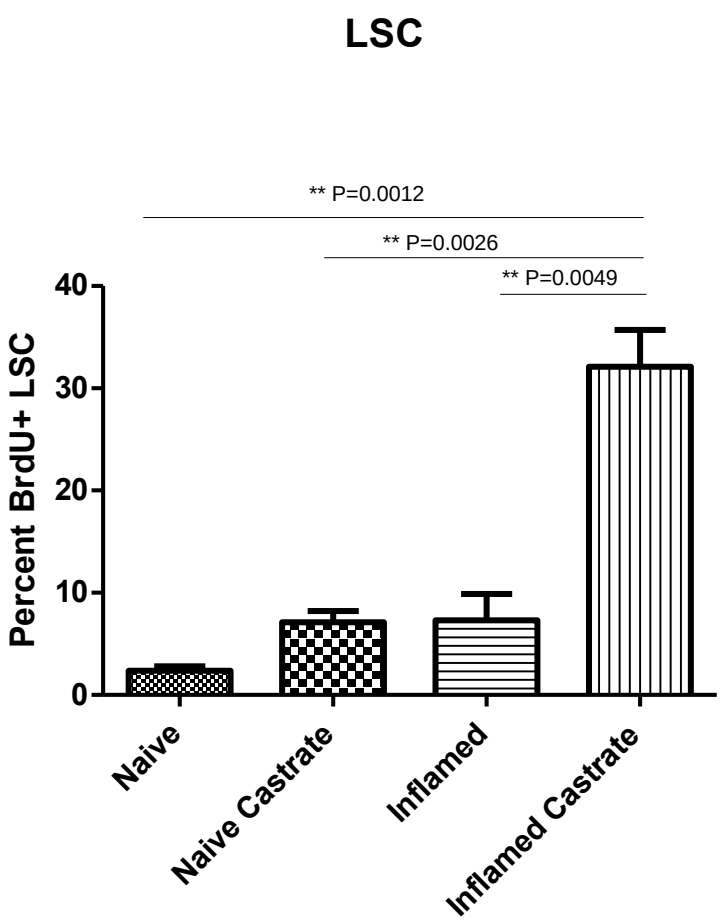

Figure 2.18. Short-term Inflammation Castration and BrdU incorporation. POET3 mice were inflamed on day 0, castrated on day 2, injected with BrdU on day 6, and harvested on day 7. Flow cytometry analysis showed significantly higher proliferation in the LSC isolated from inflamed castrate mice.

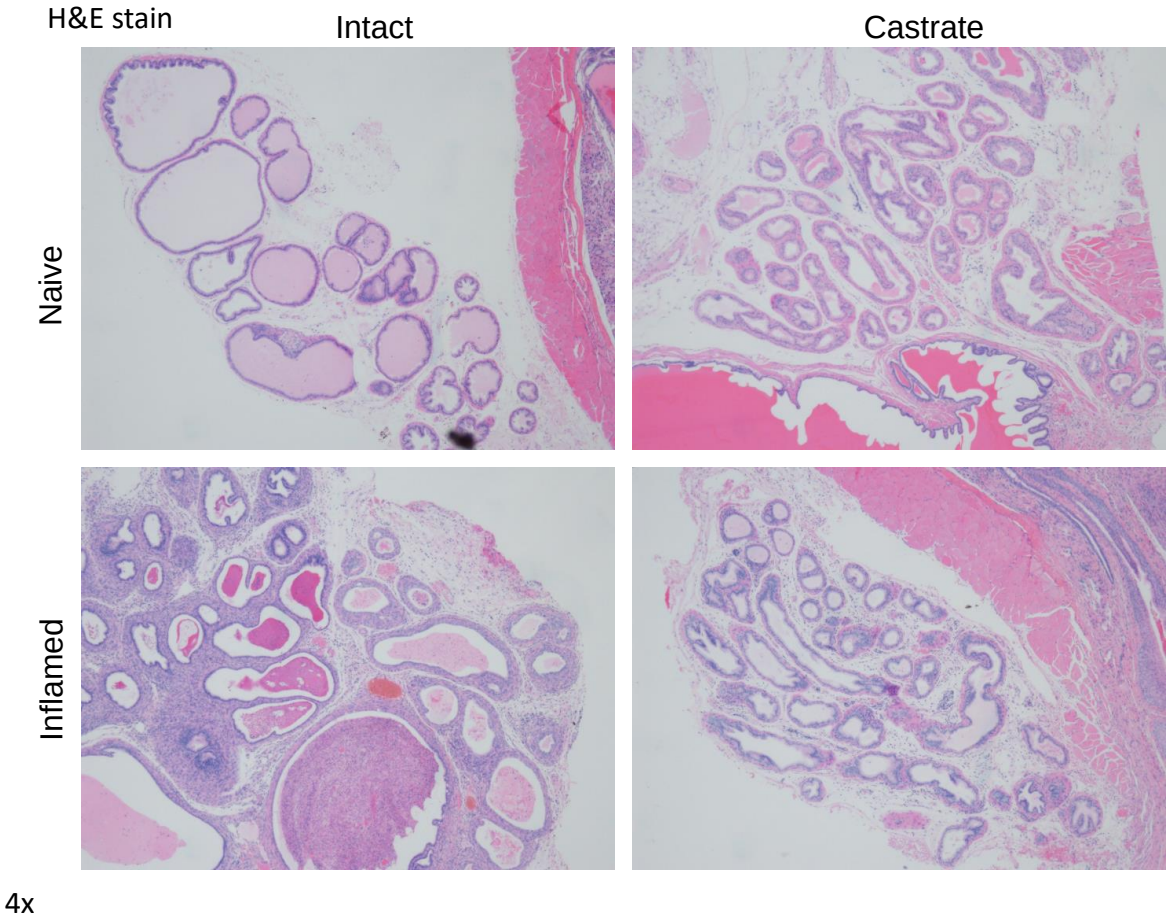

Figure 2.19. Short-term Inflammation Castration Representative H&E Staining. POET3 mice were inflamed on day 0, castrated on day 2, and harvested on day 7. H&E staining shows the state of prostatic tissues under each condition.

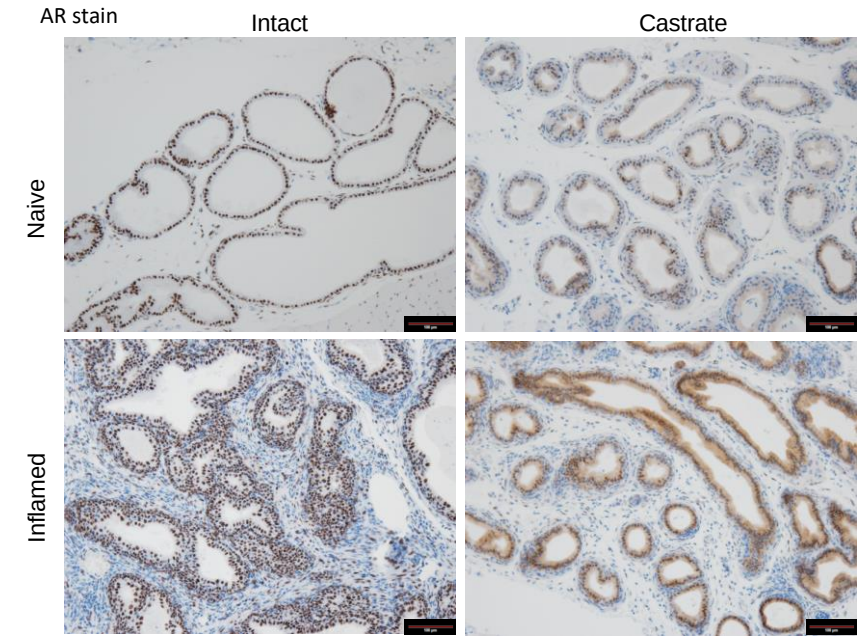

10x; scale bar =100um

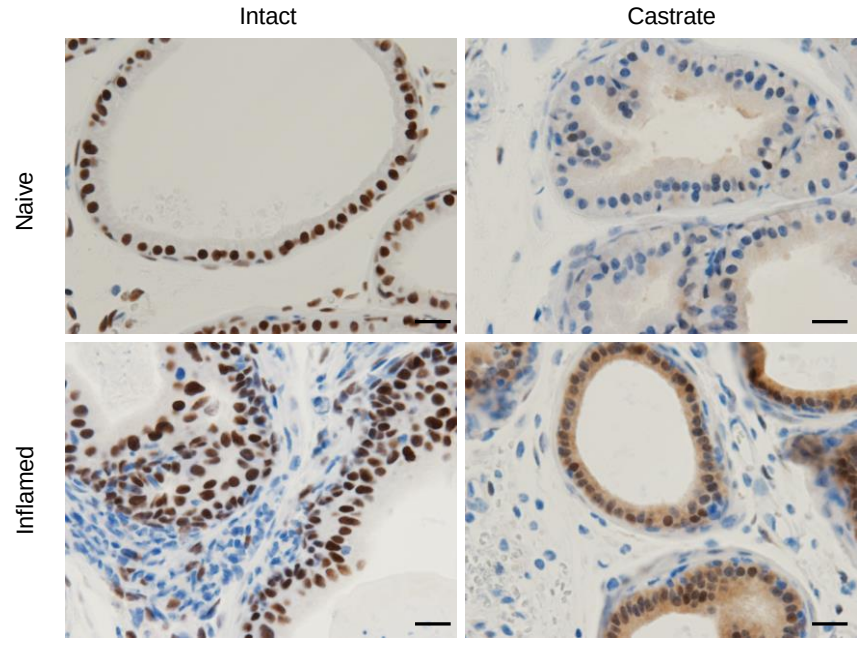

40x; scale bar =20um

Figure 2.20. Short-term Inflammation Castration Representative AR Staining. POET3 mice were inflamed on day 0, castrated on day 2, and harvested on day 7. AR staining shows maintenance of AR staining in inflamed castrate as opposed to naïve castrate.

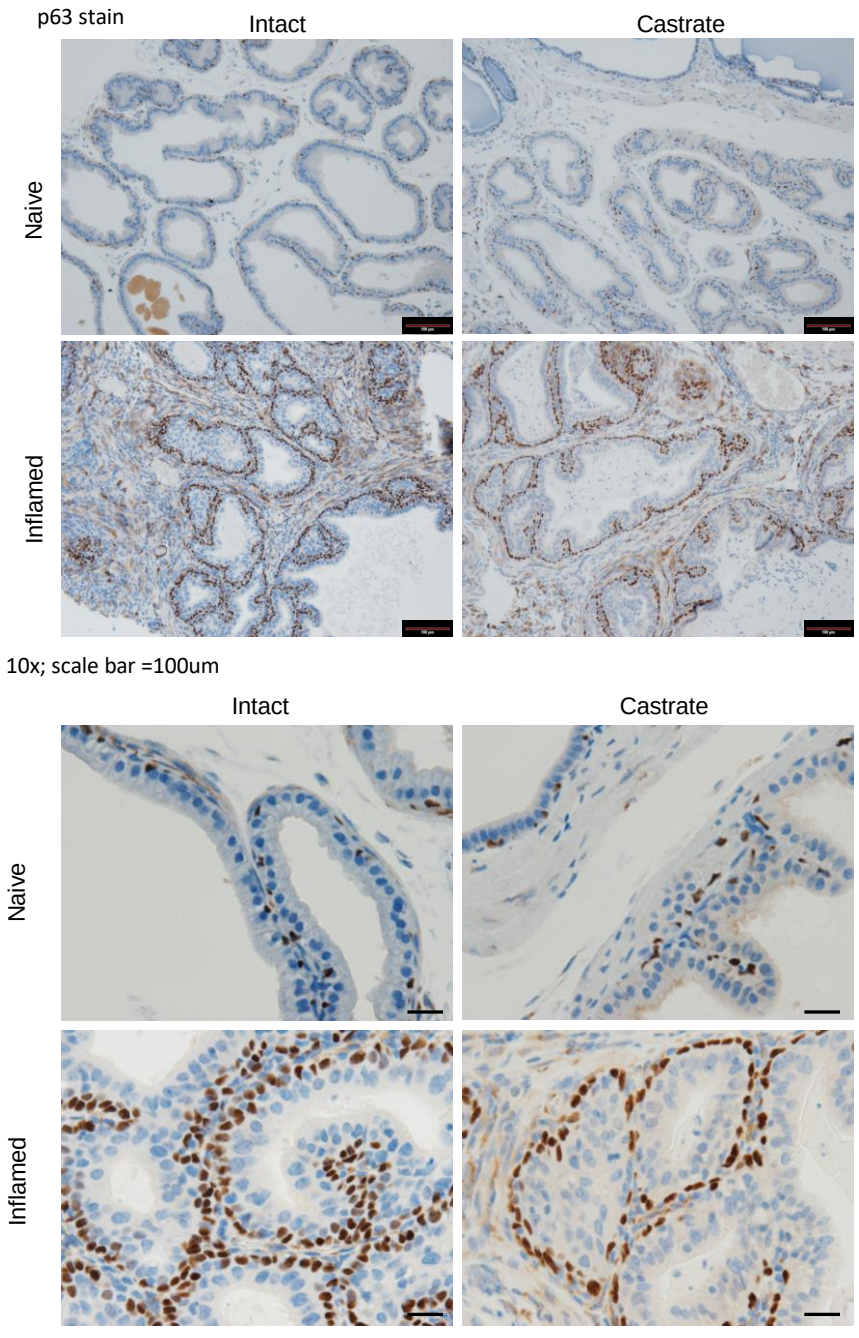

Figure 2.21. Short-term Inflammation Castration Representative p63 Staining. POET3 mice were inflamed on day 0, castrated on day 2, and harvested on day 7. P63 staining shows accumulation of basal cells in the inflamed that are maintained in the inflamed castrate.

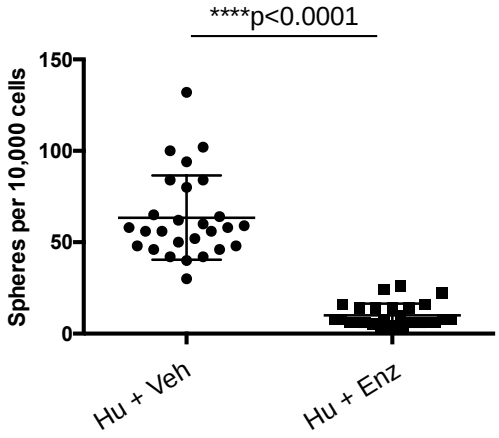

Figure 2.22. Enzalutamide Treatment of Human Organoids. Human PSC enrichments were isolated and cultured in 3D Matrigel with and without Enzalutamide (Enz). Treatment resulted in a significant decrease in organoid numbers.

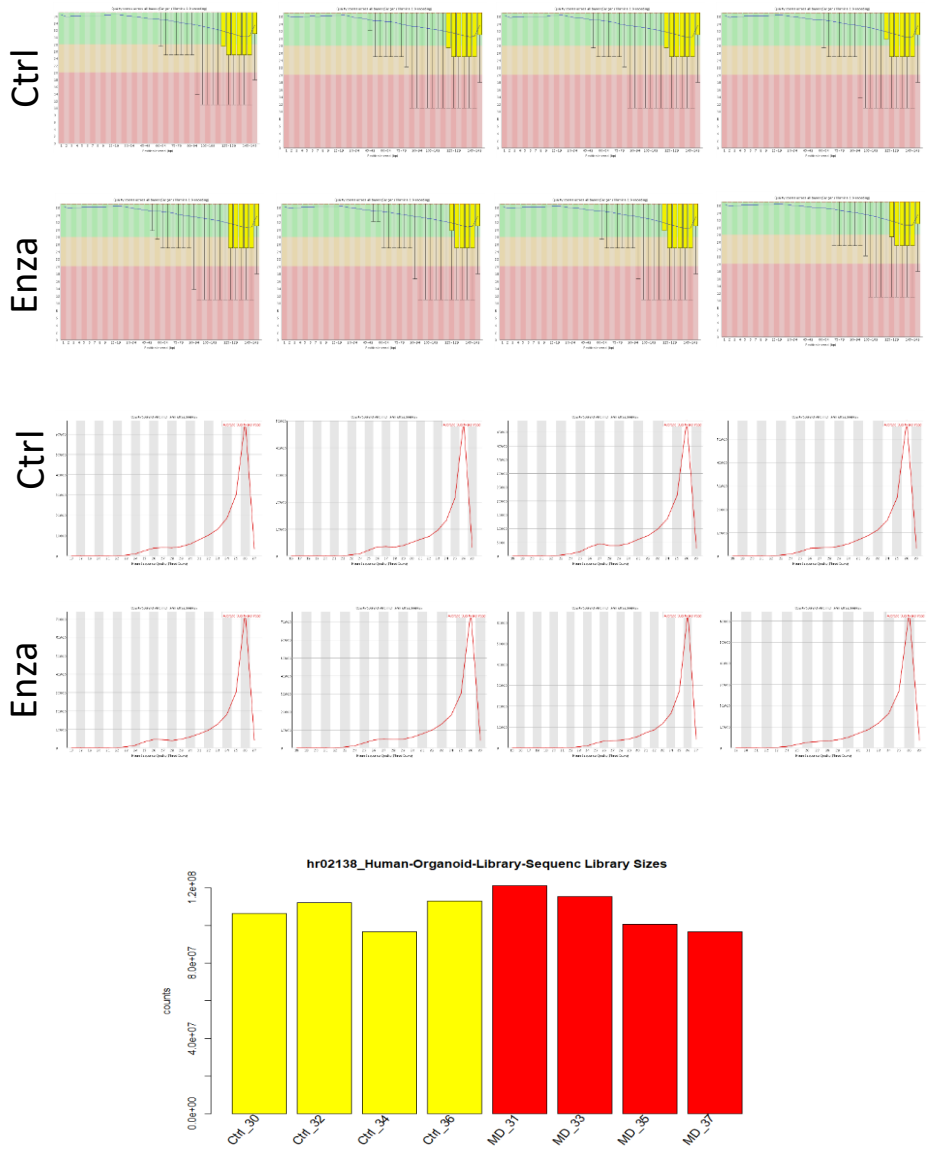

Figure 2.23. Quality Control for RNA Sequencing of Human Organoids (A) Per base sequence quality for the trimmed reads of all samples. The y-axis shows quality scores and the x-axis shows the position in the read. The red line is the median and the blue line is the mean. The yellow box represents the inter-quartile (25%-75%) range, and the upper and lower whiskers represent the 10% and 90% points. The dip in sequence quality at the end of the read is normal and is nearly always observed in Illumina sequencing data. Due in part to trimming, all positions in the reads have high quality. This graph is very typical for what was observed across all read files. **(B)** Per sequence quality score for the trimmed reads of all samples. If a subset of sequences in the FASTQ file have universally low quality scores it will show up in this plot. The Y axis shows the number of sequences and the x axis shows the mean quality score. This plot shows that the reads post-trimming have very high quality. This plot looks very similar to all the other per sequence quality score plots seen across all the trimmed FASTQ files. **(C)** Library size for each sample sequenced. The x-axis gives the sample ID and the y-axis shows the counts (read pairs aligning to features) for each sample. Overall each sample had sufficient reads aligning to perform a differential expression analysis.

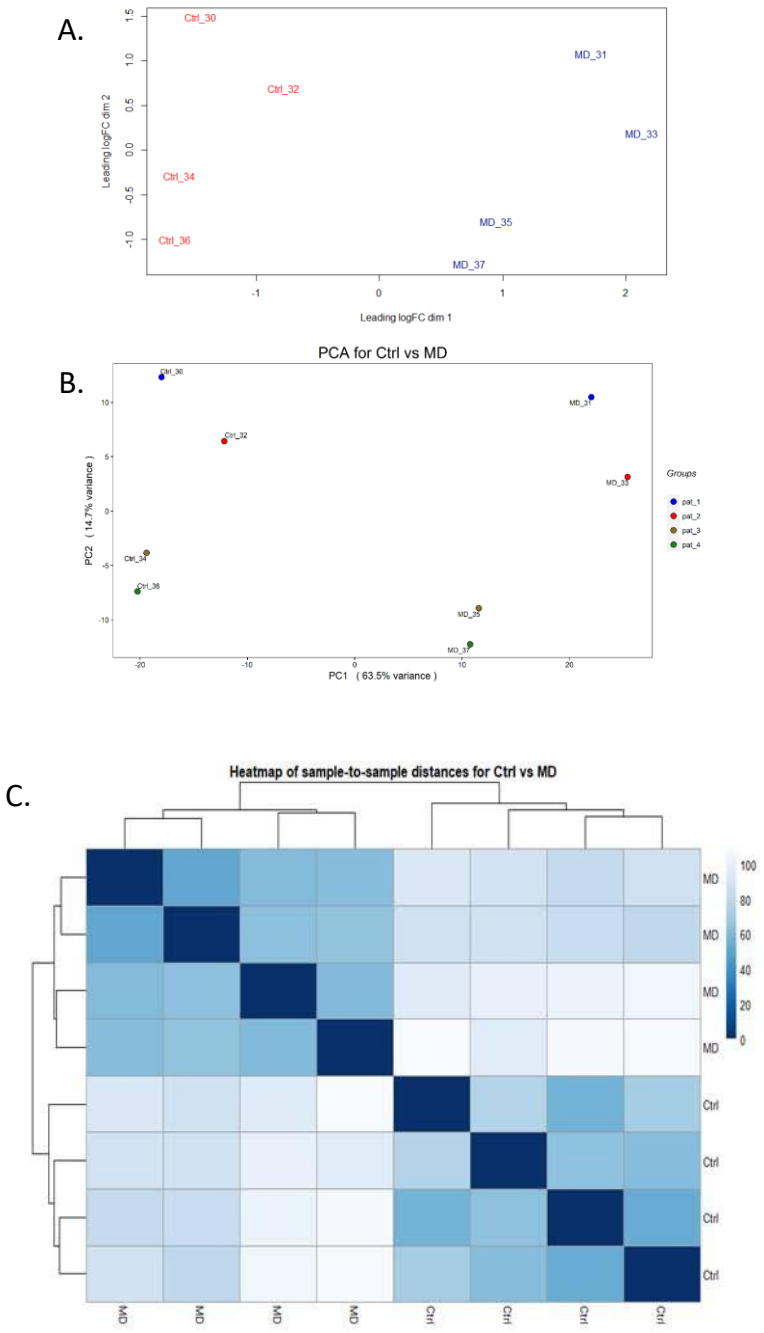

Figure 2.24. Clustering Analysis of Human Organoid RNA Sequencing. (A) MDS plot with libraries colored based on phenotypes. On the plot, baseline samples of "Ctrl" are shown in red; treatment samples of "MD" are shown in blue. The data was normalized in edgeR. It looks that there are clear separations of samples based on conditions. **(B)** PCA plot of libraries. The PCA plot shows that samples are separating based on conditions. Overall, 63.5% of the variance is captured by the first principle component (PC1, shown on the x-axis), and principle component two (PC2, shown on the y-axis) accounts for 14.7% of the variation. Data was normalized in DESeq2 and a regularized log transformation performed prior to doing the PCA. **(C).** A heatmap showing the Euclidian distances between samples, made with the DESeq2 transformed data after a regularized log transformation was performed

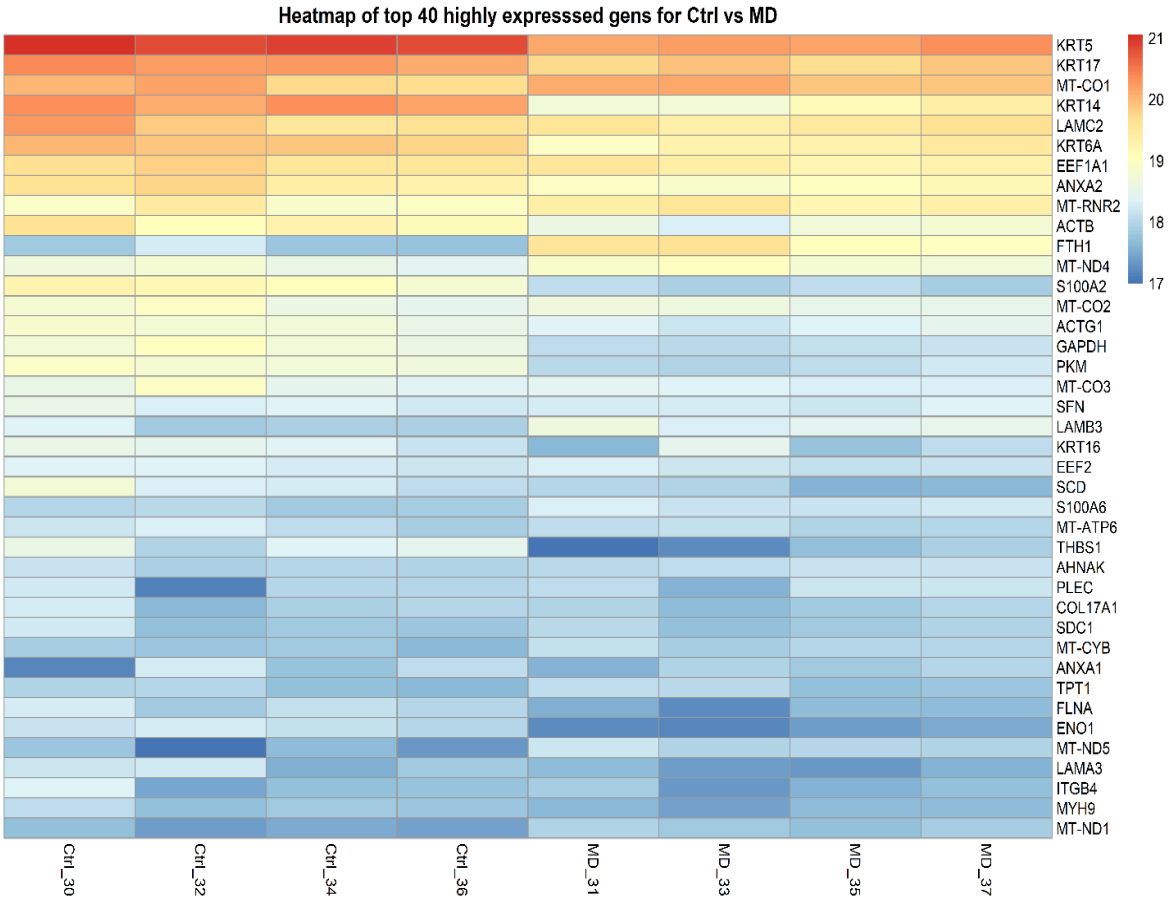

Figure 2.25. Heatmap showing the expression data of the 40 most highly expressed genes of comparison and all samples. The data show normalized counts after a regularized log transformation performed.

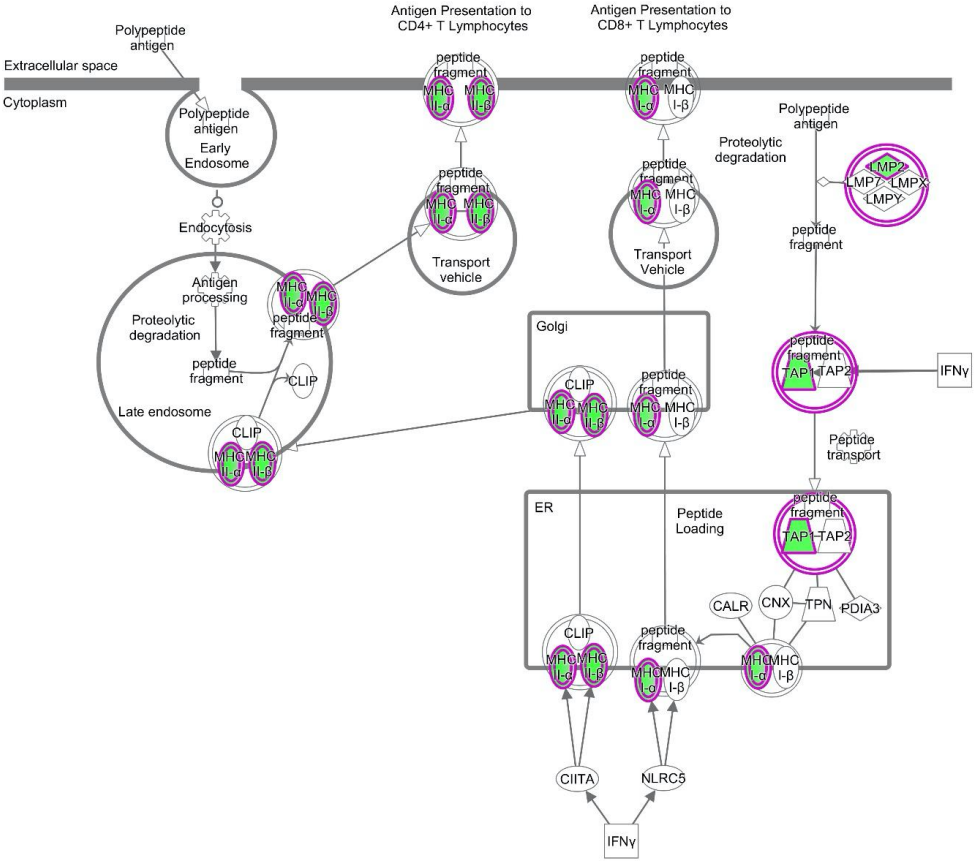

Figure 2.26. Antigen Presentation Canonical Pathway in Human Organoids. The diagram (shown on the next page) shows the antigen presentation pathway, one of the overrepresented pathways found in the BSC naïve versus inflamed comparison by IPA. Nodes represent genes, and node shape represents the class of the gene product, as shown in the legend on the right side of the diagram. Edges indicate the relationship between gene products. Genes in the pathway which are present in the differentially expressed gene list are shown outlined in pink. Upregulated molecules are colored in red and downregulated molecules, if any had been observed, would be colored in green. The intensity of the color indicates the degree of down or upregulation. The expression value used in coloring the molecules was the log p-value.

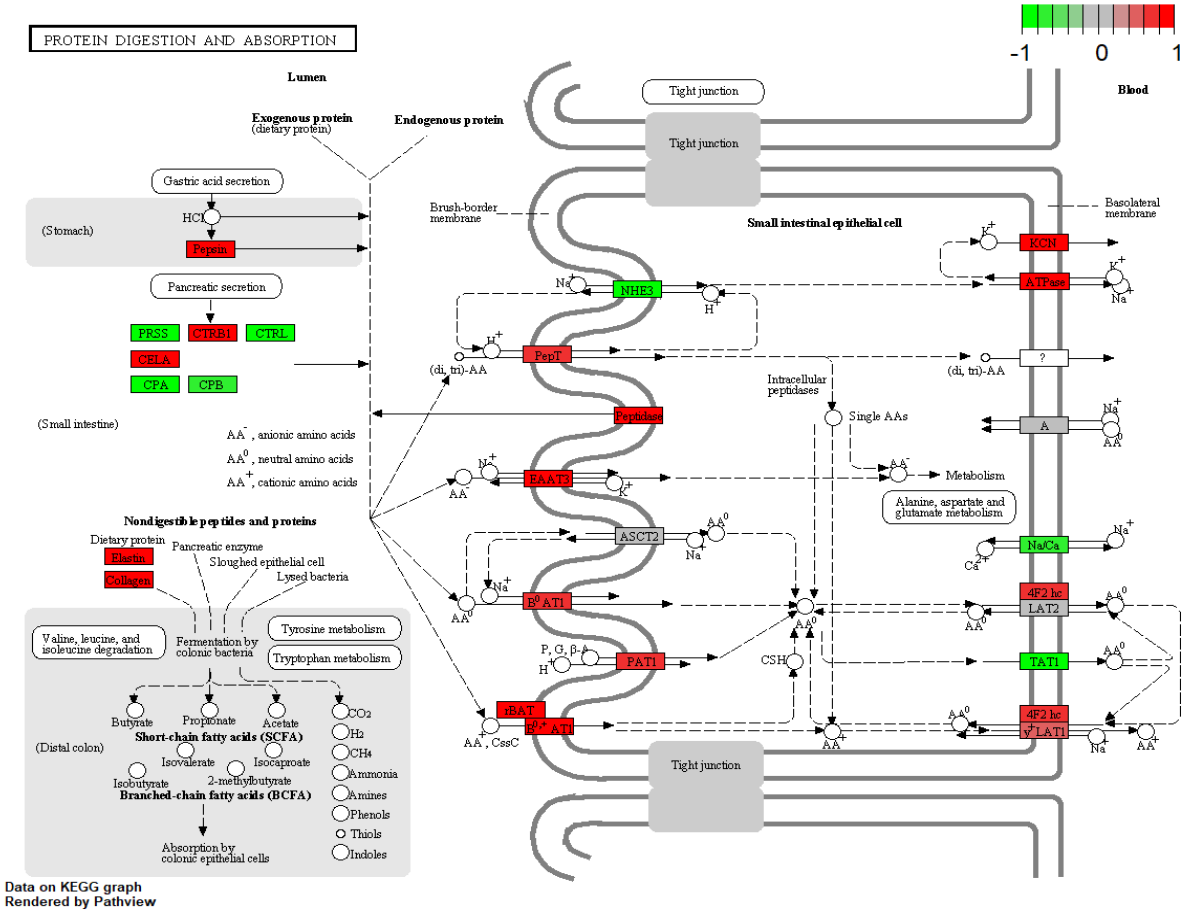

Figure 2.27. Protein Digestion and Absorption (hsa04974) in Human Organoids. The diagram shows the Protein digestion and absorption pathway, one of the overrepresented pathways by PAGE. Nodes represent genes. Edges indicate the relationship between gene products. Genes in the pathway which are present in the differentially expressed gene list are converted as pseudo colors. Upregulated molecules are colored in red, and downregulated molecules are colored in green. The intensity of the color indicates the degree of down or upregulation. The expression value used in coloring the molecules was the log fold-change. Any value outside the (-1,1) limits was truncated to the closest limit.

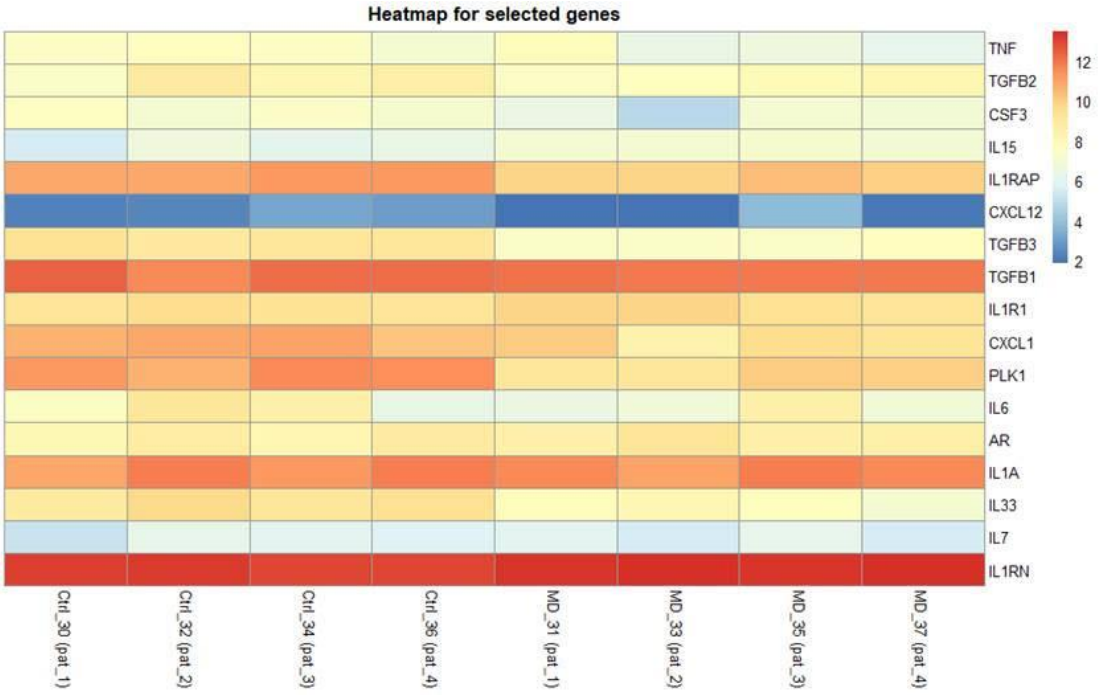

Figure 2.28. Heatmap Showing Expression Data for Genes of Interest. (AR and cytokines). The data show normalized counts after a regularized log transformation performed

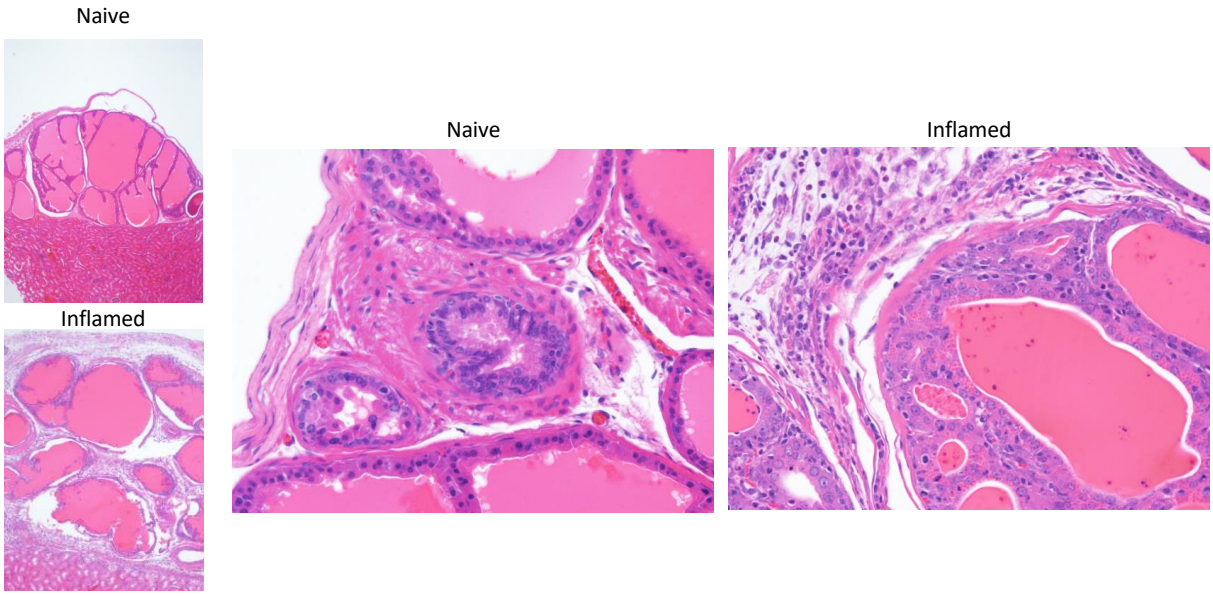

Figure 2.29. Production of Inflammable Recombinant Prostate Grafts in Renal Capsule Assay. Implanted LSC grafts produce tissues that recapitulate POET3 inflammation.

CHAPTER 3. T CELL REGULATION BY ADULT PROSTATE STEM CELLS

3.1 Abstract

Adult prostate stem cells (PSC) are a rare epithelial progenitor population in the prostate. While essential for normal homeostasis, they have also been implicated in hyperplasia and cancer initiation (1-7). Studies show that inflammation fuels hyperplastic diseases through its production of growth factors and cytokines (1, 8, 9); however, the impact of inflammatory factors on PSC and how PSC interact with infiltrating immune cells is not well studied.

To begin to examine the cross talk between epithelial PSC and immune cells, the Prostate Ovalbumin Expressing Transgenic 3 (POET3), an inducible mouse model of autoimmune T cell-induced inflammation was used. The POET3 produces epithelial and stromal hyperplasia, similar to human autoimmune inflammation (10). PSC enrichments were obtained from inflamed and non-inflamed (naïve) mouse prostates by fluorescence activated cell sorting (FACS) as described by Lucaks et al. as lineage$^-$ (CD45$^-$/CD31$^-$) stem cell antigen 1$^-$ (Sca-1) CD49f$^-$ (LSC). Single cell mRNA sequencing (described in the previous chapter) revealed significant regulation of various immune regulatory genes (table). Notably, prostates from inflamed POET3 mice showed a marked enrichment for LSC. While inflamed LSC were also found to be more proliferative, these data suggested that LSC evaded T cell-mediated apoptosis. Coupled with human BPH data indicating prominent T cell populations enriched for exhaustion and anergy genes, it was hypothesized that adult basal prostate stem cells harness immune regulatory capabilities to suppress T cell function and.

The studies described herein demonstrate 1) that LSC from inflamed POET3 mice upregulate multiple immune regulatory genes, 2) possess T cell suppressive capabilities, and 3) begin to characterize the mechanisms by which they suppress T cells. This work provides a foundation for more thorough investigation of rare stem/progenitor cells in immune regulation.

3.2 Introduction

The role of prostatitis, especially chronic prostatitis, in the development and progression of BPH has been a topic of interest for decades (9, 84, 124, 192). The correlation between the

presence of both diseases is well documented; however, the mechanism by which one may lead to or contribute to the other is poorly understood.

Cytotoxic CD8+ T cells are indispensable for clearance of viral infection and tumor cell surveillance. They possess surface receptors (TCR) that recognize specific antigens (140). When CD8+ T cells encounter that specific antigen bound by major histocompatibility complex I (MHC I), they become activated. This is characterized by proliferation, production if interferon gamma (IFNγ), and cytotoxic abilities. To prevent unchecked destruction of tissues, T cell activity is tightly controlled. When those mechanisms of control fail, it may lead to autoimmune and chronic T cell mediated inflammation (140).

Chronic prostatitis is often characterized by a persistent autoimmune component. In fact, T cells that recognizes and responds to native proteins of the prostate have been identified in patients with abacterial prostatitis (153, 193). More recent studies of the prostate have revealed a remarkably complex, dynamic balance between inflammation and immune suppression in the development and progression of hyperplastic disease (9, 27, 84, 194-197). The prostate's capability for immune regulation is made apparent by studies using the POET3 mouse model of autoimmune inflammation, in which adoptive transfer of pre-activated $CD8^+$ OT-I cells leads to epithelial and stromal hyperplasia and an influx of endogenous immune cells which persists as far as 80 days after initial inflammation (10, 166). Rather than causing complete destruction of the prostate by the OT-I, inflamed prostates become enriched for basal cells (Figure 2.21), which may contribute to repopulation of the luminal cells. This epithelial persistence points to a level of control over the infiltrating T cells.

In order to control inflammation, a variety of immune cells can halt $CD8^+$ T cell activity. During disease states such as cancer and chronic inflammation, continual suppression of T cell function may be induced by myeloid cells (especially myeloid derived suppressor cells (MDSC)), mesenchymal cells or by epithelial cancer cells (198-200). Mechanisms of suppression include expression of Arg1 (which can deplete arginine from the local environment, impacting the TCR), production of reactive nitrogen and oxygen species, and activation of T cell exhaustion and anergy through checkpoint ligands such as PD-L1 (166, 201, 202). While studies described above show that prostate stem cells (PSC) survive and proliferate during inflammation, whether they can produce factors to suppress T cell function or survive T cell attack has not been investigated.

Previous studies of POET3 inflammation demonstrate an enrichment and increased proliferative capacity of lineage$^-$, Sca-1$^+$, CD49f$^+$ (LSC) during inflammation (11), suggesting that these cells evade cytotoxic T cell-mediated apoptosis. Notably, an accumulation of LSC persists despite targeted T cell attack, hinting at the presence of suppression and escape mechanisms. Single cell RNA sequencing (scRNA-seq), described above, comparing of non-inflamed (naïve) and inflamed LSC revealed an assortment of up-regulated immune regulatory genes in the inflamed group. While the prominent mechanisms employed by MDSC and mesenchymal stem cells were not differentially expressed, there was significant modulation of multiple immune regulatory and antigen presentation genes. Along with data from human prostate organoids treated with Enzalutamide, which show modulation of the antigen presentation pathway, it is likely that mechanisms employed by PSC to manipulate and evade T cells may also be used by prostate cancer to resist immunotherapy (142, 191, 196).

The studies described herein form the foundation for an exciting new area of study: epithelial stem cell control of T cell function. Experiments compare LSC from inflamed and naïve mice, mature luminal cells, and recognized T cell suppressive MDSC. They also begin to characterize the means by which LSC may suppress T cell function.

3.3 Methods

3.3.1 OT-I Activation for Suppression

RAG1$^{-/-}$OT-I$^+$ mice (a gift from Dr. William Heath, University of Melbourne) were kept according to PACUC conditions described above. To isolate CD8$^+$ OT-I T cells, spleens from RAG1$^{-/-}$OT-I$^+$ mice were ground between frosted slides in complete RPMI-1640 medium. The resulting cell slurry was filtered through a 70 μm cell strainer before treatment with Ammonium-Chloride-Potassium (ACK) lysis buffer to remove red blood cells. Remaining splenocytes were re suspended in complete RPMI-1640, counted, and plated 2x10^6 in 24-well plates with added beta-mercaptoethanol and 1μg/ml SIINFEKL peptide (Bachem). These were allowed to activate for 24 hours before purification using FicoLite L/M according to manufacturer protocol.

3.3.2 Cell Sorting

To isolate murine MDSC, inflamed POET3 prostates were harvested and digested as described in chapter 2. Isolation was performed by Purdue Flow Cytometry and Cell Separation Core Facility.

Cells were stained using:
Zombie Live/Dead Fixable Viability Dye (Biolegend)
FITC- CD31 (Biolegend clone MEC13.3)
FITC- CD45 (Biolegend clone 30-F11)
APC- Sca-1 (Biolegend clone E13-16.7)
PE- CD49f (Biolegend clone eBioGoH3)
CD11b (Biolegend clone M1/70)
Ly-6C (Biolegend clone HK1.4)
Ly-6G (Biolegend clone 1A8)

3.3.3 Liquid Organoid Culture and Suppression Assay

After FicoLite purification of pre activated OT-I T cells, these were combined with target cells at varying ratios between 1:1 and 1:4 in 96-well ultra-low adhesion plates (Corning) with or without 0.4 μm transwell inserts and with or without treatments. All suppression assays were performed under hypoxic conditions (1% O_2). MDSC suppression experiments were performed in complete RPMI with 1μg/ml SIINFEKL peptide. LSC suppression experiments were performed in PrEGM (Lonza) with 5% Matrigel and 1μg/ml SIINFEKL peptide.

Treatments:
PD-L1 neutralizing antibody
L-NMMA
IDO1 inhibitor

3.3.4 Flow Cytometry

All samples were analyzed using a BD LSRFortessa flow cytometer. Subsequent evaluation was performed using FlowJo software.

3.4 Results

The control and suppression of T cell activity is essential for the prevention of autoimmune disease; however under pathological conditions, it may interfere with the necessary T cell function or contribute to chronic inflammation (166, 201). Various mechanisms of T cell control have been

demonstrated to occur in immune and mesenchymal cells. These include mechanisms such as nitric oxide synthesis, production of reactive oxygen species, depletion of essential factors from the local environment, activation of immune checkpoints by ligands such as PD-L1, or production of exosomes containing these factors (200, 203, 204). Single cell RNA sequencing (scRNA-seq) described in chapter two revealed differential expression of various genes associated with immune regulation (Table 3.1). While single cell RNA sequencing (scRNA-seq) did not reveal expression of suppressive genes commonly studied in MDSC (*Arg1*, *Nos2*, *Cd274* (the gene for PD-L1)), there was significant up regulation of *Ido1* and *Ido2*. Increased protein expression of PD-L1 (CD274) was also seen by flow cytometry (Figure 3.1).

The presence of immune regulatory gene expression was novel and unexpected; however, it was important to validate the finding with *in vitro* studies. To test whether the LSC were suppressive, and whether their mechanism of suppression was PD-L1, suppression assays were performed combining freshly isolated LSC and pre-activated OT-I cells at ratios of 1:1 and 1:2, with and without an anti PD-L1 neutralizing antibody. Indeed, freshly isolated inflamed LSC were able to suppress OT-I proliferation, and the addition of PD-L1 neutralizing antibody had minimal effect on T cell suppression (Figure 3.2). Based on these data, the ratio of 1:2 was determined to be appropriate for further experiments.

Since the scRNA-seq data compared naïve and inflamed LSC, it was hypothesized that immune regulatory mechanisms were activated by inflammation. Additionally, since luminal cells were not present in FACS of inflamed prostates but were apparent on histology slides (Figure 2.20) whether mature luminal cells could suppress was also tested. To assess this, a comparison of inflamed and naïve LSC was performed. Indeed, inflamed LSC were highly suppressive while luminal cells and naïve LSC were unable to suppress T cell proliferation (Figure 3.3).

The next area of interest from the scRNA-seq data was the over expression of *Ido1* and *Ido2* (Indoleamine 2, 3-dioxygenase 1 and 2). IDO1 and IDO2 function to suppress T cell activity via depletion of tryptophan from the local environment, thereby inhibiting T cell receptor (TCR) function (205-207). It was also of interest to examine recognized MDSC suppressive factors that may have been missed by scRNA-seq. Thus, a functional evaluation of these factors was performed to compare the suppression of LSC and MDSC, using inhibitors for IDO1 (Epacadostat, EPA), nitric oxide synthetase (NG-monomethyl-L-arginine, L-NMMA), and the anti PD-L1 neutralizing antibody. Consistent with previous experiments (166, 208), MDSC suppression was

inhibited by addition of LNMMA and the anti PD-L1 neutralizing antibody had minimal effect (Figure 3.3). Intriguingly, none of the tested inhibitors had an effect on LSC suppressive abilities. These data suggested that a novel suppressive mechanism may be at play.

Both soluble (reactive oxygen species, media depletion) and contact-mediated (PD-L1, checkpoint, anergy, and exhaustion induction) mechanisms can suppress T cell activity. To narrow the search for suppressive mechanisms, transwell assays were employed. Under these conditions, cell-cell contact cannot occur; thus, suppression under transwell separation would indicate that a depletion mechanism or secreted factor would be at play while loss of suppression would suggest ligand- or contact-mediated factors. While replicate experiments are necessary, transwell assay revealed that contact was required for LSC suppression of OT-I proliferation (Figure 3.4). This helped us rule out most secreted and depletion factors, allowing the focus to turn to ligand- and contact-dependent mechanisms for future experiments.

3.5 Discussion and future directions

These studies are still in the early stages; however, they point to a novel and essential role for PSC in the immune landscape of prostate disease. The implications for prostate disease are many. If the hypothesis that PSC can survive and proliferate in the chronic inflammatory environment is correct, it would be reasonable that they would be the source of the prominent basal cell nodules found in BPH (7). Coupled with the findings described in Chapter 2, that PSC-derived organoids from inflamed POET3 mice resisted treatment with enzalutamide, and those from BPH patient samples underwent changes in antigen presentation and protein digestion pathways upon treatment, these cells may also contribute to treatment resistance in BPH (120).

The findings also have implications for prostate cancer, which is resistant to immune therapy (200, 209). As studies by Zhang et al. demonstrated that prostate cancer aggression could be linked to stem cell characteristics (190), and those by Olson et al. showed that castrate conditions (which increase the presence of basal and stem cells) may be linked to poor response to CAR T cells (191), the studies of PSC immune evasion may help to explain these features. Continued research into the precise mechanisms by which these cells exert suppressive, and possibly evasive, functions would provide novel treatment targets for improved patient outcomes.

Based on the early experiments performed here, it is clear that PSC from inflamed POET3 possess strong suppressive capabilities. Whether the effects are maintained long-term and what the

biological impact of this function may be remains unclear. These aspects are the topic of studies proposed in an R21 grant (with fundable score) and will be investigated by similar experiments. Future studies will focus on manipulation of contact-dependent factors identified by scRNA-seq including *Ceacam1* (exhaustion), *Entpd1* (CD39, TCR dysfunction), and *Bax* (anergy) (210-214). These factors will be manipulated *in vitro* using inhibitors as well as *in vivo* by floxed and knockout mouse models.

Additional studies will be performed to assess the *in vivo* impact of PSC suppression. Using implanted inflammable POET3 grafts (Figure 2. 29) in transgenic mice deficient in suppressive MDSC and T regulatory cells, as well as MDSC depletion experiments, the extent of their T cell regulatory effects will be assessed.

To summarize, the data presented herein revealed a novel suppressive mechanism unique to PSC from inflamed prostates. The implications are broad and extend into the areas of BPH and cancer development and treatment resistance. These experiments set the foundation for continued and thorough study of this distinct epithelial stem cell ability.

3.6 Tables and Figures

Table 3.1. Differential Expression of Immune Regulatory Genes in Inflamed LSC vs Naïve

T cell regulation		
Gene Name	adj_p_value	log2_fc
Adam10	0.01535574	1.927666719
Bmp3	0.00046424	5.877048779
Ceacam1	0.007101201	1.8667483
Csf3	5.15E-05	2.326910404
Ido1	2.30E-28	13.08870682
Ido2	2.63E-06	8.462788392
Il33	0.001841485	1.637497658
Ptgs2	4.32E-06	4.089007094
Tgfb3	0.007213591	-7.108446735
Chemotaxis		
Cxcl10	4.22E-06	-0.946684395
Cxcl11	1.17E-06	11.04156491
Cxcl14	0.007440989	-3.150854634
Cxcl2	2.83E-09	3.316014635
Major Histocompatibility Complex		
H2.aa	1.62E-33	13.6357606
H2.ab1	2.91E-57	12.5295688
H2.d1	2.72E-20	3.197001867
H2.dmb1	8.91E-11	4.319302736
H2.k1	1.35E-17	2.838142069
H2.m3	1.12E-09	4.596759514
H2.q5	2.34E-12	9.851578536
H2.q7	2.10E-05	5.772970109

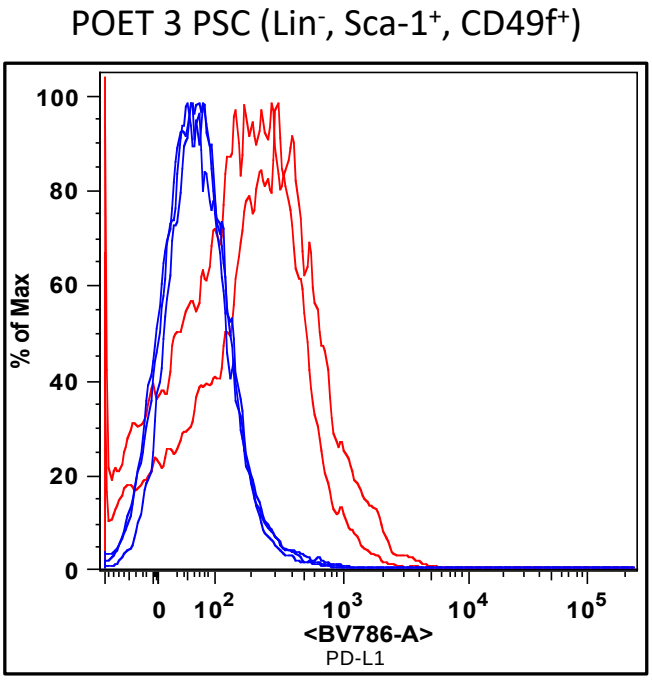

Figure 3.1. PD-L1 expression in naïve and inflamed LSC Flow cytometry analysis revealed increased PD-L1 in inflamed LSC

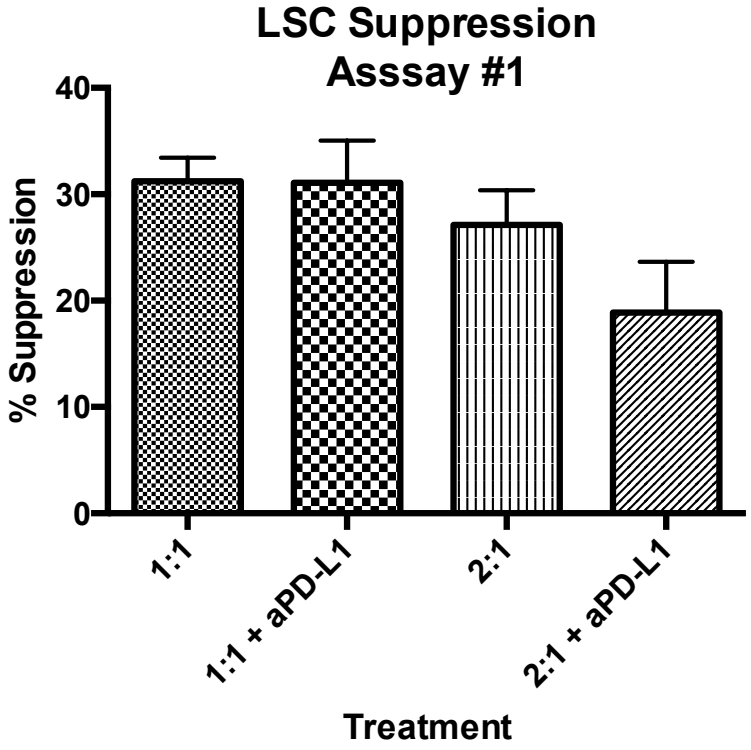

Figure 3.2. Suppression Assay With Anti-PD-L1 Neutralizing Antibody Despite the increase in PD-L1 in inflamed LSC, there was little effect of an anti PD-L1 antibody on suppression of T cells.

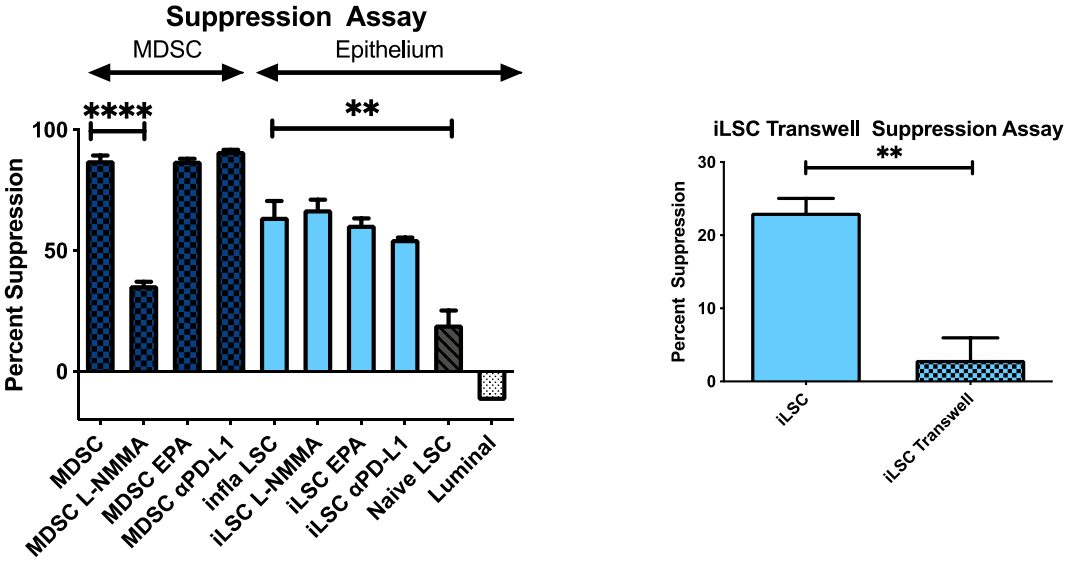

Figure 3.3. LSC Suppression Assays. An assessment of EdU incorporation to pre-activated OT-I T cells co cultured with MDSC, luminal cells, or LSC from inflamed and naïve mice. These were treated with inhibitors of various mechanisms of suppression that are recognized in other cell types. An anti PD-L1 antibody, L-NMMA, and Epacadostat (EPA) had no effect on suppression. Separation by transwell inserts significantly decreased LSC suppressive capabilities.

REFERENCES

1. Isaacs JT, Coffey DS. Etiology and disease process of benign prostatic hyperplasia. Prostate Suppl. 1989;2:33-50. Epub 1989/01/01. PubMed PMID: 2482772.

2. Jeong JH, Park SJ, Dickinson SI, Luo JL. A Constitutive Intrinsic Inflammatory Signaling Circuit Composed of miR-196b, Meis2, PPP3CC, and p65 Drives Prostate Cancer Castration Resistance. Mol Cell. 2017;65(1):154-67. Epub 2016/12/29. doi: 10.1016/j.molcel.2016.11.034. PubMed PMID: 28041912; PMCID: PMC5218896.

3. Lawson DA, Zong Y, Memarzadeh S, Xin L, Huang J, Witte ON. Basal epithelial stem cells are efficient targets for prostate cancer initiation. Proc Natl Acad Sci U S A. 2010;107(6):2610-5. Epub 2010/02/06. doi: 10.1073/pnas.0913873107

0913873107 [pii]. PubMed PMID: 20133806; PMCID: 2823887.

4. Rybak AP, Bristow RG, Kapoor A. Prostate cancer stem cells: deciphering the origins and pathways involved in prostate tumorigenesis and aggression. Oncotarget. 2015;6(4):1900-19. Epub 2015/01/18. doi: 2953 [pii]. PubMed PMID: 25595909; PMCID: 4385825.

5. Taylor RA, Toivanen R, Risbridger GP. Stem cells in prostate cancer: treating the root of the problem. Endocr Relat Cancer. 2010;17(4):R273-85. Epub 2010/09/23. doi: 10.1677/ERC-10-0145. PubMed PMID: 20660571.

6. Tomasetti C, Vogelstein B. Cancer etiology. Variation in cancer risk among tissues can be explained by the number of stem cell divisions. Science. 2015;347(6217):78-81. doi: 10.1126/science.1260825. PubMed PMID: 25554788; PMCID: PMC4446723.

7. Henry G, Malewska A, Mauck R, Gahan J, Hutchinson R, Torrealba J, Francis F, Roehrborn C, Strand D. Molecular pathogenesis of human prostate basal cell hyperplasia. Prostate. 2017;77(13):1344-55. Epub 2017/08/11. doi: 10.1002/pros.23394. PubMed PMID: 28795417; PMCID: PMC5580247.

8. Gurel B, Lucia MS, Thompson IM, Jr., Goodman PJ, Tangen CM, Kristal AR, Parnes HL, Hoque A, Lippman SM, Sutcliffe S, Peskoe SB, Drake CG, Nelson WG, De Marzo AM, Platz EA. Chronic inflammation in benign prostate tissue is associated with high-grade prostate cancer in the placebo arm of the prostate cancer prevention trial. Cancer Epidemiol Biomarkers Prev. 2014;23(5):847-56. Epub 2014/04/22. doi: 10.1158/1055-9965.EPI-13-1126 1055-9965.EPI-13-1126 [pii]. PubMed PMID: 24748218; PMCID: 4012292.

9. De Nunzio C, Kramer G, Marberger M, Montironi R, Nelson W, Schröder F, Sciarra A, Tubaro A. The controversial relationship between benign prostatic hyperplasia and prostate cancer: the role of inflammation. Eur Urol. 2011;60(1):106-17. Epub 2011/04/09. doi: 10.1016/j.eururo.2011.03.055. PubMed PMID: 21497433.

10. Haverkamp JM, Charbonneau B, Crist SA, Meyerholz DK, Cohen MB, Snyder PW, Svensson RU, Henry MD, Wang HH, Ratliff TL. An inducible model of abacterial prostatitis induces antigen specific inflammatory and proliferative changes in the murine prostate. Prostate. 2011;71(11):1139-50. Epub 2011/06/10. doi: 10.1002/pros.21327. PubMed PMID: 21656824; PMCID: 3136647.

11. Wang HH, Wang L, Jerde TJ, Chan BD, Savran CA, Burcham GN, Crist S, Ratliff TL. Characterization of autoimmune inflammation induced prostate stem cell expansion. Prostate. 2015;75(14):1620-31. Epub 2015/07/16. doi: 10.1002/pros.23043. PubMed PMID: 26174474.

12. Ittmann M. Anatomy and Histology of the Human and Murine Prostate. Cold Spring Harb Perspect Med. 2018;8(5). Epub 2018/05/01. doi: 10.1101/cshperspect.a030346. PubMed PMID: 29038334; PMCID: PMC5932577.

13. McNeal JE. The zonal anatomy of the prostate. Prostate. 1981;2(1):35-49. doi: 10.1002/pros.2990020105. PubMed PMID: 7279811.

14. Timms BG. Prostate development: a historical perspective. Differentiation. 2008;76(6):565-77. Epub 2008/05/07. doi: 10.1111/j.1432-0436.2008.00278.x. PubMed PMID: 18462432.

15. Verze P, Cai T, Lorenzetti S. The role of the prostate in male fertility, health and disease. Nat Rev Urol. 2016;13(7):379-86. Epub 2016/06/01. doi: 10.1038/nrurol.2016.89. PubMed PMID: 27245504.

16. Shappell SB, Thomas GV, Roberts RL, Herbert R, Ittmann MM, Rubin MA, Humphrey PA, Sundberg JP, Rozengurt N, Barrios R, Ward JM, Cardiff RD. Prostate pathology of genetically engineered mice: definitions and classification. The consensus report from the Bar Harbor meeting of the Mouse Models of Human Cancer Consortium Prostate Pathology Committee. Cancer Res. 2004;64(6):2270-305. doi: 10.1158/0008-5472.can-03-0946. PubMed PMID: 15026373.

17. Nath D, White JR, Bratslavsky G, Kotula L. Identification, Histological Characterization, and Dissection of Mouse Prostate Lobes for In Vitro 3D Spheroid Culture Models. J Vis Exp. 2018(139). Epub 2018/09/18. doi: 10.3791/58397. PubMed PMID: 30295668; PMCID: PMC6235197.

18. Oliveira DS, Dzinic S, Bonfil AI, Saliganan AD, Sheng S, Bonfil RD. The mouse prostate: a basic anatomical and histological guideline. Bosn J Basic Med Sci. 2016;16(1):8-13. Epub 2016/02/10. doi: 10.17305/bjbms.2016.917. PubMed PMID: 26773172; PMCID: PMC4765945.

19. Fujimoto N, Akimoto Y, Suzuki T, Kitamura S, Ohta S. Identification of prostatic-secreted proteins in mice by mass spectrometric analysis and evaluation of lobe-specific and androgen-dependent mRNA expression. J Endocrinol. 2006;190(3):793-803. doi: 10.1677/joe.1.06733. PubMed PMID: 17003280.

20. Mills JS, Needham M, Parker MG. Androgen regulated expression of a spermine binding protein gene in mouse ventral prostate. Nucleic Acids Res. 1987;15(19):7709-24. doi: 10.1093/nar/15.19.7709. PubMed PMID: 3502715; PMCID: PMC306302.

21. Leroy BE, Northrup N. Prostate cancer in dogs: comparative and clinical aspects. Vet J. 2009;180(2):149-62. Epub 2008/09/10. doi: 10.1016/j.tvjl.2008.07.012. PubMed PMID: 18786842.

22. Leav I, Schelling KH, Adams JY, Merk FB, Alroy J. Role of canine basal cells in postnatal prostatic development, induction of hyperplasia, and sex hormone-stimulated growth; and the ductal origin of carcinoma. Prostate. 2001;48(3):210-24. doi: 10.1002/pros.1100. PubMed PMID: 11494337.

23. Madewell BR, Gandour-Edwards R, DeVere White RW. Canine prostatic intraepithelial neoplasia: is the comparative model relevant? Prostate. 2004;58(3):314-7. doi: 10.1002/pros.10338. PubMed PMID: 14743472.

24. Rosenthal N, Brown S. The mouse ascending: perspectives for human-disease models. Nat Cell Biol. 2007;9(9):993-9. doi: 10.1038/ncb437. PubMed PMID: 17762889.

25. Berquin IM, Min Y, Wu R, Wu H, Chen YQ. Expression signature of the mouse prostate. J Biol Chem. 2005;280(43):36442-51. Epub 2005/07/29. doi: 10.1074/jbc.M504945200. PubMed PMID: 16055444.

26. McNeal JE. Origin and evolution of benign prostatic enlargement. Invest Urol. 1978;15(4):340-5. PubMed PMID: 75197.

27. De Marzo AM, Platz EA, Sutcliffe S, Xu J, Grönberg H, Drake CG, Nakai Y, Isaacs WB, Nelson WG. Inflammation in prostate carcinogenesis. Nat Rev Cancer. 2007;7(4):256-69. doi: 10.1038/nrc2090. PubMed PMID: 17384581; PMCID: PMC3552388.

28. Noguchi M, Stamey TA, Neal JE, Yemoto CE. An analysis of 148 consecutive transition zone cancers: clinical and histological characteristics. J Urol. 2000;163(6):1751-5. PubMed PMID: 10799175.

29. Reissigl A, Pointner J, Strasser H, Ennemoser O, Klocker H, Bartsch G. Frequency and clinical significance of transition zone cancer in prostate cancer screening. Prostate. 1997;30(2):130-5. doi: 10.1002/(sici)1097-0045(19970201)30:2<130::aid-pros8>3.0.co;2-s. PubMed PMID: 9051151.

30. de Jong M, Maina T. Of mice and humans: are they the same?--Implications in cancer translational research. J Nucl Med. 2010;51(4):501-4. Epub 2010/03/17. doi: 10.2967/jnumed.109.065706. PubMed PMID: 20237033.

31. Maser RS, Choudhury B, Campbell PJ, Feng B, Wong KK, Protopopov A, O'Neil J, Gutierrez A, Ivanova E, Perna I, Lin E, Mani V, Jiang S, McNamara K, Zaghlul S, Edkins S, Stevens C, Brennan C, Martin ES, Wiedemeyer R, Kabbarah O, Nogueira C, Histen G, Aster J, Mansour M, Duke V, Foroni L, Fielding AK, Goldstone AH, Rowe JM, Wang YA, Look AT, Stratton MR, Chin L, Futreal PA, DePinho RA. Chromosomally unstable mouse tumours have genomic alterations similar to diverse human cancers. Nature. 2007;447(7147):966-71. Epub 2007/05/21. doi: 10.1038/nature05886. PubMed PMID: 17515920; PMCID: PMC2714968.

32. Vykhovanets EV, Resnick MI, MacLennan GT, Gupta S. Experimental rodent models of prostatitis: limitations and potential. Prostate Cancer Prostatic Dis. 2007;10(1):15-29. Epub 2007/01/02. doi: 10.1038/sj.pcan.4500930. PubMed PMID: 17199136.

33. Jerde TJ, Bushman W. IL-1 induces IGF-dependent epithelial proliferation in prostate development and reactive hyperplasia. Sci Signal. 2009;2(86):ra49. Epub 2009/09/01. doi: 10.1126/scisignal.2000338. PubMed PMID: 19724062; PMCID: PMC2949294.

34. Henry GH, Malewska A, Joseph DB, Malladi VS, Lee J, Torrealba J, Mauck RJ, Gahan JC, Raj GV, Roehrborn CG, Hon GC, MacConmara MP, Reese JC, Hutchinson RC, Vezina CM, Strand DW. A Cellular Anatomy of the Normal Adult Human Prostate and Prostatic Urethra. Cell Rep. 2018;25(12):3530-42.e5. doi: 10.1016/j.celrep.2018.11.086. PubMed PMID: 30566875; PMCID: PMC6411034.

35. Hahn AM, Myers JD, McFarland EK, Lee S, Jerde TJ. Interleukin-driven insulin-like growth factor promotes prostatic inflammatory hyperplasia. J Pharmacol Exp Ther. 2014;351(3):605-15. Epub 2014/10/09. doi: 10.1124/jpet.114.218693

jpet.114.218693 [pii]. PubMed PMID: 25292180; PMCID: 4244580.

36. Lilja H, Laurell CB. The predominant protein in human seminal coagulate. Scand J Clin Lab Invest. 1985;45(7):635-41. doi: 10.3109/00365518509155271. PubMed PMID: 2866578.

37. Lilja H, Abrahamsson PA. Three predominant proteins secreted by the human prostate gland. Prostate. 1988;12(1):29-38. doi: 10.1002/pros.2990120105. PubMed PMID: 3347596.

38. Gurel B, Ali TZ, Montgomery EA, Begum S, Hicks J, Goggins M, Eberhart CG, Clark DP, Bieberich CJ, Epstein JI, De Marzo AM. NKX3.1 as a marker of prostatic origin in metastatic tumors. Am J Surg Pathol. 2010;34(8):1097-105. doi: 10.1097/PAS.0b013e3181e6cbf3. PubMed PMID: 20588175; PMCID: PMC3072223.

39. Sugimura Y, Cunha GR, Donjacour AA. Morphological and histological study of castration-induced degeneration and androgen-induced regeneration in the mouse prostate. Biol Reprod. 1986;34(5):973-83. doi: 10.1095/biolreprod34.5.973. PubMed PMID: 3730489.

40. Watabe T, Lin M, Ide H, Donjacour AA, Cunha GR, Witte ON, Reiter RE. Growth, regeneration, and tumorigenesis of the prostate activates the PSCA promoter. Proc Natl Acad Sci U S A. 2002;99(1):401-6. Epub 2001/12/18. doi: 10.1073/pnas.012574899. PubMed PMID: 11752398; PMCID: PMC117572.

41. Choi N, Zhang B, Zhang L, Ittmann M, Xin L. Adult murine prostate basal and luminal cells are self-sustained lineages that can both serve as targets for prostate cancer initiation. Cancer Cell. 2012;21(2):253-65. Epub 2012/02/22. doi: 10.1016/j.ccr.2012.01.005

S1535-6108(12)00038-4 [pii]. PubMed PMID: 22340597; PMCID: 3285423.

42. Wang X, Kruithof-de Julio M, Economides KD, Walker D, Yu H, Halili MV, Hu YP, Price SM, Abate-Shen C, Shen MM. A luminal epithelial stem cell that is a cell of origin for prostate cancer. Nature. 2009;461(7263):495-500. Epub 2009/09/11. doi: 10.1038/nature08361

nature08361 [pii]. PubMed PMID: 19741607; PMCID: 2800362.

43. Kwon OJ, Zhang L, Ittmann MM, Xin L. Prostatic inflammation enhances basal-to-luminal differentiation and accelerates initiation of prostate cancer with a basal cell origin. Proc Natl Acad Sci U S A. 2014;111(5):E592-600. Epub 2013/12/23. doi: 10.1073/pnas.1318157111. PubMed PMID: 24367088; PMCID: PMC3918789.

44. Lu TL, Huang YF, You LR, Chao NC, Su FY, Chang JL, Chen CM. Conditionally ablated Pten in prostate basal cells promotes basal-to-luminal differentiation and causes invasive prostate cancer in mice. Am J Pathol. 2013;182(3):975-91. Epub 2013/01/09. doi: 10.1016/j.ajpath.2012.11.025. PubMed PMID: 23313138.

45. Taylor RA, Toivanen R, Frydenberg M, Pedersen J, Harewood L, Collins AT, Maitland NJ, Risbridger GP, Bioresource APC. Human epithelial basal cells are cells of origin of prostate cancer, independent of CD133 status. Stem Cells. 2012;30(6):1087-96. doi: 10.1002/stem.1094. PubMed PMID: 22593016.

46. Patel GK, Chugh N, Tripathi M. Neuroendocrine Differentiation of Prostate Cancer-An Intriguing Example of Tumor Evolution at Play. Cancers (Basel). 2019;11(10). Epub 2019/09/20. doi: 10.3390/cancers11101405. PubMed PMID: 31547070; PMCID: PMC6826557.

47. Harper ME, Glynne-Jones E, Goddard L, Thurston VJ, Griffiths K. Vascular endothelial growth factor (VEGF) expression in prostatic tumours and its relationship to neuroendocrine cells. Br J Cancer. 1996;74(6):910-6. doi: 10.1038/bjc.1996.456. PubMed PMID: 8826857; PMCID: PMC2074752.

48. di Sant'Agnese PA. Neuroendocrine cells of the prostate and neuroendocrine differentiation in prostatic carcinoma: a review of morphologic aspects. Urology. 1998;51(5A Suppl):121-4. doi: 10.1016/s0090-4295(98)00064-8. PubMed PMID: 9610566.

49. Xue Y, van der Laak J, Smedts F, Schoots C, Verhofstad A, de la Rosette J, Schalken J. Neuroendocrine cells during human prostate development: does neuroendocrine cell density remain constant during fetal as well as postnatal life? Prostate. 2000;42(2):116-23. doi: 10.1002/(sici)1097-0045(20000201)42:2<116::aid-pros5>3.0.co;2-9. PubMed PMID: 10617868.

50. Kyoda Y, Ichihara K, Hashimoto K, Kobayashi K, Fukuta F, Masumori N. Distribution of Neuroendocrine Cells in the Transition Zone of the Prostate. Adv Urol. 2017;2017:8541697. Epub 2017/03/01. doi: 10.1155/2017/8541697. PubMed PMID: 28348583; PMCID: PMC5350492.

51. Kurita T, Medina RT, Mills AA, Cunha GR. Role of p63 and basal cells in the prostate. Development. 2004;131(20):4955-64. Epub 2004/09/15. doi: 10.1242/dev.01384. PubMed PMID: 15371309.

52. Donjacour AA, Cunha GR. Assessment of prostatic protein secretion in tissue recombinants made of urogenital sinus mesenchyme and urothelium from normal or androgen-insensitive mice. Endocrinology. 1993;132(6):2342-50. doi: 10.1210/endo.132.6.7684975. PubMed PMID: 7684975.

53. Pignon JC, Grisanzio C, Geng Y, Song J, Shivdasani RA, Signoretti S. p63-expressing cells are the stem cells of developing prostate, bladder, and colorectal epithelia. Proc Natl Acad Sci U S A. 2013;110(20):8105-10. Epub 2013/04/25. doi: 10.1073/pnas.1221216110. PubMed PMID: 23620512; PMCID: PMC3657776.

54. Peehl DM, Wong ST, Stamey TA. Clonal growth characteristics of adult human prostatic epithelial cells. In Vitro Cell Dev Biol. 1988;24(6):530-6. doi: 10.1007/BF02629087. PubMed PMID: 3391931.

55. Sherwood ER, Theyer G, Steiner G, Berg LA, Kozlowski JM, Lee C. Differential expression of specific cytokeratin polypeptides in the basal and luminal epithelia of the human prostate. Prostate. 1991;18(4):303-14. doi: 10.1002/pros.2990180404. PubMed PMID: 1711687.

56. Tsujimura A, Koikawa Y, Salm S, Takao T, Coetzee S, Moscatelli D, Shapiro E, Lepor H, Sun TT, Wilson EL. Proximal location of mouse prostate epithelial stem cells: a model of prostatic homeostasis. J Cell Biol. 2002;157(7):1257-65. Epub 2002/06/24. doi: 10.1083/jcb.200202067. PubMed PMID: 12082083; PMCID: PMC2173539.

57. Collins AT, Habib FK, Maitland NJ, Neal DE. Identification and isolation of human prostate epithelial stem cells based on alpha(2)beta(1)-integrin expression. J Cell Sci. 2001;114(Pt 21):3865-72. PubMed PMID: 11719553.

58. Richardson GD, Robson CN, Lang SH, Neal DE, Maitland NJ, Collins AT. CD133, a novel marker for human prostatic epithelial stem cells. J Cell Sci. 2004;117(Pt 16):3539-45. Epub 2004/06/29. doi: 10.1242/jcs.01222. PubMed PMID: 15226377.

59. Xin L, Lawson DA, Witte ON. The Sca-1 cell surface marker enriches for a prostate-regenerating cell subpopulation that can initiate prostate tumorigenesis. Proc Natl Acad Sci U S A. 2005;102(19):6942-7. Epub 2005/04/28. doi: 10.1073/pnas.0502320102. PubMed PMID: 15860580; PMCID: PMC1087514.

60. Burger PE, Xiong X, Coetzee S, Salm SN, Moscatelli D, Goto K, Wilson EL. Sca-1 expression identifies stem cells in the proximal region of prostatic ducts with high capacity to reconstitute prostatic tissue. Proc Natl Acad Sci U S A. 2005;102(20):7180-5. doi: 10.1073/pnas.0502761102. PubMed PMID: 15899981; PMCID: PMC1129148.

61. Lawson DA, Xin L, Lukacs RU, Cheng D, Witte ON. Isolation and functional characterization of murine prostate stem cells. Proc Natl Acad Sci U S A. 2007;104(1):181-6. Epub 2006/12/21. doi: 10.1073/pnas.0609684104. PubMed PMID: 17185413; PMCID: PMC1716155.

62. Xin L, Lukacs RU, Lawson DA, Cheng D, Witte ON. Self-renewal and multilineage differentiation in vitro from murine prostate stem cells. Stem Cells. 2007;25(11):2760-9. Epub 2007/07/19. doi: 10.1634/stemcells.2007-0355. PubMed PMID: 17641240.

63. Xin L, Ide H, Kim Y, Dubey P, Witte ON. In vivo regeneration of murine prostate from dissociated cell populations of postnatal epithelia and urogenital sinus mesenchyme. Proc Natl Acad Sci U S A. 2003;100 Suppl 1:11896-903. Epub 2003/08/08. doi: 10.1073/pnas.1734139100. PubMed PMID: 12909713; PMCID: PMC304104.

64. Strand DW, Aaron L, Henry G, Franco OE, Hayward SW. Isolation and analysis of discreet human prostate cellular populations. Differentiation. 2016;91(4-5):139-51. Epub 2015/11/03. doi: 10.1016/j.diff.2015.10.013. PubMed PMID: 26546040; PMCID: PMC4854811.

65. Uzgare AR, Xu Y, Isaacs JT. In vitro culturing and characteristics of transit amplifying epithelial cells from human prostate tissue. J Cell Biochem. 2004;91(1):196-205. doi: 10.1002/jcb.10764. PubMed PMID: 14689591.

66. Lukacs RU, Goldstein AS, Lawson DA, Cheng D, Witte ON. Isolation, cultivation and characterization of adult murine prostate stem cells. Nat Protoc. 2010;5(4):702-13. Epub 2010/04/03. doi: 10.1038/nprot.2010.11

nprot.2010.11 [pii]. PubMed PMID: 20360765; PMCID: 2943378.

67. Leong KG, Wang BE, Johnson L, Gao WQ. Generation of a prostate from a single adult stem cell. Nature. 2008;456(7223):804-8. Epub 2008/10/22. doi: 10.1038/nature07427. PubMed PMID: 18946470.

68. Horton C, Liu Y, Yu C, Xie Q, Wang ZA. Luminal-contact-inhibition of epithelial basal stem cell multipotency in prostate organogenesis and homeostasis. Biol Open. 2019;8(10). Epub 2019/10/01. doi: 10.1242/bio.045724. PubMed PMID: 31540905; PMCID: PMC6826291.

69. Goldstein AS, Huang J, Guo C, Garraway IP, Witte ON. Identification of a cell of origin for human prostate cancer. Science. 2010;329(5991):568-71. doi: 10.1126/science.1189992. PubMed PMID: 20671189; PMCID: PMC2917982.

70. Gelmann EP. Molecular biology of the androgen receptor. J Clin Oncol. 2002;20(13):3001-15. doi: 10.1200/JCO.2002.10.018. PubMed PMID: 12089231.

71. Brinkmann AO, Faber PW, van Rooij HC, Kuiper GG, Ris C, Klaassen P, van der Korput JA, Voorhorst MM, van Laar JH, Mulder E. The human androgen receptor: domain structure, genomic organization and regulation of expression. J Steroid Biochem. 1989;34(1-6):307-10. doi: 10.1016/0022-4731(89)90098-8. PubMed PMID: 2626022.

72. Davey RA, Grossmann M. Androgen Receptor Structure, Function and Biology: From Bench to Bedside. Clin Biochem Rev. 2016;37(1):3-15. PubMed PMID: 27057074; PMCID: PMC4810760.

73. Grino PB, Griffin JE, Wilson JD. Testosterone at high concentrations interacts with the human androgen receptor similarly to dihydrotestosterone. Endocrinology. 1990;126(2):1165-72. doi: 10.1210/endo-126-2-1165. PubMed PMID: 2298157.

74. Tan MH, Li J, Xu HE, Melcher K, Yong EL. Androgen receptor: structure, role in prostate cancer and drug discovery. Acta Pharmacol Sin. 2015;36(1):3-23. Epub 2014/06/09. doi: 10.1038/aps.2014.18. PubMed PMID: 24909511; PMCID: PMC4571323.

75. Cano LQ, Lavery DN, Bevan CL. Mini-review: Foldosome regulation of androgen receptor action in prostate cancer. Mol Cell Endocrinol. 2013;369(1-2):52-62. Epub 2013/02/08. doi: 10.1016/j.mce.2013.01.023. PubMed PMID: 23395916.

76. Nelson PS, Clegg N, Arnold H, Ferguson C, Bonham M, White J, Hood L, Lin B. The program of androgen-responsive genes in neoplastic prostate epithelium. Proc Natl Acad Sci U S A. 2002;99(18):11890-5. Epub 2002/08/16. doi: 10.1073/pnas.182376299. PubMed PMID: 12185249; PMCID: PMC129364.

77. van der Steen T, Tindall DJ, Huang H. Posttranslational modification of the androgen receptor in prostate cancer. Int J Mol Sci. 2013;14(7):14833-59. Epub 2013/07/16. doi: 10.3390/ijms140714833. PubMed PMID: 23863692; PMCID: PMC3742275.

78. Culig Z, Bartsch G, Hobisch A. Interleukin-6 regulates androgen receptor activity and prostate cancer cell growth. Mol Cell Endocrinol. 2002;197(1-2):231-8. doi: 10.1016/s0303-7207(02)00263-0. PubMed PMID: 12431817.

79. Willder JM, Heng SJ, McCall P, Adams CE, Tannahill C, Fyffe G, Seywright M, Horgan PG, Leung HY, Underwood MA, Edwards J. Androgen receptor phosphorylation at serine 515 by Cdk1 predicts biochemical relapse in prostate cancer patients. Br J Cancer. 2013;108(1):139-48. Epub 2012/12/04. doi: 10.1038/bjc.2012.480. PubMed PMID: 23321516; PMCID: PMC3553508.

80. Huggins C, Hodges CV. Studies on prostatic cancer. I. The effect of castration, of estrogen and of androgen injection on serum phosphatases in metastatic carcinoma of the prostate. 1941. J Urol. 2002;167(2 Pt 2):948-51; discussion 52. PubMed PMID: 11905923.

81. Koivisto P, Kononen J, Palmberg C, Tammela T, Hyytinen E, Isola J, Trapman J, Cleutjens K, Noordzij A, Visakorpi T, Kallioniemi OP. Androgen receptor gene amplification: a possible molecular mechanism for androgen deprivation therapy failure in prostate cancer. Cancer Res. 1997;57(2):314-9. PubMed PMID: 9000575.

82. Taplin ME, Bubley GJ, Ko YJ, Small EJ, Upton M, Rajeshkumar B, Balk SP. Selection for androgen receptor mutations in prostate cancers treated with androgen antagonist. Cancer Res. 1999;59(11):2511-5. PubMed PMID: 10363963.

83. Guo Z, Yang X, Sun F, Jiang R, Linn DE, Chen H, Kong X, Melamed J, Tepper CG, Kung HJ, Brodie AM, Edwards J, Qiu Y. A novel androgen receptor splice variant is up-regulated during prostate cancer progression and promotes androgen depletion-resistant growth. Cancer Res. 2009;69(6):2305-13. Epub 2009/02/24. doi: 10.1158/0008-5472.CAN-08-3795. PubMed PMID: 19244107; PMCID: PMC2672822.

84. Gandaglia G, Zaffuto E, Fossati N, Cucchiara V, Mirone V, Montorsi F, Briganti A. The role of prostatic inflammation in the development and progression of benign and malignant diseases. Curr Opin Urol. 2017;27(2):99-106. doi: 10.1097/MOU.0000000000000369. PubMed PMID: 27906778.

85. Palapattu GS, Sutcliffe S, Bastian PJ, Platz EA, De Marzo AM, Isaacs WB, Nelson WG. Prostate carcinogenesis and inflammation: emerging insights. Carcinogenesis. 2005;26(7):1170-81. Epub 2004/10/21. doi: 10.1093/carcin/bgh317. PubMed PMID: 15498784.

86. Sfanos KS, De Marzo AM. Prostate cancer and inflammation: the evidence. Histopathology. 2012;60(1):199-215. Epub 2012/01/04. doi: 10.1111/j.1365-2559.2011.04033.x. PubMed PMID: 22212087; PMCID: 4029103.

87. Hobisch A, Eder IE, Putz T, Horninger W, Bartsch G, Klocker H, Culig Z. Interleukin-6 regulates prostate specific protein expression in prostate carcinoma cells by activation of the androgen receptor. Cancer Research. 1998;58(20):4640-5. PubMed PMID: ISI:000076455900029.

88. Nguyen DP, Li J, Tewari AK. Inflammation and prostate cancer: the role of interleukin 6 (IL-6). BJU Int. 2014;113(6):986-92. Epub 2013/09/24. doi: 10.1111/bju.12452. PubMed PMID: 24053309.

89. Boivin WA, Jiang H, Utting OB, Hunt DW. Influence of interleukin-1alpha on androgen receptor expression and cytokine secretion by cultured human dermal papilla cells. Exp Dermatol. 2006;15(10):784-93. doi: 10.1111/j.1600-0625.2006.00462.x. PubMed PMID: 16984260.

90. Zhang B, Kwon OJ, Henry G, Malewska A, Wei X, Zhang L, Brinkley W, Zhang Y, Castro PD, Titus M, Chen R, Sayeeduddin M, Raj GV, Mauck R, Roehrborn C, Creighton CJ, Strand DW, Ittmann MM, Xin L. Non-Cell-Autonomous Regulation of Prostate Epithelial Homeostasis by Androgen Receptor. Mol Cell. 2016;63(6):976-89. Epub 2016/09/01. doi: 10.1016/j.molcel.2016.07.025. PubMed PMID: 27594448; PMCID: PMC5026614.

91. Zhang JM, An J. Cytokines, inflammation, and pain. Int Anesthesiol Clin. 2007;45(2):27-37. doi: 10.1097/AIA.0b013e318034194e. PubMed PMID: 17426506; PMCID: PMC2785020.

92. Weber A, Wasiliew P, Kracht M. Interleukin-1 (IL-1) pathway. Sci Signal. 2010;3(105):cm1. Epub 2010/01/19. doi: 10.1126/scisignal.3105cm1. PubMed PMID: 20086235.

93. Rider P, Carmi Y, Guttman O, Braiman A, Cohen I, Voronov E, White MR, Dinarello CA, Apte RN. IL-1α and IL-1β recruit different myeloid cells and promote different stages of sterile inflammation. J Immunol. 2011;187(9):4835-43. Epub 2011/09/19. doi: 10.4049/jimmunol.1102048. PubMed PMID: 21930960.

94. Rodríguez-Berriguete G, Sánchez-Espiridión B, Cansino JR, Olmedilla G, Martínez-Onsurbe P, Sánchez-Chapado M, Paniagua R, Fraile B, Royuela M. Clinical significance of both tumor and stromal expression of components of the IL-1 and TNF-α signaling pathways in prostate cancer. Cytokine. 2013;64(2):555-63. Epub 2013/09/21. doi: 10.1016/j.cyto.2013.09.003. PubMed PMID: 24063999.

95. Maund SL, Barclay WW, Hover LD, Axanova LS, Sui G, Hipp JD, Fleet JC, Thorburn A, Cramer SD. Interleukin-1α mediates the antiproliferative effects of 1,25-dihydroxyvitamin D3 in prostate progenitor/stem cells. Cancer Res. 2011;71(15):5276-86. Epub 2011/06/08. doi: 10.1158/0008-5472.CAN-10-2160. PubMed PMID: 21653679; PMCID: PMC3148300.

96. The Anatomy and Diseases of the Prostate Gland. Br Foreign Med Chir Rev. 1852;9(17):80-90. PubMed PMID: 30164048; PMCID: PMC5183671.

97. An Essay on the Treatment of Some Affections of the Prostate Gland. Br Foreign Med Rev. 1840;10(20):528-31. PubMed PMID: 30161694; PMCID: PMC5592546.

98. Magri V, Boltri M, Cai T, Colombo R, Cuzzocrea S, De Visschere P, Giuberti R, Granatieri CM, Latino MA, Larganà G, Leli C, Maierna G, Marchese V, Massa E, Matteelli A, Montanari E, Morgia G, Naber KG, Papadouli V, Perletti G, Rekleiti N, Russo GI, Sensini A, Stamatiou K, Trinchieri A, Wagenlehner FME. Multidisciplinary approach to prostatitis. Arch Ital Urol Androl. 2019;90(4):227-48. Epub 2019/01/18. doi: 10.4081/aiua.2018.4.227. PubMed PMID: 30655633.

99. Krieger JN, Nyberg L, Nickel JC. NIH consensus definition and classification of prostatitis. JAMA. 1999;282(3):236-7. doi: 10.1001/jama.282.3.236. PubMed PMID: 10422990.

100. Collins MM, Stafford RS, O'Leary MP, Barry MJ. How common is prostatitis? A national survey of physician visits. J Urol. 1998;159(4):1224-8. PubMed PMID: 9507840.

101. Krieger JN, Lee SW, Jeon J, Cheah PY, Liong ML, Riley DE. Epidemiology of prostatitis. Int J Antimicrob Agents. 2008;31 Suppl 1:S85-90. Epub 2007/12/31. doi: 10.1016/j.ijantimicag.2007.08.028. PubMed PMID: 18164907; PMCID: PMC2292121.

102. Pontari MA, Joyce GF, Wise M, McNaughton-Collins M, Project UDiA. Prostatitis. J Urol. 2007;177(6):2050-7. doi: 10.1016/j.juro.2007.01.128. PubMed PMID: 17509285.

103. Krieger JN, Riley DE, Cheah PY, Liong ML, Yuen KH. Epidemiology of prostatitis: new evidence for a world-wide problem. World J Urol. 2003;21(2):70-4. Epub 2003/04/24. doi: 10.1007/s00345-003-0329-0. PubMed PMID: 12712363.

104. Keay S, Zhang CO, Baldwin BR, Alexander RB. Polymerase chain reaction amplification of bacterial 16s rRNA genes in prostate biopsies from men without chronic prostatitis. Urology. 1999;53(3):487-91. doi: 10.1016/s0090-4295(98)00553-6. PubMed PMID: 10096371.

105. Krieger JN, Riley DE. Bacteria in the chronic prostatitis-chronic pelvic pain syndrome: molecular approaches to critical research questions. J Urol. 2002;167(6):2574-83. PubMed PMID: 11992091.

106. Melissa M. Norström, ER, Lars Henningsohn, Victor Levitsk, Berit Sundberg, Jonas Mattsson, Michael Uhlin. Progression of benign prostatic hyperplasia is associated with pro-inflammatory mediators and chronic activation of prostate-infiltrating lymphocytes. Oncotarget. 2016;7(17).

107. Torkko KC, Wilson RS, Smith EE, Kusek JW, van Bokhoven A, Lucia MS. Prostate Biopsy Markers of Inflammation are Associated with Risk of Clinical Progression of Benign Prostatic Hyperplasia: Findings from the MTOPS Study. J Urol. 2015;194(2):454-61. Epub 2015/03/28. doi: 10.1016/j.juro.2015.03.103. PubMed PMID: 25828974.

108. Gao Y, Wei L, Wang C, Huang Y, Li W, Li T, Mo C, Qin H, Zhong X, Wang Y, Tan A, Mo Z, Jiang Y, Hu Y. Chronic prostatitis alters the prostatic microenvironment and accelerates preneoplastic lesions in C57BL/6 mice. Biol Res. 2019;52(1):30. Epub 2019/05/14. doi: 10.1186/s40659-019-0237-4. PubMed PMID: 31088536; PMCID: PMC6518623.

109. Bates JP, Derakhshandeh R, Jones L, Webb TJ. Mechanisms of immune evasion in breast cancer. BMC Cancer. 2018;18(1):556. Epub 2018/05/11. doi: 10.1186/s12885-018-4441-3. PubMed PMID: 29751789; PMCID: PMC5948714.

110. Fu X, Xiao J, Wei Y, Li S, Liu Y, Yin J, Sun K, Sun H, Wang H, Zhang Z, Zhang BT, Sheng C, Wang H, Hu P. Combination of inflammation-related cytokines promotes long-term muscle stem cell expansion. Cell Res. 2015;25(6):655-73. Epub 2015/05/16. doi: 10.1038/cr.2015.58. PubMed PMID: 25976405; PMCID: PMC4456625.

111. Kruslin B, Tomas D, Dzombeta T, Milkovic-Perisa M, Ulamec M. Inflammation in Prostatic Hyperplasia and Carcinoma-Basic Scientific Approach. Front Oncol. 2017;7:77. Epub 2017/05/11. doi: 10.3389/fonc.2017.00077. PubMed PMID: 28487844; PMCID: PMC5403898.

112. Berry SJ, Coffey DS, Walsh PC, Ewing LL. The development of human benign prostatic hyperplasia with age. J Urol. 1984;132(3):474-9. PubMed PMID: 6206240.

113. Lim KB. Epidemiology of clinical benign prostatic hyperplasia. Asian J Urol. 2017;4(3):148-51. Epub 2017/06/09. doi: 10.1016/j.ajur.2017.06.004. PubMed PMID: 29264223; PMCID: PMC5717991.

114. Basatac C, Cicek MC. A huge benign prostatic hyperplasia presenting with renal failure. J Surg Case Rep. 2015;2015(6). Epub 2015/06/01. doi: 10.1093/jscr/rjv060. PubMed PMID: 26034239; PMCID: PMC4450250.

115. Macey MR, Raynor MC. Medical and Surgical Treatment Modalities for Lower Urinary Tract Symptoms in the Male Patient Secondary to Benign Prostatic Hyperplasia: A Review. Semin Intervent Radiol. 2016;33(3):217-23. doi: 10.1055/s-0036-1586142. PubMed PMID: 27582609; PMCID: PMC5005076.

116. Shapiro E, Hartanto V, Lepor H. The response to alpha blockade in benign prostatic hyperplasia is related to the percent area density of prostate smooth muscle. Prostate. 1992;21(4):297-307. doi: 10.1002/pros.2990210406. PubMed PMID: 1281322.

117. Roehrborn CG, Barkin J, Siami P, Tubaro A, Wilson TH, Morrill BB, Gagnier RP. Clinical outcomes after combined therapy with dutasteride plus tamsulosin or either monotherapy in men with benign prostatic hyperplasia (BPH) by baseline characteristics: 4-year results from the randomized, double-blind Combination of Avodart and Tamsulosin (CombAT) trial. BJU Int. 2011;107(6):946-54. Epub 2011/02/18. doi: 10.1111/j.1464-410X.2011.10124.x. PubMed PMID: 21332630.

118. McConnell JD, Roehrborn CG, Bautista OM, Andriole GL, Dixon CM, Kusek JW, Lepor H, McVary KT, Nyberg LM, Clarke HS, Crawford ED, Diokno A, Foley JP, Foster HE, Jacobs SC, Kaplan SA, Kreder KJ, Lieber MM, Lucia MS, Miller GJ, Menon M, Milam DF, Ramsdell JW, Schenkman NS, Slawin KM, Smith JA, Group MToPSMR. The long-term effect of doxazosin, finasteride, and combination therapy on the clinical progression of benign prostatic hyperplasia. N Engl J Med. 2003;349(25):2387-98. doi: 10.1056/NEJMoa030656. PubMed PMID: 14681504.

119. Wei JT, Calhoun E, Jacobsen SJ. Urologic diseases in america project: benign prostatic hyperplasia. J Urol. 2008;179(5 Suppl):S75-80. doi: 10.1016/j.juro.2008.03.141. PubMed PMID: 18405761.

120. Strand DW, Costa DN, Francis F, Ricke WA, Roehrborn CG. Targeting phenotypic heterogeneity in benign prostatic hyperplasia. Differentiation. 2017;96:49-61. Epub 2017/08/04. doi: 10.1016/j.diff.2017.07.005. PubMed PMID: 28800482; PMCID: PMC5669834.

121. Roehrborn CG. Pathology of benign prostatic hyperplasia. Int J Impot Res. 2008;20 Suppl 3:S11-8. doi: 10.1038/ijir.2008.55. PubMed PMID: 19002119.

122. Robert G, Descazeaud A, Nicolaïew N, Terry S, Sirab N, Vacherot F, Maillé P, Allory Y, de la Taille A. Inflammation in benign prostatic hyperplasia: a 282 patients' immunohistochemical analysis. Prostate. 2009;69(16):1774-80. doi: 10.1002/pros.21027. PubMed PMID: 19670242; PMCID: PMC2833181.

123. Aaron-Brooks LM, Sasaki T, Vickman RE, Wei L, Franco OE, Ji Y, Crawford SE, Hayward SW. Hyperglycemia and T Cell infiltration are associated with stromal and epithelial prostatic hyperplasia in the nonobese diabetic mouse. Prostate. 2019;79(9):980-93. Epub 2019/04/18. doi: 10.1002/pros.23809. PubMed PMID: 30999385; PMCID: PMC6591734.

124. Irani J, Levillain P, Goujon JM, Bon D, Doré B, Aubert J. Inflammation in benign prostatic hyperplasia: correlation with prostate specific antigen value. J Urol. 1997;157(4):1301-3. doi: 10.1016/s0022-5347(01)64957-7. PubMed PMID: 9120926.

125. Kramer G, Marberger M. Could inflammation be a key component in the progression of benign prostatic hyperplasia? Curr Opin Urol. 2006;16(1):25-9. PubMed PMID: 16385197.

126. Mishra VC, Allen DJ, Nicolaou C, Sharif H, Hudd C, Karim OM, Motiwala HG, Laniado ME. Does intraprostatic inflammation have a role in the pathogenesis and progression of benign prostatic hyperplasia? BJU Int. 2007;100(2):327-31. doi: 10.1111/j.1464-410X.2007.06910.x. PubMed PMID: 17617139.

127. Theyer G, Kramer G, Assmann I, Sherwood E, Preinfalk W, Marberger M, Zechner O, Steiner GE. Phenotypic characterization of infiltrating leukocytes in benign prostatic hyperplasia. Lab Invest. 1992;66(1):96-107. PubMed PMID: 1370561.

128. Laidlaw BJ, Craft JE, Kaech SM. The multifaceted role of CD4(+) T cells in CD8(+) T cell memory. Nat Rev Immunol. 2016;16(2):102-11. Epub 2016/01/19. doi: 10.1038/nri.2015.10. PubMed PMID: 26781939; PMCID: PMC4860014.

129. Steiner G, Gessl A, Kramer G, Schöllhammer A, Förster O, Marberger M. Phenotype and function of peripheral and prostatic lymphocytes in patients with benign prostatic hyperplasia. J Urol. 1994;151(2):480-4. doi: 10.1016/s0022-5347(17)34998-4. PubMed PMID: 7506795.

130. Bostwick DG, Brawer MK. Prostatic intra-epithelial neoplasia and early invasion in prostate cancer. Cancer. 1987;59(4):788-94. doi: 10.1002/1097-0142(19870215)59:4<788::aid-cncr2820590421>3.0.co;2-i. PubMed PMID: 2433020.

131. Bray F, Ferlay J, Soerjomataram I, Siegel RL, Torre LA, Jemal A. Global cancer statistics 2018: GLOBOCAN estimates of incidence and mortality worldwide for 36 cancers in 185 countries. CA Cancer J Clin. 2018;68(6):394-424. Epub 2018/09/12. doi: 10.3322/caac.21492. PubMed PMID: 30207593.

132. Siegel RL, Miller KD, Jemal A. Cancer statistics, 2020. CA Cancer J Clin. 2020;70(1):7-30. Epub 2020/01/08. doi: 10.3322/caac.21590. PubMed PMID: 31912902.

133. Potosky AL, Miller BA, Albertsen PC, Kramer BS. The role of increasing detection in the rising incidence of prostate cancer. JAMA. 1995;273(7):548-52. PubMed PMID: 7530782.

134. Marcus DM, Goodman M, Jani AB, Osunkoya AO, Rossi PJ. A comprehensive review of incidence and survival in patients with rare histological variants of prostate cancer in the United States from 1973 to 2008. Prostate Cancer Prostatic Dis. 2012;15(3):283-8. Epub 2012/02/21. doi: 10.1038/pcan.2012.4. PubMed PMID: 22349984.

135. Harris WP, Mostaghel EA, Nelson PS, Montgomery B. Androgen deprivation therapy: progress in understanding mechanisms of resistance and optimizing androgen depletion. Nat Clin Pract Urol. 2009;6(2):76-85. doi: 10.1038/ncpuro1296. PubMed PMID: 19198621; PMCID: PMC2981403.

136. Scher HI, Fizazi K, Saad F, Taplin ME, Sternberg CN, Miller K, de Wit R, Mulders P, Chi KN, Shore ND, Armstrong AJ, Flaig TW, Flechon A, Mainwaring P, Fleming M, Hainsworth JD, Hirmand M, Selby B, Seely L, de Bono JS. Increased survival with enzalutamide in prostate cancer after chemotherapy. N Engl J Med. 2012;367(13):1187-97. Epub 2012/08/17. doi: 10.1056/NEJMoa1207506. PubMed PMID: 22894553.

137. Scher HI, Fizazi K, Saad F, Taplin M-E, Sternberg CN, Miller K, De Wit R, Mulders P, Hirmand M, Selby B, De Bono JS. Effect of MDV3100, an androgen receptor signaling inhibitor (ARSI), on overall survival in patients with prostate cancer postdocetaxel: Results from the phase III AFFIRM study. Journal of Clinical Oncology. 2012;30(5_suppl):LBA1-LBA. doi: 10.1200/jco.2012.30.5_suppl.lba1. PubMed PMID: 28142898.

138. Couzin-Frankel J. Breakthrough of the year 2013. Cancer immunotherapy. Science. 2013;342(6165):1432-3. doi: 10.1126/science.342.6165.1432. PubMed PMID: 24357284.

139. Wahid B, Ali A, Rafique S, Waqar M, Wasim M, Wahid K, Idrees M. An overview of cancer immunotherapeutic strategies. Immunotherapy. 2018;10(11):999-1010. doi: 10.2217/imt-2018-0002. PubMed PMID: 30149763.

140. Andersen MH, Schrama D, Thor Straten P, Becker JC. Cytotoxic T cells. J Invest Dermatol. 2006;126(1):32-41. doi: 10.1038/sj.jid.5700001. PubMed PMID: 16417215.

141. Rusch T, Bayry J, Werner J, Shevchenko I, Bazhin AV. Immunotherapy as an Option for Cancer Treatment. Arch Immunol Ther Exp (Warsz). 2018;66(2):89-96. Epub 2017/10/12. doi: 10.1007/s00005-017-0491-5. PubMed PMID: 29026920.

142. Kwon ED, Hurwitz AA, Foster BA, Madias C, Feldhaus AL, Greenberg NM, Burg MB, Allison JP. Manipulation of T cell costimulatory and inhibitory signals for immunotherapy of prostate cancer. Proc Natl Acad Sci U S A. 1997;94(15):8099-103. doi: 10.1073/pnas.94.15.8099. PubMed PMID: 9223321; PMCID: PMC21563.

143. Holl EK, McNamara MA, Healy P, Anand M, Concepcion RS, Breland CD, Dumbudze I, Tutrone R, Shore N, Armstrong AJ, Harrison M, Wallace JA, Wu Y, George DJ. Prolonged PSA stabilization and overall survival following sipuleucel-T monotherapy in metastatic castration-resistant prostate cancer patients. Prostate Cancer Prostatic Dis. 2019. Epub 2019/04/12. doi: 10.1038/s41391-019-0144-3. PubMed PMID: 30980027.

144. Laccetti AL, Subudhi SK. Immunotherapy for metastatic prostate cancer: immuno-cold or the tip of the iceberg? Curr Opin Urol. 2017;27(6):566-71. doi: 10.1097/MOU.0000000000000433. PubMed PMID: 28825923; PMCID: PMC6351068.

145. Silvestri I, Cattarino S, Aglianò AM, Collalti G, Sciarra A. Beyond the Immune Suppression: The Immunotherapy in Prostate Cancer. Biomed Res Int. 2015;2015:794968. Epub 2015/06/16. doi: 10.1155/2015/794968. PubMed PMID: 26161414; PMCID: PMC4486485.

146. Ludwig M, Steltz C, Huwe P, Schäffer R, Altmannsberger M, Weidner W. Immunocytological analysis of leukocyte subpopulations in urine specimens before and after prostatic massage. Eur Urol. 2001;39(3):277-82. doi: 10.1159/000052453. PubMed PMID: 11275719.

147. Bostwick DG, de la Roza G, Dundore P, Corica FA, Iczkowski KA. Intraepithelial and stromal lymphocytes in the normal human prostate. Prostate. 2003;55(3):187-93. doi: 10.1002/pros.10224. PubMed PMID: 12692784.

148. Haverkamp JM, Charbonneau B, Crist SA, Meyerholz DK, Cohen MB, Snyder PW, Svensson RU, Henry MD, Wang H-H, Ratliff TL. An inducible model of abacterial prostatitis induces antigen specific inflammatory and proliferative changes in the murine prostate. The Prostate. 2011;71(11):1139-50. doi: 10.1002/pros.21327.

149. Maccioni M, Rivero VE, Riera CM. Prostatein (or rat prostatic steroid binding protein) is a major autoantigen in experimental autoimmune prostatitis. Clin Exp Immunol. 1998;112(2):159-65. doi: 10.1046/j.1365-2249.1998.00588.x. PubMed PMID: 9649176; PMCID: PMC1904968.

150. Rivero V, Carnaud C, Riera CM. Prostatein or steroid binding protein (PSBP) induces experimental autoimmune prostatitis (EAP) in NOD mice. Clin Immunol. 2002;105(2):176-84. doi: 10.1006/clim.2002.5281. PubMed PMID: 12482391.

151. Klyushnenkova EN, Ponniah S, Rodriguez A, Kodak J, Mann DL, Langerman A, Nishimura MI, Alexander RB. CD4 and CD8 T-lymphocyte recognition of prostate specific antigen in granulomatous prostatitis. J Immunother. 2004;27(2):136-46. doi: 10.1097/00002371-200403000-00007. PubMed PMID: 14770085.

152. Motrich RD, Maccioni M, Molina R, Tissera A, Olmedo J, Riera CM, Rivero VE. Presence of INFgamma-secreting lymphocytes specific to prostate antigens in a group of chronic prostatitis patients. Clin Immunol. 2005;116(2):149-57. doi: 10.1016/j.clim.2005.03.011. PubMed PMID: 15993362.

153. Alexander RB, Brady F, Ponniah S. Autoimmune prostatitis: evidence of T cell reactivity with normal prostatic proteins. Urology. 1997;50(6):893-9. doi: 10.1016/S0090-4295(97)00456-1. PubMed PMID: 9426720.

154. Ebelt K, Babaryka G, Frankenberger B, Stief CG, Eisenmenger W, Kirchner T, Schendel DJ, Noessner E. Prostate cancer lesions are surrounded by FOXP3+, PD-1+ and B7-H1+ lymphocyte clusters. Eur J Cancer. 2009;45(9):1664-72. Epub 2009/03/21. doi: 10.1016/j.ejca.2009.02.015. PubMed PMID: 19318244.

155. Ebelt K, Babaryka G, Figel AM, Pohla H, Buchner A, Stief CG, Eisenmenger W, Kirchner T, Schendel DJ, Noessner E. Dominance of CD4+ lymphocytic infiltrates with disturbed effector cell characteristics in the tumor microenvironment of prostate carcinoma. Prostate. 2008;68(1):1-10. doi: 10.1002/pros.20661. PubMed PMID: 17948280.

156. Xie Q, Liu Y, Cai T, Horton C, Stefanson J, Wang ZA. Dissecting cell-type-specific roles of androgen receptor in prostate homeostasis and regeneration through lineage tracing. Nat Commun. 2017;8:14284. Epub 2017/01/23. doi: 10.1038/ncomms14284. PubMed PMID: 28112153; PMCID: PMC5264212.

157. Toivanen R, Shen MM. Prostate organogenesis: tissue induction, hormonal regulation and cell type specification. Development. 2017;144(8):1382-98. doi: 10.1242/dev.148270. PubMed PMID: 28400434; PMCID: PMC5399670.

158. Crowell PD, Goldstein AS. Functional evidence that progenitor cells near sites of inflammation are precursors for aggressive prostate cancer. Mol Cell Oncol. 2017;4(2):e1279723. Epub 2017/01/13. doi: 10.1080/23723556.2017.1279723. PubMed PMID: 28401184; PMCID: PMC5383352.

159. Yan J, De Melo J, Cutz JC, Aziz T, Tang D. Aldehyde dehydrogenase 3A1 associates with prostate tumorigenesis. Br J Cancer. 2014;110(10):2593-603. Epub 2014/04/26. doi: 10.1038/bjc.2014.201

bjc2014201 [pii]. PubMed PMID: 24762960; PMCID: 4021532.

160. Austin DC, Strand DW, Love HL, Franco OE, Grabowska MM, Miller NL, Hameed O, Clark PE, Matusik RJ, Jin RJ, Hayward SW. NF-κB and androgen receptor variant 7 induce expression of SRD5A isoforms and confer 5ARI resistance. Prostate. 2016;76(11):1004-18. Epub 2016/05/16. doi: 10.1002/pros.23195. PubMed PMID: 27197599; PMCID: PMC4912960.

161. Koryakina Y, Ta HQ, Gioeli D. Androgen receptor phosphorylation: biological context and functional consequences. Endocr Relat Cancer. 2014;21(4):T131-45. Epub 2014/01/14. doi: 10.1530/ERC-13-0472. PubMed PMID: 24424504; PMCID: PMC4437516.

162. Watson PA, Ellwood-Yen K, King JC, Wongvipat J, Lebeau MM, Sawyers CL. Context-dependent hormone-refractory progression revealed through characterization of a novel murine prostate cancer cell line. Cancer Res. 2005;65(24):11565-71. doi: 10.1158/0008-5472.CAN-05-3441. PubMed PMID: 16357166.

163. Watson PA, Chen YF, Balbas MD, Wongvipat J, Socci ND, Viale A, Kim K, Sawyers CL. Constitutively active androgen receptor splice variants expressed in castration-resistant prostate cancer require full-length androgen receptor. Proc Natl Acad Sci U S A. 2010;107(39):16759-65. Epub 2010/09/09. doi: 10.1073/pnas.1012443107

1012443107 [pii]. PubMed PMID: 20823238; PMCID: 2947883.

164. Yuan X, Cai C, Chen S, Yu Z, Balk SP. Androgen receptor functions in castration-resistant prostate cancer and mechanisms of resistance to new agents targeting the androgen axis. Oncogene. 2014;33(22):2815-25. Epub 2013/06/12. doi: 10.1038/onc.2013.235

onc2013235 [pii]. PubMed PMID: 23752196.

165. Lindmark F, Zheng SL, Wiklund F, Bälter KA, Sun J, Chang B, Hedelin M, Clark J, Johansson JE, Meyers DA, Adami HO, Isaacs W, Grönberg H, Xu J. Interleukin-1 receptor antagonist haplotype associated with prostate cancer risk. Br J Cancer. 2005;93(4):493-7. doi: 10.1038/sj.bjc.6602729. PubMed PMID: 16106254; PMCID: PMC2361575.

166. Haverkamp JM, Crist SA, Elzey BD, Cimen C, Ratliff TL. In vivo suppressive function of myeloid-derived suppressor cells is limited to the inflammatory site. Eur J Immunol. 2011;41(3):749-59. doi: 10.1002/eji.201041069. PubMed PMID: 21287554; PMCID: PMC3089902.

167. Buenrostro JD, Giresi PG, Zaba LC, Chang HY, Greenleaf WJ. Transposition of native chromatin for fast and sensitive epigenomic profiling of open chromatin, DNA-binding proteins and nucleosome position. Nat Methods. 2013;10(12):1213-8. Epub 2013/10/06. doi: 10.1038/nmeth.2688. PubMed PMID: 24097267; PMCID: PMC3959825.

168. Bolger AM, Lohse M, Usadel B. Trimmomatic: a flexible trimmer for Illumina sequence data. Bioinformatics. 2014;30(15):2114-20. doi: 10.1093/bioinformatics/btu170. PubMed PMID: 24695404; PMCID: 4103590.

169. Andrews S. FastQC2010.

170. Gordon A. FastX-Toolkit. 2009.

171. Trapnell C, Pachter L, Salzberg SL. TopHat: discovering splice junctions with RNA-Seq. Bioinformatics. 2009;25(9):1105-11. doi: 10.1093/bioinformatics/btp120. PubMed PMID: 19289445; PMCID: 2672628.

172. Kim D, Pertea G, Trapnell C, Pimentel H, Kelley R, Salzberg SL. TopHat2: accurate alignment of transcriptomes in the presence of insertions, deletions and gene fusions. Genome biology. 2013;14(4):R36. doi: 10.1186/gb-2013-14-4-r36. PubMed PMID: 23618408; PMCID: 4053844.

173. Anders S, Pyl PT, Huber W. HTSeq--a Python framework to work with high-throughput sequencing data. Bioinformatics. 2015;31(2):166-9. doi: 10.1093/bioinformatics/btu638. PubMed PMID: 25260700; PMCID: 4287950.

174. Li H, Handsaker B, Wysoker A, Fennell T, Ruan J, Homer N, Marth G, Abecasis G, Durbin R, Genome Project Data Processing S. The Sequence Alignment/Map format and SAMtools. Bioinformatics. 2009;25(16):2078-9. doi: 10.1093/bioinformatics/btp352. PubMed PMID: 19505943; PMCID: 2723002.

175. Robinson MD, McCarthy DJ, Smyth GK. edgeR: a Bioconductor package for differential expression analysis of digital gene expression data. Bioinformatics. 2010;26(1):139-40. doi: 10.1093/bioinformatics/btp616. PubMed PMID: 19910308; PMCID: 2796818.

176. Robinson MD, Oshlack A. A scaling normalization method for differential expression analysis of RNA-seq data. Genome biology. 2010;11(3):R25. doi: 10.1186/gb-2010-11-3-r25. PubMed PMID: 20196867; PMCID: 2864565.

177. McCarthy DJ, Chen Y, Smyth GK. Differential expression analysis of multifactor RNA-Seq experiments with respect to biological variation. Nucleic acids research. 2012;40(10):4288-97. doi: 10.1093/nar/gks042. PubMed PMID: 22287627; PMCID: 3378882.

178. Kramer A, Green J, Pollard J, Jr., Tugendreich S. Causal analysis approaches in Ingenuity Pathway Analysis. Bioinformatics. 2014;30(4):523-30. doi: 10.1093/bioinformatics/btt703. PubMed PMID: 24336805; PMCID: 3928520.

179. Dobin A, Davis CA, Schlesinger F, Drenkow J, Zaleski C, Jha S, Batut P, Chaisson M, Gingeras TR. STAR: ultrafast universal RNA-seq aligner. Bioinformatics. 2013;29(1):15-21. Epub 2012/10/25. doi: 10.1093/bioinformatics/bts635. PubMed PMID: 23104886; PMCID: PMC3530905.

180. Love MI, Huber W, Anders S. Moderated estimation of fold change and dispersion for RNA-seq data with DESeq2. Genome biology. 2014;15(12):550. doi: 10.1186/s13059-014-0550-8. PubMed PMID: 25516281; PMCID: 4302049.

181. Cao Y, Jia SF, Chakravarty G, de Crombrugghe B, Kleinerman ES. The osterix transcription factor down-regulates interleukin-1 alpha expression in mouse osteosarcoma cells. Mol Cancer Res. 2008;6(1):119-26. doi: 10.1158/1541-7786.MCR-07-0090. PubMed PMID: 18234967; PMCID: PMC2929177.

182. Chua CW, Shibata M, Lei M, Toivanen R, Barlow LJ, Bergren SK, Badani KK, McKiernan JM, Benson MC, Hibshoosh H, Shen MM. Single luminal epithelial progenitors can generate prostate organoids in culture. Nat Cell Biol. 2014;16(10):951-61, 1-4. Epub 2014/09/23. doi: 10.1038/ncb3047

ncb3047 [pii]. PubMed PMID: 25241035; PMCID: 4183706.

183. Kwon OJ, Zhang L, Xin L. Stem Cell Antigen-1 Identifies a Distinct Androgen-Independent Murine Prostatic Luminal Cell Lineage with Bipotent Potential. Stem Cells. 2016;34(1):191-202. Epub 2015/10/27. doi: 10.1002/stem.2217. PubMed PMID: 26418304; PMCID: PMC4816225.

184. Marker PC, Donjacour AA, Dahiya R, Cunha GR. Hormonal, cellular, and molecular control of prostatic development. Dev Biol. 2003;253(2):165-74. doi: 10.1016/s0012-1606(02)00031-3. PubMed PMID: 12645922.

185. Yip CKY, Bansal S, Wong SY, Lau AJ. Identification of Galeterone and Abiraterone as Inhibitors of Dehydroepiandrosterone Sulfonation Catalyzed by Human Hepatic Cytosol, SULT2A1, SULT2B1b, and SULT1E1. Drug Metab Dispos. 2018;46(4):470-82. Epub 2018/02/07. doi: 10.1124/dmd.117.078980. PubMed PMID: 29436390.

186. Chhipa RR, Halim D, Cheng J, Zhang HY, Mohler JL, Ip C, Wu Y. The direct inhibitory effect of dutasteride or finasteride on androgen receptor activity is cell line specific. Prostate. 2013;73(14):1483-94. Epub 2013/06/28. doi: 10.1002/pros.22696. PubMed PMID: 23813737; PMCID: PMC3992475.

187. Wu Y, Chhipa RR, Zhang H, Ip C. The antiandrogenic effect of finasteride against a mutant androgen receptor. Cancer Biol Ther. 2011;11(10):902-9. Epub 2011/05/15. doi: 10.4161/cbt.11.10.15187. PubMed PMID: 21386657; PMCID: PMC3116931.

188. Lamb AD, Massie CE, Neal DE. The transcriptional programme of the androgen receptor (AR) in prostate cancer. BJU Int. 2014;113(3):358-66. Epub 2013/09/24. doi: 10.1111/bju.12415. PubMed PMID: 24053777.

189. Irikura VM, Lagraoui M, Hirsh D. The epistatic interrelationships of IL-1, IL-1 receptor antagonist, and the type I IL-1 receptor. J Immunol. 2002;169(1):393-8. PubMed PMID: 12077269.

190. Zhang D, Park D, Zhong Y, Lu Y, Rycaj K, Gong S, Chen X, Liu X, Chao HP, Whitney P, Calhoun-Davis T, Takata Y, Shen J, Iyer VR, Tang DG. Stem cell and neurogenic gene-expression profiles link prostate basal cells to aggressive prostate cancer. Nat Commun. 2016;7:10798. Epub 2016/02/29. doi: 10.1038/ncomms10798. PubMed PMID: 26924072; PMCID: PMC4773505.

191. Olson BM, Gamat M, Seliski J, Sawicki T, Jeffery J, Ellis L, Drake CG, Weichert J, McNeel DG. Prostate Cancer Cells Express More Androgen Receptor (AR) Following Androgen Deprivation, Improving Recognition by AR-Specific T Cells. Cancer Immunol Res. 2017;5(12):1074-85. Epub 2017/10/21. doi: 10.1158/2326-6066.cir-16-0390. PubMed PMID: 29051161; PMCID: PMC5873299.

192. Fibbi B, Penna G, Morelli A, Adorini L, Maggi M. Chronic inflammation in the pathogenesis of benign prostatic hyperplasia. Int J Androl. 2010;33(3):475-88. Epub 2009/06/08. doi: 10.1111/j.1365-2605.2009.00972.x. PubMed PMID: 19508330.

193. Donadio AC, Depiante-Depaoli M. Inflammatory cells and MHC class II antigens expression in prostate during time-course experimental autoimmune prostatitis development. Clin Immunol Immunopathol. 1997;85(2):158-65. doi: 10.1006/clin.1997.4427. PubMed PMID: 9344698.

194. De Marzo AM, Nakai Y, Nelson WG. Inflammation, atrophy, and prostate carcinogenesis. Urol Oncol. 2007;25(5):398-400. Epub 2007/09/11. doi: S1078-1439(07)00139-1 [pii]

10.1016/j.urolonc.2007.05.007. PubMed PMID: 17826659.

195. Le B, Schaeffer AJ. Chronic prostatitis. BMJ Clin Evid. 2011;2011. Epub 2011/07/04. PubMed PMID: 21736764; PMCID: PMC3275320.

196. Shen YC, Ghasemzadeh A, Kochel CM, Nirschl TR, Francica BJ, Lopez-Bujanda ZA, Carrera Haro MA, Tam A, Anders RA, Selby MJ, Korman AJ, Drake CG. Combining intratumoral Treg depletion with androgen deprivation therapy (ADT): preclinical activity in the Myc-CaP model. Prostate Cancer Prostatic Dis. 2018;21(1):113-25. Epub 2017/12/06. doi: 10.1038/s41391-017-0013-x. PubMed PMID: 29203894; PMCID: PMC5897134.

197. Ylitalo EB, Thysell E, Jernberg E, Lundholm M, Crnalic S, Egevad L, Stattin P, Widmark A, Bergh A, Wikström P. Subgroups of Castration-resistant Prostate Cancer Bone Metastases Defined Through an Inverse Relationship Between Androgen Receptor Activity and Immune Response. Eur Urol. 2017;71(5):776-87. Epub 2016/08/03. doi: 10.1016/j.eururo.2016.07.033. PubMed PMID: 27497761.

198. de Oliveira Bravo M, Carvalho JL, Saldanha-Araujo F. Adenosine production: a common path for mesenchymal stem-cell and regulatory T-cell-mediated immunosuppression. Purinergic Signal. 2016;12(4):595-609. Epub 2016/08/26. doi: 10.1007/s11302-016-9529-0. PubMed PMID: 27557887; PMCID: PMC5124006.

199. Gabrilovich DI, Nagaraj S. Myeloid-derived suppressor cells as regulators of the immune system. Nat Rev Immunol. 2009;9(3):162-74. doi: 10.1038/nri2506. PubMed PMID: 19197294; PMCID: PMC2828349.

200. Krueger TE, Thorek DLJ, Meeker AK, Isaacs JT, Brennen WN. Tumor-infiltrating mesenchymal stem cells: Drivers of the immunosuppressive tumor microenvironment in prostate cancer? Prostate. 2019;79(3):320-30. Epub 2018/11/28. doi: 10.1002/pros.23738. PubMed PMID: 30488530; PMCID: PMC6549513.

201. Kumar V, Patel S, Tcyganov E, Gabrilovich DI. The Nature of Myeloid-Derived Suppressor Cells in the Tumor Microenvironment. Trends Immunol. 2016;37(3):208-20. Epub 2016/02/10. doi: 10.1016/j.it.2016.01.004. PubMed PMID: 26858199; PMCID: PMC4775398.

202. Noman MZ, Desantis G, Janji B, Hasmim M, Karray S, Dessen P, Bronte V, Chouaib S. PD-L1 is a novel direct target of HIF-1alpha, and its blockade under hypoxia enhanced MDSC-mediated T cell activation. J Exp Med. 2014;211(5):781-90. doi: 10.1084/jem.20131916. PubMed PMID: 24778419; PMCID: PMC4010891.

203. Sato K, Ozaki K, Oh I, Meguro A, Hatanaka K, Nagai T, Muroi K, Ozawa K. Nitric oxide plays a critical role in suppression of T-cell proliferation by mesenchymal stem cells. Blood. 2007;109(1):228-34. Epub 2006/09/19. doi: 10.1182/blood-2006-02-002246. PubMed PMID: 16985180.

204. van den Akker F, Vrijsen KR, Deddens JC, Buikema JW, Mokry M, van Laake LW, Doevendans PA, Sluijter JPG. Suppression of T cells by mesenchymal and cardiac progenitor cells is partly mediated via extracellular vesicles. Heliyon. 2018;4(6):e00642. Epub 2018/06/06. doi: 10.1016/j.heliyon.2018.e00642. PubMed PMID: 30003150; PMCID: PMC6040605.

205. Liu M, Wang X, Wang L, Ma X, Gong Z, Zhang S, Li Y. Targeting the IDO1 pathway in cancer: from bench to bedside. J Hematol Oncol. 2018;11(1):100. Epub 2018/08/02. doi: 10.1186/s13045-018-0644-y. PubMed PMID: 30068361; PMCID: PMC6090955.

206. Zhai L, Ladomersky E, Lenzen A, Nguyen B, Patel R, Lauing KL, Wu M, Wainwright DA. IDO1 in cancer: a Gemini of immune checkpoints. Cell Mol Immunol. 2018;15(5):447-57. Epub 2018/01/29. doi: 10.1038/cmi.2017.143. PubMed PMID: 29375124; PMCID: PMC6068130.

207. Zhou QH, Han H, Lu JB, Liu TY, Huang KB, Deng CZ, Li ZS, Chen JP, Yao K, Qin ZK, Liu ZW, Li YH, Guo SJ, Ye YL, Zhou FJ, Liu RY. Up-regulation of indoleamine 2,3-dioxygenase 1 (IDO1) expression and catalytic activity is associated with immunosuppression and poor prognosis in penile squamous cell carcinoma patients. Cancer Commun (Lond). 2020;40(1):3-15. Epub 2020/03/03. doi: 10.1002/cac2.12001. PubMed PMID: 32125093; PMCID: PMC7163927.

208. Cimen Bozkus C, Elzey BD, Crist SA, Ellies LG, Ratliff TL. Expression of Cationic Amino Acid Transporter 2 Is Required for Myeloid-Derived Suppressor Cell-Mediated Control of T Cell Immunity. J Immunol. 2015;195(11):5237-50. Epub 2015/10/21. doi: 10.4049/jimmunol.1500959. PubMed PMID: 26491198; PMCID: PMC4655170.

209. Barach YS, Lee JS, Zang X. T cell coinhibition in prostate cancer: new immune evasion pathways and emerging therapeutics. Trends Mol Med. 2011;17(1):47-55. doi: 10.1016/j.molmed.2010.09.006. PubMed PMID: 20971039; PMCID: PMC3039708.

210. Huang YH, Zhu C, Kondo Y, Anderson AC, Gandhi A, Russell A, Dougan SK, Petersen BS, Melum E, Pertel T, Clayton KL, Raab M, Chen Q, Beauchemin N, Yazaki PJ, Pyzik M, Ostrowski MA, Glickman JN, Rudd CE, Ploegh HL, Franke A, Petsko GA, Kuchroo VK, Blumberg RS. CEACAM1 regulates TIM-3-mediated tolerance and exhaustion. Nature. 2015;517(7534):386-90. Epub 2014/11/05. doi: 10.1038/nature13848. PubMed PMID: 25363763; PMCID: PMC4297519.

211. Adamiak M, Bujko K, Brzezniakiewicz-Janus K, Kucia M, Ratajczak J, Ratajczak MZ. The Inhibition of CD39 and CD73 Cell Surface Ectonucleotidases by Small Molecular Inhibitors Enhances the Mobilization of Bone Marrow Residing Stem Cells by Decreasing the Extracellular Level of Adenosine. Stem Cell Rev Rep. 2019;15(6):892-9. Epub 2019/09/15. doi: 10.1007/s12015-019-09918-y. PubMed PMID: 31520298; PMCID: PMC6925070.

212. Allard B, Longhi MS, Robson SC, Stagg J. The ectonucleotidases CD39 and CD73: Novel checkpoint inhibitor targets. Immunol Rev. 2017;276(1):121-44. Epub 2017/03/05. doi: 10.1111/imr.12528. PubMed PMID: 28258700; PMCID: PMC5338647.

213. Mescher MF, Popescu FE, Gerner M, Hammerbeck CD, Curtsinger JM. Activation-induced non-responsiveness (anergy) limits CD8 T cell responses to tumors. Semin Cancer Biol. 2007;17(4):299-308. Epub 2007/07/28. doi: 10.1016/j.semcancer.2007.06.008. PubMed PMID: 17656106; PMCID: PMC2693139.

214. Mognol GP, Spreafico R, Wong V, Scott-Browne JP, Togher S, Hoffmann A, Hogan PG, Rao A, Trifari S. Exhaustion-associated regulatory regions in CD8(+) tumor-infiltrating T cells. Proc Natl Acad Sci U S A. 2017;114(13):E2776-E85. Epub 2017/03/12. doi: 10.1073/pnas.1620498114. PubMed PMID: 28283662; PMCID: PMC5380094.